

Chapter 10



<https://doi.org/10.32685/pub.esp.36.2019.10>
Published online 15 May 2020

Cretaceous Record from a Mariana– to an Andean–Type Margin in the Central Cordillera of the Colombian Andes

Agustín CARDONA^{1*}, Santiago LEÓN² , Juan S. JARAMILLO³ , Victor A. VALENCIA⁴ , Sebastian ZAPATA⁵ , Andrés PARDO–TRUJILLO⁶ , Axel K. SCHMITT⁷ , Dany MEJÍA⁸ , and Juan Camilo ARENAS⁹

Abstract The Cretaceous tectonic evolution of the western margin of South America involves a shift from an extensional convergent margin toward a more compressional setting that marks the beginning of the Andean Orogeny. In the Colombian Andes, this changing scenario is recorded in the Cretaceous sedimentary and magmatic rocks of the Central Cordillera. A review of field relationships, together with analysis of integrated provenance constraints, including sandstone petrography and detrital zircon geochronology from various localities, suggests that during the Early Cretaceous until the Aptian – Albian, siliciclastic basin fills were characterized by transgressive fining-upward trends, with prominent first-cycle quartzose provenances that indicate strong chemical weathering in the source areas. Jurassic, Triassic, and older detrital zircon U–Pb ages suggest that the igneous and metamorphic rocks forming the basement of the Central Cordillera were the main sources. Furthermore, the presence of Early Cretaceous detrital ages between 120 and 100 Ma, together with interlayered volcanic rocks at the top of the sequence characterized by mixed arc-like, MORB, and E–MORB geochemical signatures, can be related to the evolution of an extensional arc with associated back-arc basin formation. Plutonic rocks with ca. 98 Ma crystallization ages show Nd, Sr, Hf, and O isotope evidence for the existence of thinned continental crust that may account for the dominant mantle signature. By ca. 93 Ma, the Early Cretaceous sedimentary sequences were deformed and intruded by plutonic rocks, which conversely show isotopic fingerprints characteristic of crustal signatures that can be explained by the involvement of thicker crust that promoted melt interaction with the more radiogenic host rocks.

This tectonic change from a Mariana– to an Andean–type subduction style was probably triggered by regional–scale plate kinematic reorganizations, as suggested by similar coeval tectonic scenarios along the entire South American margin, and set the conditions for the construction of the Andean chain.

Keywords: Cretaceous, back-arc, intra-arc, Andean Orogeny, Geochemistry.

Resumen La evolución tectónica del borde occidental de Suramérica durante el Cretácico está marcada por el cambio de un margen convergente extensional hacia una configuración más compresiva que marca el inicio de la Orogenia Andina. En los Andes

Citation: Cardona, A., León, S., Jaramillo, J.S., Valencia, V., Zapata, S., Pardo-Trujillo, A., Schmitt, A.K., Mejía, D. & Arenas, J.C. 2020. Cretaceous record from a Mariana– to an Andean–type margin in the Central Cordillera of the Colombian Andes. In: Gómez, J. & Pinilla-Pachon, A.O. (editors), *The Geology of Colombia, Volume 2 Mesozoic. Servicio Geológico Colombiano, Publicaciones Geológicas Especiales 36*, p. 335–373. Bogotá. <https://doi.org/10.32685/pub.esp.36.2019.10>

- 1 agcardonamo@unal.edu.co
Universidad Nacional de Colombia
Sede Medellín
Facultad de Minas
Departamento de Procesos y Energía
Grupo de Investigación en Geología y Geofísica (EGEO)
Medellín, Colombia
 - 2 sleonva@gmail.com
Universidad Nacional de Colombia
Sede Medellín
Grupo de Investigación en Geología y Geofísica (EGEO)
Medellín, Colombia
Smithsonian Tropical Research Institute
Ancón, Panamá
 - 3 jusjaramillori@unal.edu.co
Universidad Nacional de Colombia
Sede Medellín
Facultad de Minas
Departamento de Materiales y Minerales
Grupo de Investigación en Geología y Geofísica (EGEO)
Medellín, Colombia
 - 4 victor.valencia@wsu.edu
Washington State University
School of the Environment
Pullman, USA
 - 5 szapatah@gmail.com
Smithsonian Tropical Research Institute
Ancón, Panamá
Missouri University of Science and Technology
Department of Geology and Geophysics
USA
 - 6 andres.pardo@ucaldas.edu.co
Universidad de Caldas
Instituto de Investigaciones en Estratigrafía (IIES)
Manizales, Colombia
 - 7 Axel.Schmitt@geow.uni-heidelberg.de
Heidelberg University
Institute of Earth Sciences
Heidelberg, Germany
 - 8 dymejiav@unal.edu.co
Universidad Nacional de Colombia
Sede Medellín
Facultad de Minas
Departamento de Materiales y Minerales
Grupo de Investigación en Geología y Geofísica (EGEO)
Medellín, Colombia
 - 9 Universidad Nacional de Colombia
Sede Medellín
Departamento de Geociencias y Medio Ambiente
Medellín, Colombia
- * Corresponding author

Supplementary Information:

S: <https://www2.sgc.gov.co/LibroGeologiaColombia/tgc/sgcpubesp36201910s.pdf>

colombianos, este cambio está registrado en las rocas sedimentarias y magmáticas cretácicas de la cordillera Central. La revisión de las relaciones de campo, junto con el análisis de procedencia de rocas siliciclásticas (petrografía de areniscas y geocronología en circones detríticos de varias localidades), sugiere que durante el Cretácico Temprano hasta el Aptiano–Albiano el relleno siliciclástico de la cuenca se caracterizó por tener un carácter transgresivo granodecreciente y una composición cuarzosa con componentes de primer ciclo asociados a condiciones de meteorización intensa en el área fuente. Las edades U–Pb en circón jurásicas, triásicas y más antiguas sugieren que las fuentes principales fueron las rocas ígneas y metamórficas que conforman el basamento de la cordillera Central. Además, la presencia de edades detríticas del Cretácico Temprano entre 120 y 100 Ma, junto con la de rocas volcánicas intercaladas al tope de la secuencia que se caracterizan por una mezcla de firmas geoquímicas de arco, MORB y E–MORB, puede estar relacionada con la evolución de un arco extensional y la formación de una cuenca de retroarco. Las rocas plutónicas con edades de cristalización de ca. 98 Ma muestran evidencias isotópicas de Nd, Sr, Hf y O de afinidad mantélica que estarían asociadas a la existencia de una corteza continental adelgazada. A los ca. 93 Ma, las secuencias sedimentarias del Cretácico Temprano fueron deformadas e intruidas por rocas plutónicas, las cuales en cambio muestran características isotópicas corticales que pueden explicarse por la participación de una corteza más gruesa que promovió la interacción del fundido con las rocas caja más radiogénicas.

Este cambio tectónico de un estilo de subducción de tipo Marianas a uno de tipo andino es común en toda la margen continental suramericana y estaría asociado con reorganizaciones cinemáticas a escala de placas que marcarían el inicio de la construcción de la cadena andina.

Palabras clave: *Cretácico, retroarco, intraarco, Orogenia Andina, geoquímica.*

1. Introduction

During the Cretaceous, the western margin of South America experienced a major change from a dominantly extensional system (Mariana–type) toward a more compressional tectonic style (Chile–type; Uyeda & Kanamori, 1979; Stern, 2012), which marks the initiation of the Andean orogeny (see reviews in Tunik et al., 2010; Horton, 2018). Whereas the Mesozoic – Cenozoic tectonic evolution of the central and southern Andean segments was characterized by a subduction–dominated orogeny, the northern Andes constitutes a classic accretionary orogen in which interspersed terrane accretion and subduction tectonics were responsible for orogenic growth (see a review in Ramos, 2009). With such a complex scenario and the continuous superimposition of tectonic events, clear discrimination between subduction–dominated extensional and compressional tectonics remains a major challenge.

The long–term spatiotemporal and compositional changes in magmatic rocks integrated with the stratigraphic and provenance evolution of contemporaneous basins are sensitive markers of the evolution of convergent margins and can be used to address alternating settings between extension and compression (Busby, 2012; Cawood et al., 2009; Marsaglia, 2012).

In this contribution, we present a review of published field observations and petrographic, geochronological, and

geochemical data, together with new results from magmatic and detrital zircon U–Pb geochronology, whole–rock geochemistry, zircon Hf and O isotopes, sandstone petrography, and field relationships of Cretaceous units from selected localities exposed between the two flanks of the Central Cordillera of the Colombian Andes (Figure 1). The analysis of available data and the new data presented here allows documenting an Aptian – Albian extensional margin associated with the formation of different intra–arc and back–arc extensional domains, which were inverted and deformed before 90 Ma and subsequently experienced the formation of a younger Late Cretaceous arc and the collision of an intra–oceanic terrane.

The Early to Late Cretaceous record in the Central Cordillera provides additional constraints on the continental–scale transition from extension to compression that gave rise to the Andean Orogeny (Horton, 2018; Tunik et al., 2010).

2. Geological Setting

Within the Colombian Andes, the Cretaceous geological record is found in three different tectonostratigraphic domains, which closely coincide with major morphostructural features represented by the three main cordilleras and the intervening Magdalena and Cauca valleys (Figures 1, 2).

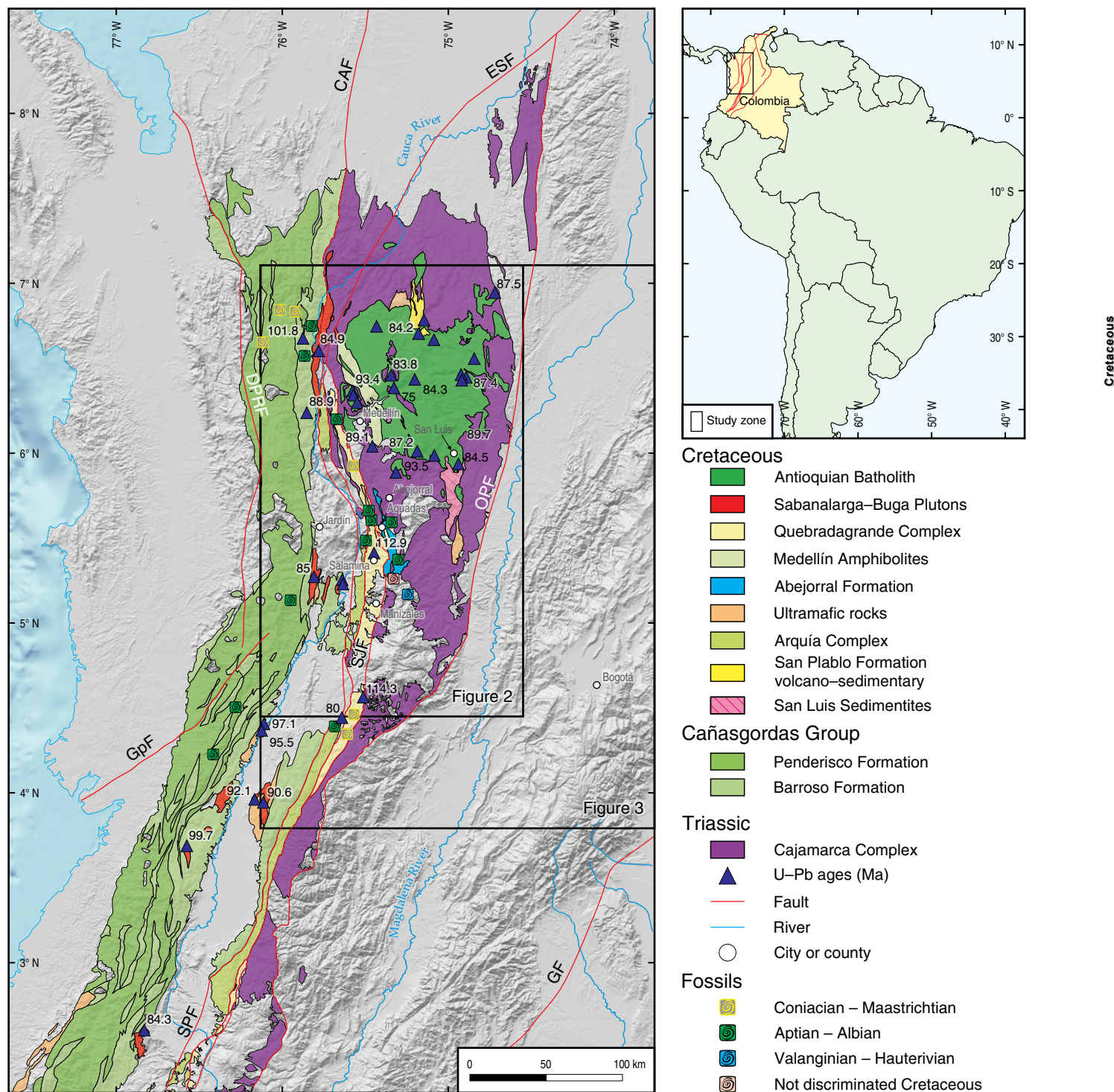


Figure 1. Regional geological map of the Colombian Andes showing the locations of the pre-Cretaceous and Cretaceous units, as well as the published U–Pb geochronology from the magmatic units (modified after Gómez et al., 2015; Jaramillo et al., 2017). (CAF) Cauca–Almaguer Fault; (ESF) Espíritu Santo Fault; (DPRF) Dabeiba–Pueblo Rico Fault; (OPF) Otú–Pericos Fault; (SJF) San Jerónimo Fault; (GpF) Garrapata Fault; (SPF) Silvia–Pijao Fault; (GF) Guacáramo Fault.

In the Magdalena valley and the Eastern Cordillera, Cretaceous sedimentary rocks accumulated over Jurassic volcanic and siliciclastic units and correspond to a former extensional basin filling interval that ended in the Berriasian (Kammer &

Sánchez, 2006; Sarmiento–Rojas et al., 2006). These units are considered para–autochthonous and/or northward–transported domains that nearly achieved their modern paleogeographic positions west of the reference craton during the Late Jurassic

(Bayona *et al.*, 2006). The Early Cretaceous extension–dominated setting switched to eustatic–dominated sedimentation with coeval tectonic quiescence and thermal subsidence. This sedimentary record can be traced eastward in the Llanos Basin and includes associated volcanogenic clays and tuffs ranging in age from the Hauterivian to the Turonian (Villamil & Arango, 1998; Villamil, 1999; Sarmiento–Rojas *et al.*, 2006), as well as minor gabbroic bodies with Ar–Ar ages between 136 and 74 Ma (Vásquez *et al.*, 2010).

In the Central Cordillera, the Early Cretaceous units are represented by a series of discontinuous siliciclastic sequences that crop out on both flanks and along its axis (Figure 2). These sequences overlie Permian – Triassic and Jurassic metamorphic rocks and are characterized by an apparent fining–upward pattern from predominantly sandstone/conglomeratic beds toward a mudstone–dominated sequence (see review in Nivia *et al.*, 2006; Zapata *et al.*, 2018). Fossil remnants, including ammonites, bivalves, and gastropods, have shown that sedimentary accumulation extended from the Berriasian to the Aptian (see compilation in Botero & González, 1983; González, 2001). Volcanic flows and small gabbroic bodies have been found in association with some of these sedimentary sequences (Rodríguez & Celada–Arango, 2018; Zapata *et al.*, 2018).

Two different hypothetical geodynamic settings have been considered for the evolution of the Central Cordillera sediments: a passive margin that collided with an intra–oceanic arc (Toussaint, 1996; Moreno–Sánchez *et al.*, 2008) or a back–arc basin that formed during the Early Cretaceous (Nivia *et al.*, 2006; Villagómez *et al.*, 2011; Cochrane *et al.*, 2014a; Spikings *et al.*, 2015; Zapata *et al.*, 2018). The paleogeographic position where these basins accumulated also remains controversial, with some authors considering an autochthonous origin connected to depocenters located in the Eastern Cordillera domains (Etayo–Serna *et al.*, 1969) and other authors arguing for exotic positions farther to the south probably correlated with coeval terranes in Ecuador (Toussaint, 1996; Pindell & Kennan, 2009).

In the western flank of the Central Cordillera and the Cauca Valley that separates it from the Western Cordillera, a series of highly deformed volcano–sedimentary units also considered Aptian – Albian in age crop out and are affected by a major fault system (Cauca–Romeral; Nivia *et al.*, 2006). These units include gabbroic rocks associated with serpentinized peridotites (Álvarez, 1987; González, 2001) and are in fault contact with intermediate– to high–pressure metamorphic rocks with Lu–Hf and Ar–Ar peaks and cooling ages between 137 and 110 Ma (García–Ramírez *et al.*, 2017), as well as younger ages of ca. 64 Ma (Bustamante *et al.*, 2011). These units are also interspersed with Triassic and older igneous and metamorphic rocks (Vinasco *et al.*, 2006; Cochrane *et al.*, 2014a; Zapata *et al.*, 2018). The volcano–sedimentary units have been considered either as part of a fringing arc associated with the formation of a back–arc basin (Nivia *et al.*, 2006; Villagómez *et al.*, 2011; Cochrane *et al.*, 2014b; Spikings *et al.*, 2015) or as an allochthonous oceanic arc that collided with a passive margin (Toussaint, 1996; Moreno–Sánchez & Pardo–Trujillo, 2003).

Following the formation of these extensional basins related to a back–arc or intra–arc setting, prominent plutonic activity formed intrusions with ages between 98 and 72 Ma in the Early Cretaceous and older basement of the Central Cordillera (Ibañez–Mejía *et al.*, 2007; Ordóñez–Carmona *et al.*, 2007; Restrepo–Moreno *et al.*, 2007; Leal–Mejía, 2011; Villagómez *et al.*, 2011). This magmatism represents the construction of a continental arc that was active until the Maastrichtian – Paleocene collision of the South American margin with an intra–oceanic arc (Villagómez *et al.*, 2011; Spikings *et al.*, 2015; Jaramillo *et al.*, 2017). Several plutonic bodies with ages between 90 Ma and 78 Ma also intrude the Cretaceous extensional related volcano–sedimentary unit exposed to the west (Villagómez *et al.*, 2011; Jaramillo *et al.*, 2017).

In contrast, the Western Cordillera includes a high–density basaltic sequence characterized by deformed and undeformed lava flows, pillow lavas, and minor pyroclastic rocks, which have been interpreted as remnants of an oceanic plateau likely related to the Caribbean Large Igneous Province that formed in southern latitudes (CLIP; Kerr *et al.*, 1997; Villagómez *et al.*, 2011; Zapata *et al.*, 2017; Hincapié–Gómez *et al.*, 2018). This basaltic province presents minor intercalations of mudstones and cherts with Berriasian to Albian fossil remnants that are intruded by plateau–related gabbroic and tonalitic bodies with ca. 98 Ma crystallization ages (Villagómez *et al.*, 2011; Weber *et al.*, 2015). These units are also intruded by arc–related granitoids and gabbroic rocks with zircon U–Pb ages between 80 and 90 Ma (Villagómez *et al.*, 2011; Zapata *et al.*, 2017), which are locally associated with volcanic units of Campanian age (Spadea & Espinosa, 1996). Late Cretaceous and younger sandstones with quartz–rich compositions overlie these volcanic units and represent the stratigraphic record of their juxtaposition against the continental margin (León *et al.*, 2018).

Several lines of evidence, including exhumation trends in the Central and Western Cordilleras (Villagómez & Spikings, 2013), changes in the nature of the magmatic record along the western flank of the Central Cordillera (Jaramillo *et al.*, 2017) and major changes in the sedimentary environments and the associated provenances in the eastern basins (Villamil, 1999), have suggested that during the Late Cretaceous – Paleocene, the different units described above were fully juxtaposed (Toussaint, 1996; Villagómez *et al.*, 2011; Spikings *et al.*, 2015) and subsequently segmented and dispersed by strike–slip fault systems along the margin (Pindell & Kennan, 2009; Montes *et al.*, 2010).

Several lines of evidence, including exhumation trends in the Central and Western Cordilleras (Villagómez & Spikings, 2013), changes in the nature of the magmatic record along the western flank of the Central Cordillera (Jaramillo *et al.*, 2017) and major changes in the sedimentary environments and the associated provenances in the eastern basins (Villamil, 1999), have suggested that during the Late Cretaceous – Paleocene, the different units described above were fully juxtaposed (Toussaint, 1996; Villagómez *et al.*, 2011; Spikings *et al.*, 2015) and subsequently segmented and dispersed by strike–slip fault systems along the margin (Pindell & Kennan, 2009; Montes *et al.*, 2010).

3. Methods and Approach

In this contribution, we present a review of published geological constraints from Lower to Upper Cretaceous sedimentary

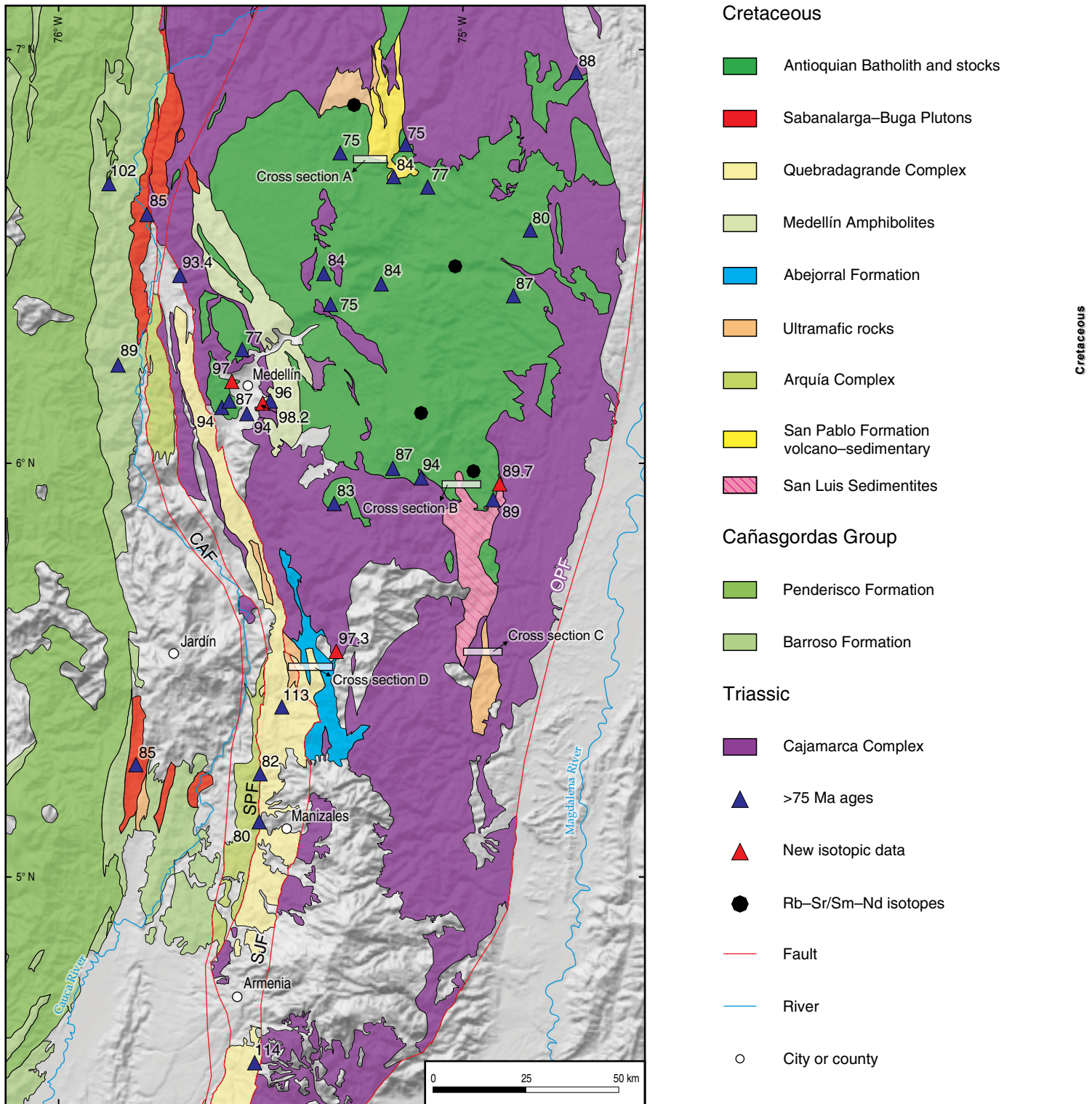


Figure 2. Geological map of the sampled and discussed regions in the Central Cordillera (modified after Gómez et al., 2015). (CAF) Cauca–Almaguer Fault; (OPF) Otú–Pericos Fault; (SJF) San Jerónimo Fault; (SPF) Silvia–Pijao Fault. See the cross sections A, B, C, and D in Figure 4.

and magmatic rocks of the Central Cordillera. Although some of the available constraints are mainly from basic geological cartography, the descriptions are remarkably objective and

remain valid. These results are integrated with new field observations together with sandstone petrography, geochemical analyses, U–Pb zircon geochronology, and zircon oxygen and

hafnium isotopes from two localities of the Cretaceous units exposed in the western and eastern flanks of the Central Cordillera in the Department of Antioquia near the city of Medellín and cross section B (Figures 2 and 3).

Our approach follows the concept of tectonic facies (Robertson, 1994), which integrates field and laboratory analysis to identify tectonostratigraphic associations, which can be used to recognize discrete tectonic settings and test their geological evolution.

To avoid repetition, we integrated both the published and the new data in a single section. The locations of the samples analyzed in this study are presented in Table 1, and the results from sandstone petrography of samples from the San Luis Sedimentites in Table 2.

3.1. Zircon U–Pb LA–ICP–MS Geochronology

After zircon separation using conventional techniques, including crushing, pulverization, water table, and heavy liquid gravity concentration, LA–ICP–MS U–Pb zircon analyses were obtained from 4 granitic rocks and 4 sandstone samples at the Washington State University Geoanalytical Lab, using a New Wave Nd:YAG UV 213–nm laser coupled to a Thermo Finnigan Element 2 single collector, double–focusing, magnetic sector ICP–MS following the analytical protocol of Chang *et al.* (2006). For this study, the Plešovice zircon was used as the main standard, which is characterized by a $^{238}\text{U}/^{206}\text{Pb}$ age of 337.13 ± 0.37 Ma (Sláma *et al.*, 2008). Common Pb represents a large proportion of the total Pb in Mesozoic and younger U–poor zircons. However, common Pb is typically not significant in LA–ICP–MS analyses, most likely because it is concentrated in cracks and inclusions, which can be avoided by appropriately selecting the crystals. When this is not possible, the influence of common Pb is easy to recognize on Tera–Wasserburg diagrams because analyses tend to line up on a steep linear trajectory that can be anchored at a reasonable $^{207}\text{Pb}/^{206}\text{Pb}$ common lead composition (y –intercept) (DeGraaff–Surplless *et al.*, 2002). Common Pb corrections were made on these analyses using the ^{207}Pb method (Williams, 1998). Uranium–lead ages were processed and calculated using Isoplot 4.15 (Ludwig, 2003). Analytical data from the detrital zircons are presented in Table 1, Supplementary Information, and data from the magmatic rocks are presented in Table 3.

3.2. Whole–Rock Geochemistry

Whole–rock geochemical analyses of five magmatic rocks from the Cretaceous Altavista Stock and San Diego Gabbro were conducted at the ALS Minerals Laboratories (the results are presented in Table 4).

After crushing, splitting, and pulverizing, an aliquot of 0.1 g is added to a $\text{LiBO}_2/\text{Li}_2\text{B}_4\text{O}_7$ flux, mixed and fused in a furnace

at 1000 °C. The resulting melt is then cooled and dissolved in 100 mL of 4% HNO_3 /2% HCl . This solution is then analyzed for major oxides by inductively coupled plasma atomic emission spectroscopy (ICP–AES), and the results are corrected for spectral interelement interferences. For trace and rare earth elements, an aliquot of 0.1 g is added to a $\text{LiBO}_2/\text{Li}_2\text{B}_4\text{O}_7$ flux (1.8 g), mixed and fused in a furnace at 1025 °C. The resulting melt is cooled and dissolved in a mixture containing HNO_3 , HCl , and HF . This solution is then analyzed by ICP–MS. Data handling, plotting, and interpretation are performed using the software GCD Toolkit 4.1 (Janoušek *et al.*, 2006).

3.3. Hafnium Isotopes

Hf isotope geochemistry was determined at the GeoAnalytical Lab of Washington State University using a Thermo Finnigan Neptune™ MC–ICP–MS equipped with 9 Faraday collectors interfaced with a New Wave™ 213 nm UP Nd–YAG laser. The results are presented in Table 5.

The laser was operated at a pulse rate of 10 Hz and a fluence of 10–12 J/cm². The laser spot size was 30 μm. The carrier gas consisted of purified He plus small quantities of N₂ to minimize oxide formation and increase Hf sensitivity. The total Hf signal achieved was between 2 and 6 V. The data were acquired in static mode with 60 s integrations. Details of the analytical procedures and data treatment were after (Vervoort *et al.*, 2004; Dufrane *et al.*, 2007). For the Hf–depleted mantle model ages (Hf TDM), we used $^{176}\text{Hf}/^{177}\text{Hf}$ and $^{176}\text{Lu}/^{177}\text{Hf}$ for the individual zircon samples to determine their initial $^{176}\text{Hf}/^{177}\text{Hf}$ ratios at their crystallization ages. Projection back from zircon crystallization was calculated using a present value of 0.0093 for $^{176}\text{Lu}/^{177}\text{Hf}$ in the crust (Vervoort & Patchett, 1996; Amelin *et al.*, 2002). The depleted mantle Hf evolution curve was calculated from present–day depleted mantle values of $^{176}\text{Hf}/^{177}\text{Hf}$ DM(0) = 0.283225 and $^{176}\text{Lu}/^{177}\text{Hf}$ DM(0) = 0.038512 (Vervoort & Blichert–Toft, 1999).

3.4. Oxygen Isotopes

Oxygen isotopes in zircon were analyzed using the CAMECA IMS 1280–HR ion microprobe at Heidelberg University. The procedures of multicollection analysis of oxygen isotopes (^{16}O and ^{18}O) using two Faraday cup (FC) detectors were similar to those presented in Trail *et al.* (2007) as modified by Schmitt *et al.* (2017).

A 2–3 nA Cs⁺ primary beam was focused to 10–15 μm using a focused beam rastered over 10 μm. FC backgrounds were recorded during an initial 30 s of presputtering and averaged over the duration of the analysis session. Mass fractionation was corrected by analyzing the 91 500 reference zircon in pairs with interspersed blocks of six unknowns (91500 $\delta^{18}\text{O}$ = +9.86‰; Wiedenbeck *et al.*, 2004; δ values are relative to Vien-

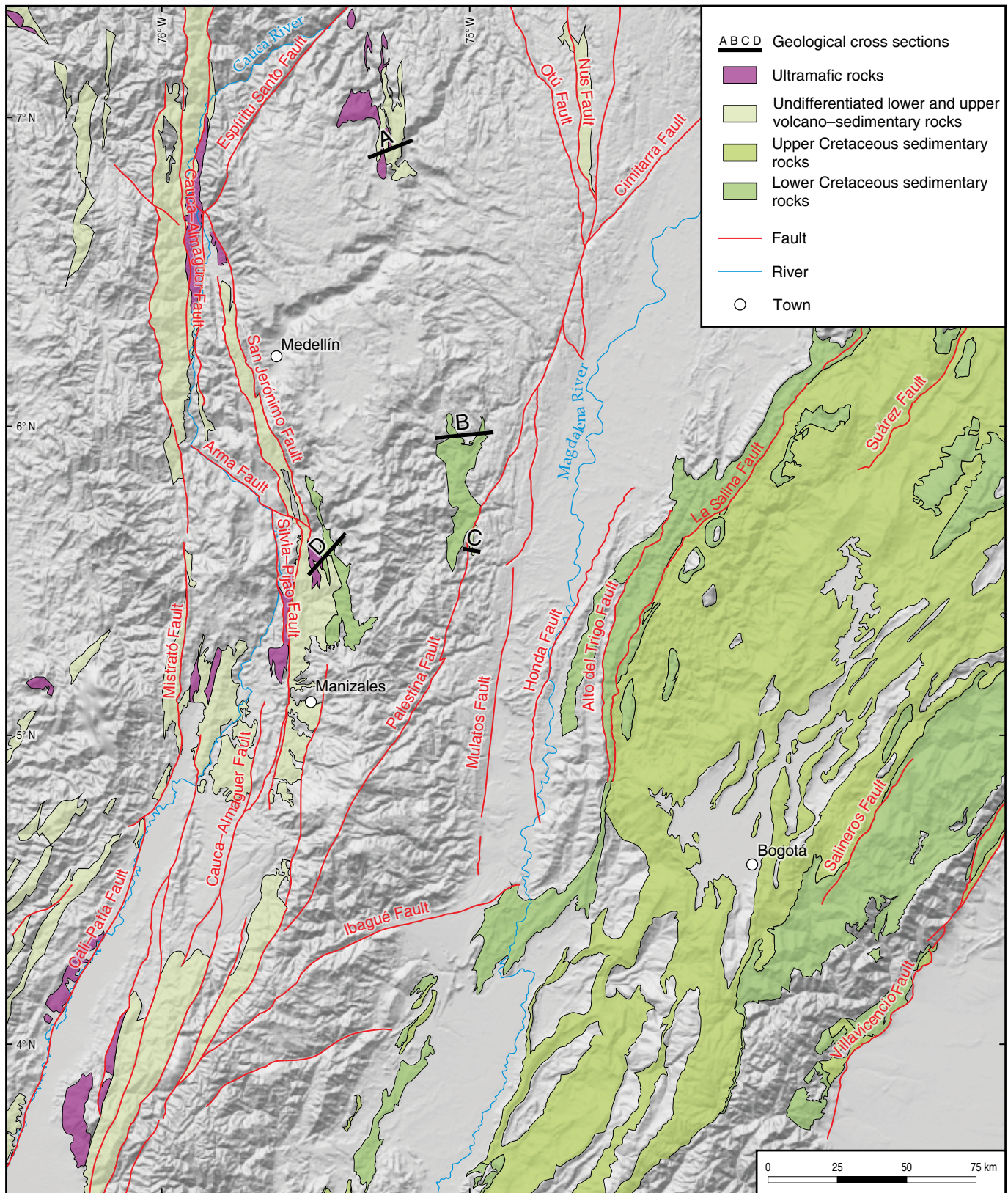


Figure 3. Distribution of Cretaceous rocks in the Colombian Andes (modified after Gómez et al., 2015). Geological cross sections A, B, C, and D are presented in Figure 4.

Table 1. Sample locations.

Sample code	N	W	Geologic unit	Lithology	Analysis
JCA-045	6.27423	-75.62193	Altavista Stock	Quartz monzonite	U-Pb LA-ICP-MS
JCA-046	6.22818	-75.56890	San Diego Gabbro	Gabbroic diorite	U-Pb LA-ICP-MS
DM-056	5.57991	-75.36080		Porphyry andesitic	U-Pb LA-ICP-MS and Hf
AG-01	6.01612	-74.94476	Antioquian Batholith	Quartz diorite	U-Pb LA-ICP-MS
QG-W-01	5.07222	-75.44886	Quebradagrande Complex	Sandstone	Detrital U-Pb LA-ICP-MS
MQA-4A	5.07197	-75.44895	Quebradagrande Complex	Quartz conglomerate	Detrital U-Pb LA-ICP-MS
JCA036	6.27423	-75.62193	Altavista Stock	Quartz diorite	Geochemistry
JCA037	6.27423	-75.62193	Altavista Stock	Gabbro	Geochemistry
JCA038	6.27423	-75.62193	Altavista Stock	Andesitic porphyry	Geochemistry
JCA043	6.22818	-75.56890	San Diego Gabbro	Gabbro	Geochemistry
DM-TM-084	5.99307	-75.03510	San Luis Sedimentites	Sandstone	Petrography
DM-TM-076	5.99593	-75.02480	San Luis Sedimentites	Sandstone	Petrography

Table 2. Petrographical results from the San Luis Sedimentites.

Sample	Qzm	Qzi	Qzmet	Ltmet	Ltsed	Pg	K
DM-TM-084	85	85	46	3	8	22	8
DM-TM-076	70	65	29	1	3	18	3

(Qzm) monocrystalline quartz; (Qzi) polycrystalline igneous quartz; (Qzmet) polycrystalline metamorphic quartz; (Ltmet) metamorphic lithic; (Ltsed) sedimentary lithic; (Pg) plagioclase; (K) alkaline feldspar.

na standard mean ocean water, VSMOW; $^{18}\text{O}/^{16}\text{O} = 0.0020052$; Baertschi, 1976). The reproducibility in $\delta^{18}\text{O}$ was 0.15‰ (1 standard deviation, $n = 24$). A secondary reference zircon FC1 ($\delta^{18}\text{O} = 5.4\text{‰}$; Ickert et al., 2008) was analyzed under the same conditions, and a $\delta^{18}\text{O}$ value of $5.56 \pm 0.15\text{‰}$ ($n = 6$) was obtained, attesting to the accuracy of the method within stated uncertainties.

4. Results

4.1. Review of the Early Cretaceous Sedimentary Record in the Central Cordillera and New Observations

Several discontinuous belts of fossiliferous siliciclastic Lower Cretaceous rocks are exposed along the axis and both flanks of the Central Cordillera (Figure 2). All of them are overlying Triassic or Jurassic schist and gneissic rocks that have been included in the Cajamarca Complex (Vinasco et al., 2006; Blanco-Quintero et al., 2014; Cochrane et al., 2014b; Bustamante et al., 2017; Rodríguez et al., 2018) and show local evidence of intense deformation by folding and faulting, as well as local low-grade metamorphic overprinting that formed slates and flattened metaconglomerates. In some segments of the cordil-

lera, the eastern and western belts are separated more than 50 km by the pre-Cretaceous metamorphic basement.

In the western flank of the Central Cordillera, between the Departments of Antioquia and Caldas, different names have been used to refer units with similar lithofacies, including the Abejorral Formation (González, 1980), the Aranzázu-Manizales Metasedimentary Complex (Lozano et al., 1975), the “Valle Alto”, “San Félix”, and “El Establo” units (Rodríguez & Rojas, 1985), and the “Eastern” interval near the city of Manizales (Gómez-Cruz et al., 1995).

These sequences include basal oligomictic quartzose conglomerates and coarse-grained sandstones with thicknesses between 40 and 240 m. Interlayered fine-grained sandstones, mudstones, siliceous mudstones, and chert with polymictic conglomerate beds overlie the coarse-grained units and may reach thicknesses between 160 and 1910 m. The greater stratigraphic thicknesses may be an artifact of repetition associated with the superimposed deformation (Figure 4). These units yield Berriasian to middle Albian fossil fauna and have been interpreted as transgressive successions that evolved from fluvial-deltaic to marine platform environments (Lozano et al., 1975; Etayo-Serna, 1985; Rodríguez & Rojas, 1985; Gómez-Cruz et al., 1995; Quiroz, 2005; Zapata et al., 2018). Magmatic activity associated with fine-grained facies has recently been recognized in the form of interlayered tuffs and dikes near the town of Abejorral (Antioquia), which suggests that sedimentation and volcanism were contemporaneous (Zapata et al., 2018). In this contribution, we report the presence of a porphyritic body that intrudes a sequence of mudstones and siltstones of the Abejorral Formation near the town of Salamina in the state Caldas Department.

Several segmented and deformed siliciclastic units also crop out along the eastern flank of the Central Cordillera approximately 50 km to the east and both north and south from the main exposures of the Abejorral Formation. These sequences trend N-S,

Table 3. U–Pb LA–ICP–MS geochronological results from the analyzed intrusive bodies (Altavista, San Diego, and Antioquia).

Department of the Environment, Washington State University		Isotopic ratios										Ages							
Sample	U (ppm)	Pb 207 Corrected					Non Corrected					206Pb/238U		207Pb/206Pb		Best age (Ma)	2σ Abs error (Ma)		
		U/Th	206Pb/238U	2σ Abs error	206Pb/238U	2σ Abs error	207Pb/206Pb	2σ Abs error	207Pb/206Pb	2σ Abs error	207Pb/206Pb	2σ Abs error	(Ma) (207 Corr)	(Ma)	(Ma)				
JCA-045_1	1241	0.3	0.10276	0.00468	0.01485	0.00046	0.825	67.1453	2.0541	0.0502	0.0013	99.3	4.3	95.0	2.9	203.7	30.5	95.0	2.9
JCA-045_2	1372	0.3	0.10170	0.00453	0.01521	0.00047	0.837	65.6973	2.0198	0.0485	0.0012	98.3	4.2	97.3	3.0	123.2	29.4	97.3	3.0
JCA-045_3	1014	0.4	0.10415	0.00485	0.01551	0.00050	0.828	64.4056	2.0550	0.0487	0.0013	100.6	4.5	99.2	3.2	133.2	31.3	99.2	3.2
JCA-045_4	1859	0.2	0.10669	0.00445	0.01512	0.00046	0.866	65.8769	1.9861	0.0512	0.0011	102.9	4.1	96.7	2.9	249.2	24.7	96.7	2.9
JCA-045_5	955	0.5	0.11109	0.00535	0.01517	0.00049	0.817	65.4894	2.1001	0.0531	0.0015	107.0	4.9	97.1	3.1	333.7	31.9	97.1	3.1
JCA-045_6	1132	0.3	0.10328	0.00463	0.01543	0.00047	0.833	64.7666	1.9875	0.0485	0.0012	99.8	4.3	98.7	3.0	126.1	30.0	98.7	3.0
JCA-045_7	1728	0.4	0.10264	0.00423	0.01530	0.00047	0.874	65.2928	1.9836	0.0486	0.0010	99.2	3.9	97.9	3.0	130.7	24.3	97.9	3.0
JCA-045_8	500	0.9	0.10600	0.00594	0.01594	0.00058	0.791	62.7350	2.2947	0.0482	0.0017	102.3	5.4	101.9	3.7	111.1	41.0	101.9	3.7
JCA-045_9	1530	0.3	0.10124	0.00471	0.01487	0.00045	0.811	67.1098	2.0367	0.0494	0.0014	97.9	4.3	95.2	2.9	165.2	32.6	95.2	2.9
JCA-045_10	2021	0.3	0.10001	0.00428	0.01504	0.00049	0.886	66.4656	2.1818	0.0482	0.0010	96.8	4.0	96.2	3.1	110.6	24.0	96.2	3.1
JCA-045_11	547	0.6	0.10732	0.00611	0.01544	0.00053	0.761	64.5841	2.1908	0.0504	0.0019	103.5	5.6	98.7	3.3	214.8	43.4	98.7	3.3
JCA-045_12	3223	0.2	0.10364	0.00416	0.01564	0.00047	0.880	63.9292	1.9038	0.0481	0.0010	100.1	3.8	100.1	3.0	102.1	23.3	100.1	3.0
JCA-045_13	3670	0.3	0.10383	0.00444	0.01532	0.00053	0.912	65.1954	2.2474	0.0492	0.0009	100.3	4.1	98.0	3.4	155.9	21.1	98.0	3.4
JCA-045_14	2536	0.3	0.09994	0.00414	0.01505	0.00047	0.887	66.4295	2.0951	0.0482	0.0010	96.7	3.8	96.3	3.0	107.3	23.3	96.3	3.0
JCA-045_15	3443	0.2	0.10148	0.00438	0.01513	0.00050	0.888	66.0270	2.1954	0.0486	0.0010	98.1	4.0	96.8	3.2	130.5	24.0	96.8	3.2
JCA-045_16	1667	0.4	0.10327	0.00440	0.01484	0.00047	0.869	67.1516	2.1007	0.0505	0.0011	99.8	4.0	95.0	3.0	216.2	25.1	95.0	3.0
JCA-045_17	1209	0.3	0.10833	0.00470	0.01608	0.00048	0.836	62.1391	1.8396	0.0489	0.0012	104.4	4.3	102.8	3.0	141.7	28.7	102.8	3.0
JCA-045_18	882	0.4	0.10116	0.00544	0.01490	0.00059	0.848	67.0016	2.6686	0.0492	0.0014	97.8	5.0	95.3	3.8	159.4	33.6	95.3	3.8
JCA-045_19	426	0.7	0.10443	0.00546	0.01477	0.00049	0.790	67.4305	2.2382	0.0513	0.0017	100.9	5.0	94.5	3.1	254.1	37.3	94.5	3.1
JCA-045_20	459	1.1	0.10569	0.00574	0.01484	0.00050	0.778	67.0791	2.2567	0.0517	0.0018	102.0	5.3	94.9	3.2	270.6	39.7	94.9	3.2
JCA-046_1	1085	0.4	0.10397	0.00540	0.01543	0.00048	0.772	64.7219	2.0253	0.0489	0.0017	100.4	5.0	98.7	3.1	141.0	39.5	98.7	3.1
JCA-046_2	1282	0.4	0.10477	0.00490	0.01576	0.00051	0.828	63.4334	2.0321	0.0482	0.0013	101.2	4.5	100.8	3.2	109.7	31.7	100.8	3.2
JCA-046_3	1354	0.6	0.10514	0.00492	0.01541	0.00052	0.847	64.7781	2.1739	0.0495	0.0013	101.5	4.5	98.6	3.3	171.1	29.6	98.6	3.3
JCA-046_4	605	1.1	0.10372	0.00560	0.01523	0.00054	0.796	65.5443	2.3173	0.0494	0.0017	100.2	5.1	97.4	3.4	166.7	38.7	97.4	3.4
JCA-046_5	1829	0.3	0.14750	0.00705	0.01472	0.00054	0.876	65.7814	2.3297	0.0727	0.0017	139.7	6.2	94.2	3.3	1004.7	23.1	94.2	3.3
JCA-046_6	367	1.1	0.18299	0.01245	0.01472	0.00062	0.763	64.2634	2.5666	0.0901	0.0038	170.6	10.6	94.2	3.8	1428.6	40.1	94.2	3.8
JCA-046_7	401	0.8	0.12206	0.00751	0.01558	0.00063	0.786	63.4533	2.5255	0.0568	0.0022	116.9	6.8	99.7	4.0	484.2	41.9	99.7	4.0
JCA-046_8	2132	0.3	0.09888	0.00443	0.01493	0.00051	0.878	66.9584	2.2837	0.0480	0.0011	95.7	4.1	95.6	3.2	100.4	25.9	95.6	3.2
JCA-046_9	893	0.7	0.10581	0.00565	0.01527	0.00056	0.815	65.2950	2.3863	0.0503	0.0016	102.1	5.2	97.7	3.6	206.9	36.3	97.7	3.6
JCA-046_10	486	0.7	0.10092	0.00595	0.01545	0.00050	0.734	64.7761	2.1005	0.0474	0.0020	97.6	5.5	98.8	3.2	68.1	48.7	98.8	3.2
JCA-046_11	511	0.5	0.11094	0.00583	0.01570	0.00052	0.783	63.4248	2.0749	0.0512	0.0017	106.8	5.3	100.4	3.3	251.8	38.2	100.4	3.3

Table 3. U–Pb LA–ICP–MS geochronological results from the analyzed intrusive bodies (Altavista, San Diego, and Antioquia) (continued).

		Isotopic ratios										Ages							
		Pb 207 Corrected					Non Corrected												
Sample	U (ppm)	U/Th	²⁰⁷ Pb/ ²⁰⁶ Pb	2σ Abs error	²⁰⁶ Pb/ ²³⁸ U	2s Abs error	Corr. Coef.	²³⁵ U/ ²³⁸ U	2σ Abs error	²⁰⁷ Pb/ ²⁰⁶ Pb	2σ Abs error	²⁰⁶ Pb/ ²³⁸ U	2σ Abs error	Best age	2σ Abs error				
Name														(Ma)	(Ma)				
														(Ma) (207 Corr)	(Ma)				
JCA-046_12	515	0.7	0.10312	0.00566	0.01526	0.00052	0.774	65.4367	2.2113	0.0490	0.0018	99.7	5.2	97.6	3.3	148.1	41.4	97.6	3.3
JCA-046_13	930	0.6	0.10398	0.00475	0.01563	0.00049	0.832	63.9668	2.0123	0.0483	0.0013	100.4	4.4	100.0	3.1	111.8	30.6	100.0	3.1
JCA-046_14	460	0.9	0.10374	0.00561	0.01565	0.00055	0.791	63.8983	2.2340	0.0481	0.0016	100.2	5.2	100.1	3.5	103.1	39.7	100.1	3.5
JCA-046_15	1224	0.5	0.09936	0.00449	0.01500	0.00046	0.830	66.6674	2.0542	0.0480	0.0013	96.2	4.1	96.0	2.9	101.6	30.5	96.0	2.9
JCA-046_16	480	0.7	0.10477	0.00562	0.01465	0.00052	0.803	67.9338	2.4174	0.0519	0.0017	101.2	5.2	93.7	3.3	280.5	36.9	93.7	3.3
JCA-046_17	3108	0.3	0.10236	0.00410	0.01542	0.00047	0.895	64.8489	1.9930	0.0482	0.0009	99.0	3.8	98.6	3.0	106.9	21.8	98.6	3.0
JCA-046_18	1161	0.7	0.10237	0.00465	0.01547	0.00050	0.849	64.6331	2.1068	0.0480	0.0012	99.0	4.3	99.0	3.2	98.6	29.0	99.0	3.2
JCA-046_19	999	0.7	0.10153	0.00461	0.01539	0.00049	0.839	64.9936	2.0676	0.0478	0.0012	98.2	4.2	98.4	3.1	91.8	30.0	98.4	3.1
JCA-046_20	1029	0.6	0.10785	0.00556	0.01545	0.00058	0.843	64.5014	2.4115	0.0506	0.0014	104.0	5.1	98.8	3.7	223.7	32.4	98.8	3.7
AG-01_1	442	0.3	0.09151	0.00519	0.01388	0.00047	0.758	72.0371	2.4205	0.0478	0.0018	88.9	4.8	88.9	3.0	89.9	44.6	88.9	3.0
AG-01_2	955	0.3	0.09564	0.00484	0.01408	0.00045	0.791	70.8804	2.2699	0.0493	0.0016	92.7	4.5	90.1	2.9	160.1	36.9	90.1	2.9
AG-01_3	310	0.3	0.09829	0.00622	0.01405	0.00051	0.743	70.9108	2.5870	0.0507	0.0022	95.2	5.7	89.9	3.3	228.9	49.4	89.9	3.3
AG-01_4	422	0.3	0.12867	0.01543	0.01277	0.00050	0.650	75.7602	2.8662	0.0731	0.0070	122.9	13.8	81.8	3.2	1015.8	94.2	81.8	3.2
AG-01_5	279	0.3	0.20064	0.02189	0.01352	0.00071	0.675	68.3075	3.3098	0.1076	0.0083	185.7	18.2	86.6	4.3	1759.5	68.7	86.6	4.3
AG-01_6	360	0.3	0.09565	0.00600	0.01397	0.00051	0.746	71.4332	2.6114	0.0497	0.0021	92.7	5.6	89.4	3.3	179.6	49.3	89.4	3.3
AG-01_7	301	0.3	0.09530	0.00631	0.01439	0.00051	0.721	69.4940	2.4824	0.0480	0.0023	92.4	5.8	92.1	3.3	101.6	55.1	92.1	3.3
AG-01_8	629	0.3	0.10049	0.00647	0.01377	0.00054	0.759	72.1494	2.8303	0.0529	0.0023	97.2	6.0	88.2	3.5	325.9	47.7	88.2	3.5
AG-01_9	231	0.3	0.09640	0.00678	0.01398	0.00055	0.729	71.3235	2.8221	0.0500	0.0025	93.5	6.3	89.5	3.5	195.4	56.4	89.5	3.5
AG-01_10	388	0.3	0.09013	0.00553	0.01405	0.00050	0.743	71.2944	2.5173	0.0465	0.0020	87.6	5.1	89.9	3.2	25.0	50.2	89.9	3.2
AG-01_11	317	0.3	0.10078	0.00728	0.01428	0.00057	0.720	69.7401	2.7550	0.0512	0.0026	97.5	6.7	91.4	3.6	249.5	58.2	91.4	3.6
AG-01_12	435	0.3	0.09130	0.00542	0.01397	0.00049	0.755	71.6075	2.5232	0.0474	0.0019	88.7	5.0	89.4	3.1	69.1	47.1	89.4	3.1
AG-01_13	375	0.3	0.10117	0.00734	0.01376	0.00050	0.700	72.1606	2.6214	0.0533	0.0028	97.9	6.8	88.1	3.2	342.7	59.3	88.1	3.2
AG-01_14	542	0.4	0.09123	0.00595	0.01363	0.00063	0.817	73.2973	3.4070	0.0485	0.0019	88.6	5.5	87.3	4.0	125.9	44.4	87.3	4.0
AG-01_15	677	0.3	0.09247	0.00466	0.01390	0.00044	0.791	71.8793	2.2939	0.0482	0.0015	89.8	4.3	89.0	2.8	110.8	37.1	89.0	2.8
AG-01_16	631	0.3	0.09657	0.00531	0.01458	0.00050	0.777	68.5634	2.3473	0.0480	0.0017	93.6	4.9	93.3	3.2	100.8	41.6	93.3	3.2
AG-01_17	436	0.2	0.09206	0.00583	0.01358	0.00050	0.746	73.5011	2.7205	0.0492	0.0021	89.4	5.4	87.0	3.2	155.7	49.9	87.0	3.2
AG-01_18	388	0.2	0.09041	0.00579	0.01379	0.00051	0.743	72.5375	2.7009	0.0475	0.0021	87.9	5.4	88.3	3.3	76.9	51.6	88.3	3.3
AG-01_19	595	0.3	0.10576	0.00633	0.01413	0.00056	0.791	70.2030	2.7475	0.0543	0.0020	102.1	5.8	90.4	3.5	383.4	41.2	90.4	3.5
AG-01_20	554	0.3	0.09369	0.00622	0.01413	0.00066	0.807	70.7667	3.2861	0.0481	0.0019	90.9	5.8	90.4	4.2	104.3	46.4	90.4	4.2
AG-01_21	553	0.4	0.09683	0.00481	0.01458	0.00046	0.794	68.5701	2.1676	0.0482	0.0015	93.8	4.4	93.3	2.9	107.7	36.4	93.3	2.9

Table 3. U–Pb LA–ICP–MS geochronological results from the analyzed intrusive bodies (Altavista, San Diego, and Antioquia) (continued).

Department of the Environment, Washington State University		Isotopic ratios										Ages							
Sample	U (ppm)	U/Th	$^{207}\text{Pb}/^{235}\text{U}$ Corrected	$^{207}\text{Pb}/^{238}\text{U}$ 2 σ Abs error	$^{206}\text{Pb}/^{238}\text{U}$ 2 σ Abs error	Corr. Coef.	$^{28}\text{U}/^{235}\text{Pb}$ Non Corrected	$^{207}\text{Pb}/^{206}\text{Pb}$ 2 σ Abs error	$^{207}\text{Pb}/^{206}\text{Pb}$ 2 σ Abs error	$^{207}\text{Pb}/^{206}\text{Pb}$ 2 σ Abs error	$^{207}\text{Pb}/^{206}\text{Pb}$ (Ma) (207 Corr)	$^{206}\text{Pb}/^{238}\text{U}$ 2 σ Abs error	$^{206}\text{Pb}/^{238}\text{U}$ 2 σ Abs error	$^{206}\text{Pb}/^{238}\text{U}$ 2 σ Abs error	Best age	2 σ Abs error			
																	(Ma)	(Ma)	(Ma)
DM-056_1	100	1.8	0.09562	0.00907	0.01527	0.00071	0.724	65.7082	3.0561	0.0454	0.0032	92.7	8.4	97.7	4.5	0.0	49.1	97.7	4.5
DM-056_2	290	1.0	0.09663	0.00605	0.01516	0.00051	0.779	66.0890	2.2307	0.0462	0.0019	93.7	5.6	97.0	3.3	8.7	49.9	97.0	3.3
DM-056_3	189	1.3	0.10458	0.00668	0.01544	0.00056	0.785	64.6646	2.3241	0.0491	0.0021	101.0	6.1	98.8	3.5	153.5	48.4	98.8	3.5
DM-056_4	152	1.0	0.12042	0.01383	0.01464	0.00068	0.700	67.2831	3.0872	0.0597	0.0052	115.5	12.5	93.7	4.3	591.2	92.0	93.7	4.3
DM-056_5	135	1.2	0.09890	0.00820	0.01508	0.00078	0.786	66.3443	3.4457	0.0476	0.0025	95.8	7.6	96.5	5.0	77.7	61.8	96.5	5.0
DM-056_6	100	1.4	0.10365	0.00988	0.01532	0.00069	0.719	65.1730	2.9118	0.0491	0.0034	100.1	9.1	98.0	4.4	150.8	80.3	98.0	4.4
DM-056_7	106	1.8	0.10589	0.00909	0.01507	0.00063	0.732	66.1030	2.7610	0.0510	0.0032	102.2	8.3	96.4	4.0	239.0	69.9	96.4	4.0
DM-056_8	94	1.6	0.10229	0.01370	0.01542	0.00084	0.692	64.8431	3.5524	0.0481	0.0050	98.9	12.6	98.6	5.4	104.9	118.3	98.6	5.4
DM-056_9	121	1.8	0.10199	0.00879	0.01526	0.00066	0.735	65.4732	2.8372	0.0485	0.0030	98.6	8.1	97.7	4.2	121.8	71.1	97.7	4.2
DM-056_10	109	1.1	0.10138	0.00933	0.01547	0.00077	0.742	64.6707	3.2182	0.0475	0.0031	98.0	8.6	99.0	4.9	75.4	74.9	99.0	4.9
DM-056_11	109	1.6	0.10275	0.00990	0.01549	0.00085	0.750	64.5614	3.5290	0.0481	0.0032	99.3	9.1	99.1	5.4	105.1	76.3	99.1	5.4
DM-056_12	214	1.2	0.10310	0.00831	0.01480	0.00077	0.798	67.3376	3.4976	0.0505	0.0025	99.6	7.6	94.7	4.9	218.9	56.8	94.7	4.9
DM-056_13	110	1.7	0.10926	0.00969	0.01561	0.00078	0.754	63.8484	3.1824	0.0508	0.0031	105.3	8.8	99.8	5.0	230.5	68.3	99.8	5.0
DM-056_14	136	1.5	0.09880	0.00851	0.01537	0.00078	0.766	65.1912	3.3105	0.0466	0.0027	95.7	7.9	98.3	5.0	30.6	67.6	98.3	5.0
DM-056_15	104	1.5	0.10388	0.01254	0.01537	0.00117	0.771	64.9912	4.9583	0.0490	0.0039	100.4	11.5	98.3	7.5	149.3	89.6	98.3	7.5
DM-056_16	138	1.7	0.09700	0.00831	0.01535	0.00080	0.775	65.3406	3.4102	0.0458	0.0026	94.0	7.7	98.2	5.1	0.0	56.0	98.2	5.1
DM-056_17	110	1.6	0.10746	0.00906	0.01504	0.00059	0.729	66.1518	2.5977	0.0518	0.0032	103.6	8.3	96.2	3.8	277.2	68.9	96.2	3.8
DM-056_18	95	2.1	0.10809	0.00958	0.01490	0.00060	0.723	66.7323	2.6817	0.0526	0.0034	104.2	8.8	95.3	3.8	312.9	72.6	95.3	3.8
DM-056_19	98	1.3	0.10098	0.00929	0.01542	0.00070	0.728	64.8919	2.9543	0.0475	0.0032	97.7	8.5	98.6	4.5	74.1	77.4	98.6	4.5
DM-056_20	146	0.6	0.10435	0.00776	0.01551	0.00065	0.769	64.4212	2.7079	0.0488	0.0024	100.8	7.1	99.2	4.2	138.6	57.5	99.2	4.2
DM-056_21	108	1.6	0.09602	0.00734	0.01516	0.00064	0.760	66.1276	2.7911	0.0459	0.0024	93.1	6.8	97.0	4.1	0.4	55.7	97.0	4.1
DM-056_22	97	1.6	0.10395	0.00916	0.01493	0.00067	0.735	66.7764	2.9791	0.0505	0.0032	100.4	8.4	95.5	4.3	218.5	71.2	95.5	4.3
DM-056_23	66	2.4	0.09748	0.01054	0.01503	0.00078	0.713	66.6121	3.4411	0.0470	0.0038	94.4	9.7	96.2	5.0	51.2	92.9	96.2	5.0
DM-056_24	174	2.0	0.10609	0.00805	0.01514	0.00056	0.744	65.8070	2.4430	0.0508	0.0027	102.4	7.4	96.9	3.6	232.6	61.2	96.9	3.6
DM-056_25	190	1.3	0.10585	0.00746	0.01497	0.00054	0.756	66.4981	2.3692	0.0513	0.0025	102.2	6.8	95.8	3.4	252.9	55.6	95.8	3.4
DM-056_26	113	2.1	0.10162	0.00768	0.01508	0.00058	0.748	66.2409	2.5293	0.0489	0.0026	98.3	7.1	96.5	3.7	142.1	61.4	96.5	3.7
DM-056_27	141	1.7	0.10283	0.00900	0.01499	0.00070	0.742	66.5727	3.0824	0.0498	0.0031	99.4	8.3	95.9	4.4	184.1	70.0	95.9	4.4
DM-056_28	93	2.0	0.11843	0.01050	0.01566	0.00072	0.738	63.2963	2.8963	0.0548	0.0034	113.6	9.5	100.2	4.6	406.0	68.3	100.2	4.6
DM-056_29	121	1.5	0.10360	0.00830	0.01505	0.00059	0.738	66.2812	2.5859	0.0499	0.0029	100.1	7.6	96.3	3.8	191.6	65.6	96.3	3.8
DM-056_30	104	1.8	0.09789	0.00820	0.01522	0.00060	0.730	65.8208	2.6156	0.0467	0.0029	94.8	7.6	97.4	3.9	31.4	71.9	97.4	3.9
DM-056_31	94	2.0	0.09949	0.00934	0.01585	0.00071	0.721	63.2773	2.8272	0.0455	0.0032	96.3	8.6	101.4	4.5	0.0	53.7	101.4	4.5

Table 4. Whole-rock geochemistry from the Altavista and San Diego Plutons.

Sample	JCA036	JCA037	JCA038	JCA043
Rock type	Quartz diorite	Gabbro	Andesitic porphyry	Gabbro
Unit	Altavista	Altavista	Altavista	San Diego
SiO ₂	67.4	63.9	56.9	54.6
Al ₂ O ₃	16.8	15.6	15.8	16.15
Fe ₂ O ₃	4.12	5.36	6.71	7.19
MgO	0.83	2.67	3.42	5.93
CaO	2.87	5.23	7.48	9.36
Na ₂ O	6.51	5.48	2.99	3.73
K ₂ O	1.59	0.67	0.8	0.43
TiO ₂	0.51	0.92	0.76	0.85
P ₂ O ₅	0.15	0.2	0.23	0.12
MnO	0.06	0.14	0.15	0.14
Cr ₂ O ₃		0.01	0.01	0.01
Ni	0	0	0	0
Sc	0	0	0	0
LOI	0.36	0.44	4.5	1.03
Sum	101.28	100.67	99.85	99.59
Cr	30	60	60	100
Pb				
Ba	487	193.5	356	169.5
Co	0	0	0	0
Cs	2.05	1.25	0.59	0.49
Ga	21.2	18.9	18.2	14.7
Hf	8.4	4	3.4	2.7
Nb	10.6	14.4	4.3	5
Rb	48.6	27.8	18.1	9.4
Sn	3	3	2	2
Sr	243	240	493	289
Ta	0.6	0.9	0.3	0.3
Th	4.42	3.26	1.64	1.41
U	1.99	1.39	0.73	0.47
V	87	95	148	172
W	1	1	1	1
Zr	406	168	122	98
Y	25	37.2	21	22
La	21.2	14.4	10.3	8.5
Ce	43.3	37.7	23.4	21.2
Pr	4.96	4.98	3.23	2.93
Nd	18.3	20.9	14.1	13.3
Sm	4.02	4.87	3.02	3.23
Eu	1.31	1.21	1	1.28
Gd	4.28	5.64	3.68	4.13
Tb	0.65	0.9	0.63	0.75

Table 4. Whole-rock geochemistry from the Altavista and San Diego Plutons (*continued*).

Sample	JCA036	JCA037	JCA038	JCA043
Rock type	Quartz diorite	Gabbro	Andesitic porphyry	Gabbro
Unit	Altavista	Altavista	Altavista	San Diego
Dy	3.82	6.11	3.44	4.35
Ho	0.9	1.28	0.73	0.8
Er	2.66	4.13	2.42	2.4
Tm	0.41	0.62	0.32	0.35
Yb	2.96	4.67	2.18	2.27
Lu	0.49	0.62	0.36	0.39
Rb/Sr	0.20	0.12	0.04	0.03
Sr/Y	9.72	6.45	23.48	13.14
Sr/Y thickness	18.84	15.21	34.11	22.63

have received different lithostratigraphic names (e.g., San Luis, Amalfi, and Berlin Sedimentites, and the San Pablo and La Soledad Formations), overlie Triassic and older metamorphic rocks of the Cajamarca Complex, and are also intruded by Upper Cretaceous plutons (Feininger et al., 1972; Hall et al., 1972; Barrero & Vesga, 1976; Naranjo, 1983). The fossil content of mudstones from these units suggests Valanginian to Aptian – Albian accumulation ages. Although precise stratigraphic analysis from these units is still missing, cartographic and field observations indicate that they are represented by fining-upward sequences in which coarse-grained conglomeratic and sandstone levels are overlain by upper fine-grained siliciclastic facies associations.

The coarse-grained association includes intercalations of sandstones and conglomerates, which in the San Luis Sedimentites are characterized by thicknesses of a few centimeters to hundreds of meters (Feininger et al., 1972). Sandstones are mainly quartzose in composition, whereas conglomerates include oligomictic (white quartz and chert) or polymictic conglomerates that may include metavolcanic, schist, and/or gabbroic clasts in the San Luis Sedimentites, as well as in the San Pablo Formation and the Berlin Sedimentites (Feininger et al., 1972; Hall et al., 1972; Naranjo, 1983). The quartzose conglomerates have been reported overlying the metamorphic basement (Feininger et al., 1972; Hall et al., 1972; Naranjo, 1983; Pimiento, 2011).

The fine-grained facies include mostly fossiliferous Lower Cretaceous black shales (up to 80%; see review in González, 2001) intercalated with chert, siltstones, graywackes, and intraformational conglomerates with shale and sandstone fragments, which may reach thicknesses of 600–1000 m (Feininger et al., 1972; Hall et al., 1972; Gómez & Lizcano, 1990). Significant variations and lateral differences in the stratigraphic thickness between distinct localities is a commonly reported feature. The La Soledad Formation, which is one of the northern expressions

Table 5. Hf isotope results for zircons from the Aguadas porphyritic unit.

Sample	measured		corrected		2SE	¹⁷⁶ Lu/ ¹⁷⁷ Hf	2SE	¹⁷⁶ Yb/ ¹⁷⁷ Hf	2SE	¹⁷⁸ Hf/ ¹⁷⁷ Hf	2SE	¹⁸⁰ Hf/ ¹⁷⁷ Hf	2SE	Total Hf beam	Age	¹⁷⁶ Hf/ ¹⁷⁷ Hf _i	EHf0	2SE	EHf _i
	¹⁷⁶ Hf/ ¹⁷⁷ Hf	¹⁷⁶ Hf/ ¹⁷⁷ Hf	2SE	¹⁷⁶ Lu/ ¹⁷⁷ Hf															
DM56_1	0.282958	0.2830121	0.000036	0.002089	0.000067	0.0504	0.0018	1.467149	0.000041	1.88694	0.0001	14.5	94.4	0.283008412	8.0	1.3	10.0		
DM56_2	0.282949	0.2830031	0.00003	0.001171	0.000018	0.0263	0.0004	1.467186	0.000042	1.887079	0.000091	16.44	97.2	0.283000967	7.7	1.1	9.8		
DM56_3	0.282937	0.2829911	0.000026	0.000881	0.000039	0.01948	0.00082	1.46717	0.000033	1.887001	0.000084	17.68	98.7	0.282989468	7.3	0.9	9.4		
DM56_4	0.282966	0.2830201	0.000026	0.001068	0.00005	0.0232	0.001	1.467173	0.000032	1.88699	0.00011	17.41	93.9	0.283018224	8.3	0.9	10.3		
DM56_5	0.283019	0.2830731	0.000028	0.00319	0.00025	0.0805	0.0064	1.467178	0.000031	1.887	0.000082	14.78	99.0	0.283067207	10.2	1.0	12.2		
DM56_6	0.282946	0.2830001	0.000033	0.001426	0.000071	0.0336	0.0017	1.467165	0.000037	1.88695	0.000081	18.13	98.0	0.282997483	7.6	1.2	9.7		
DM56_7	0.282946	0.2830001	0.000025	0.001099	0.000022	0.02485	0.00048	1.467187	0.000035	1.886991	0.000081	15.49	98.5	0.282998071	7.6	0.9	9.7		
DM56_8	0.282928	0.2829821	0.000024	0.001542	0.000048	0.037	0.0014	1.467171	0.000035	1.88695	0.000071	15.9	97.2	0.282979289	7.0	0.8	9.0		
DM56_9	0.282965	0.2830191	0.000036	0.00128	0.000093	0.0306	0.0021	1.467153	0.000042	1.88694	0.00012	18.56	96.2	0.283016797	8.3	1.3	10.3		
DM56_10	0.282955	0.2830091	0.000029	0.001196	0.000021	0.02749	0.00065	1.467133	0.000031	1.887	0.00011	16.33	99.6	0.283006687	7.9	1.0	10.1		
DM56_11	0.282972	0.2830261	0.00003	0.00195	0.00024	0.0476	0.0061	1.467147	0.000032	1.886874	0.000095	15.13	97.2	0.283022557	8.5	1.1	10.6		
DM56_12	0.282974	0.2830281	0.000023	0.00176	0.00012	0.0406	0.0029	1.467179	0.000034	1.886947	0.000084	16.97	97.2	0.283024902	8.6	0.8	10.6		
DM56_13	0.282982	0.2830361	0.000032	0.001103	0.000059	0.0243	0.0013	1.46714	0.000031	1.886876	0.00009	17.18	97.2	0.283034097	8.9	1.1	11.0		

of the Lower Cretaceous sedimentites of the Central Cordillera, presents interlayered spilitized basaltic lava flows at its top, which include embedded fragments of the host sedimentary rocks (Hall et al., 1972).

All the units described above are intruded by Upper Cretaceous granodioritic to quartz dioritic rocks, which are part of the composite Antioquian Batholith with a protracted magmatic history spanning from 97 Ma to 84 Ma (Figures 2, 3; Ibañez-Mejía et al., 2007; Leal-Mejía, 2011; Villagómez et al., 2011; Duque-Trujillo et al., 2018). Our new field and petrographic observations of the San Luis Sedimentites, together with similar published results in the same unit as well as in the La Soledad Formation and Berlin Sedimentites (Feininger et al., 1972; Hall et al., 1972), have shown that granitoid bodies intrude formerly folded and foliated low-grade Lower Cretaceous metasedimentary rocks (Figure 4), producing an undeformed thermal aureole. In the San Luis Sedimentites, petrographic observations of andalusite porphyroblasts and mica needles cut the schistose fabric defined by the orientation of white mica and suggest that contact metamorphism reached the hornblende-hornfels facies.

Field observations in the Abejorral Formation and in the San Luis Sedimentites near the towns of Aguadas and San Luis, as well as previously published maps and reports from correlatable units (Zapata et al., 2018), show that all of these rocks are characterized by the presence of asymmetric folding with relatively steep limbs and are commonly faulted against the metamorphic basement (Figure 4).

West of the Abejorral Formation, in the western flank of the Central Cordillera, a series of Cretaceous siliciclastic sequences crops out and is characterized by interlayered fine-grained sandstones and mudstones with volcanic (pyroclastic and effusive) rocks (Gómez-Cruz et al., 1995; Tamayo & Correa, 2010; Zapata et al., 2018). These sequences are

often exclusively composed of volcanic rocks with basaltic composition, including pillow lavas, and are locally associated with gabbroic bodies and highly deformed serpentized peridotites, which have been included in the Quebradagrande Complex and/or the Cauca Ophiolitic Complex (González, 1980, 2001; Álvarez, 1987; Rodríguez & Cetina, 2016; Zapata et al., 2018).

4.2. Sandstone Petrography

Quantitative published petrographic data from the Abejorral Formation and Quebradagrande Complex were reviewed (Quiroz, 2005; Tamayo & Correa, 2010; Zapata et al., 2018), together with two newly analyzed samples from the San Luis Sedimentites. Additionally, qualitative descriptions were revised in order to assess the compositional character and provenance of the Lower Cretaceous sedimentary units exposed in the Central Cordillera of Colombia. Both the Folk (1974) and Garzanti (2016) classification and provenance diagrams were used to analyze sandstone compositions.

Sandstones from the Abejorral Formation and the upper segment of the Valle Alto Formation are medium- to coarse-grained, with angular to subangular and low-sphericity particles dominantly composed of monocrystalline and polycrystalline quartz and metamorphic lithic fragments, with minor muscovite and sedimentary lithic fragments (Gómez-Cruz et al., 1995; Quiroz, 2005; Tamayo & Correa, 2010; Zapata et al., 2018). In the QFL diagram of Folk (1974), samples plot within the litharenite, sublitharenite, and quartzarenite fields, whereas in the tectonic discrimination diagram of Garzanti (2016), they plot within the recycled orogen and continental block fields (Figure 5).

The Lower Cretaceous sandstones included in the Quebradagrande Complex and the upper Abejorral segment include

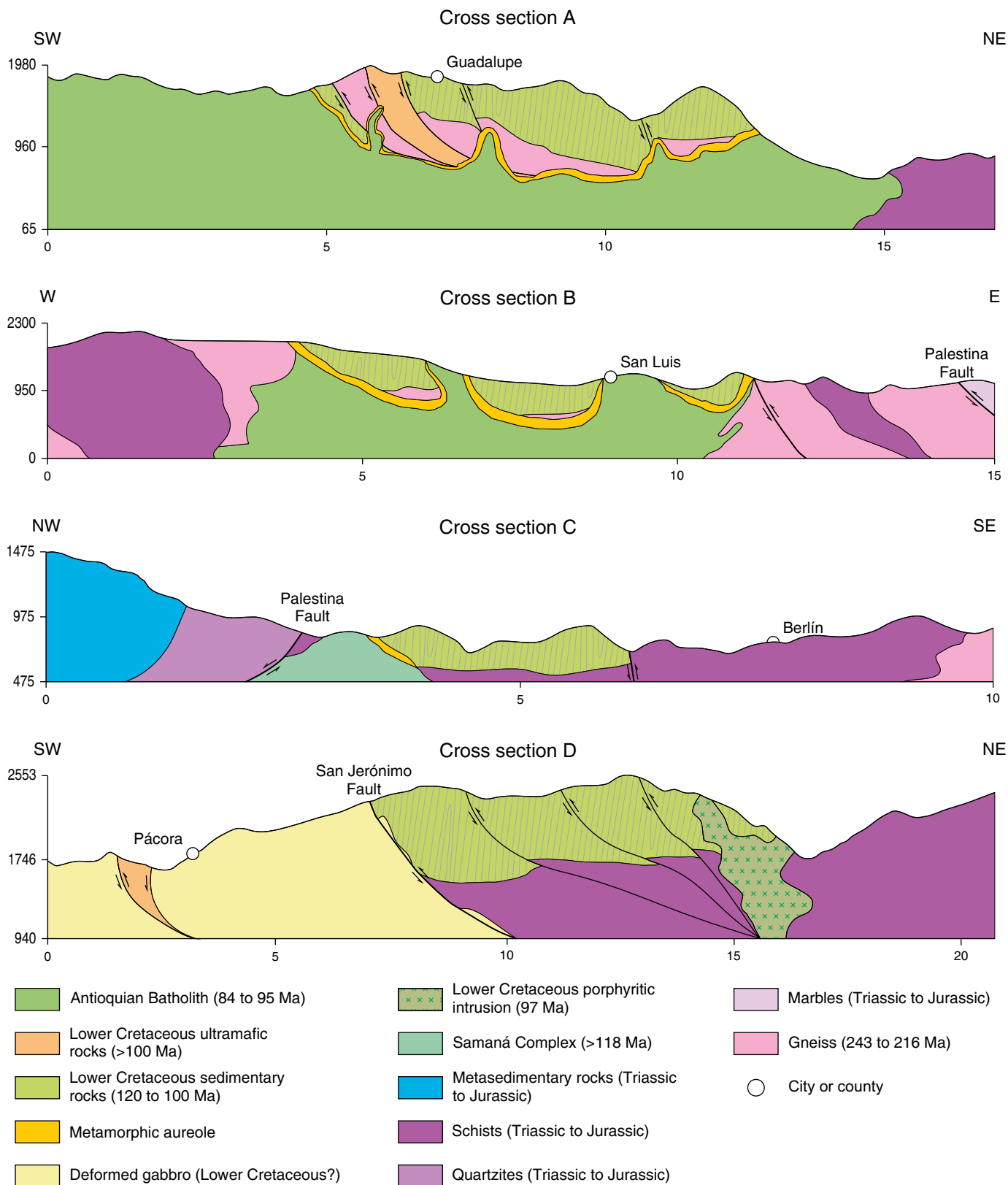


Figure 4. Geological cross sections from the Lower Cretaceous units showing the relation between deformation and magmatic intrusions. The cross-section locations are given in Figure 2. Cross section A includes the San Pablo Formation in the northern segment of the Central Cordillera (after Álvarez et al., 1975). Cross section B includes the San Luis Sedimentites in the eastern segment of the Central Cordillera (new field data, after Feininger et al., 1972). Cross section C includes the Berlin Sedimentites on the eastern flank of the Central Cordillera (after Barrero & Vesga, 1976). Cross section D includes the Abejorral Formation on the western flank of the Central Cordillera (new field data).

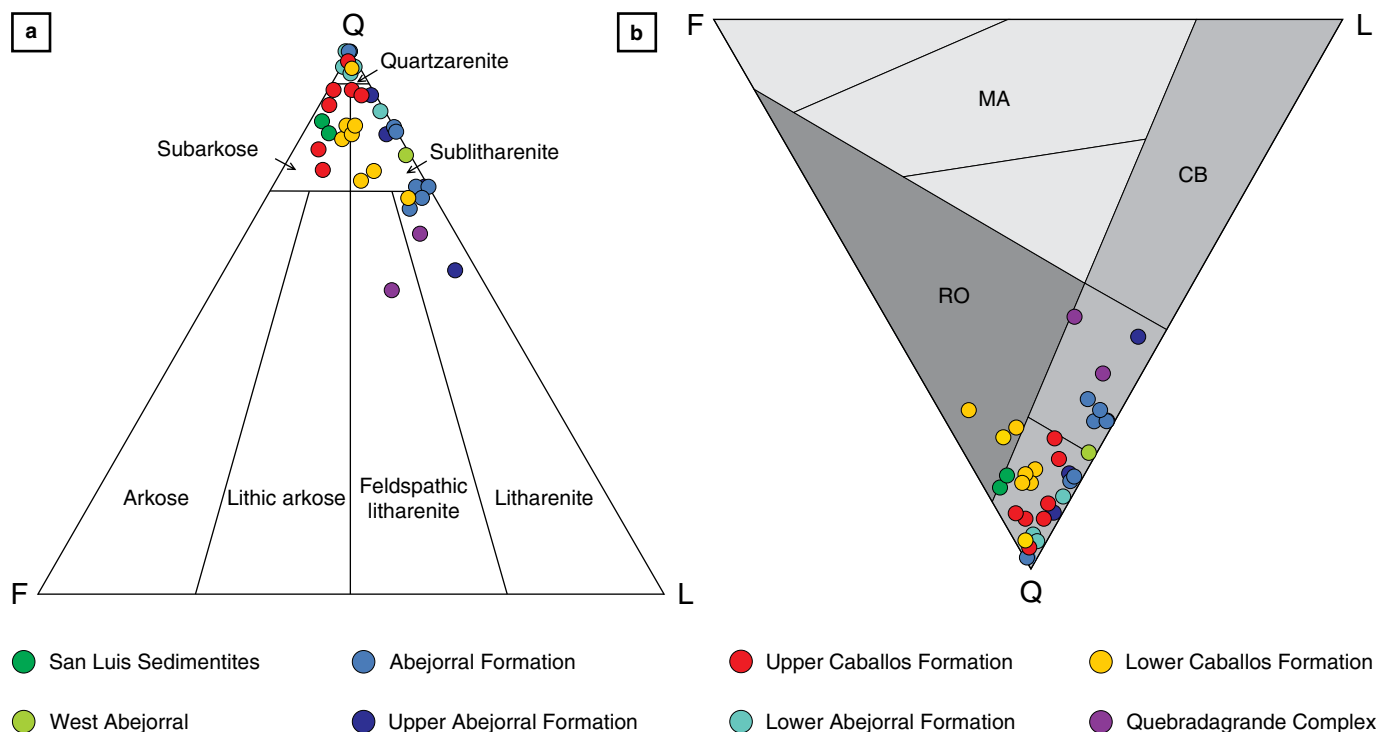


Figure 5. Sandstone petrography compilation and new data from the Abejorral Formation (Tamayo & Correa, 2010) and the San Luis Sedimentites. **(a)** Sandstone classification after Folk (1974). **(b)** Sandstone classification diagram after Garzanti (2016). Abbreviations: (MA) magmatic arc; (RO) recycled orogen; (CB) continental block.

schistose and volcanic lithics, as well as abundant (<70%) foliated polycrystalline and monocrystalline quartz with undulatory and straight extinction (Tamayo & Correa, 2010; Jaramillo et al., 2017; Zapata et al., 2018).

The San Luis Sedimentites include medium- to coarse-grained sandstones, with angular to subangular and low-sphericity particles, also dominantly composed of monocrystalline igneous and polycrystalline metamorphic quartz, with minor sedimentary and metamorphic lithic fragments and feldspar. In the QFL diagram of Folk (1974), the samples plot within the subarkose field, whereas in the tectonic discrimination diagram of Garzanti (2016), they plot within the continental block field (Figure 5).

Descriptions of sandstones from the San Pablo and La Soledad Formations in the northern segment of the Central Cordillera, as well as the Berlin Sedimentites, suggest that they are fine- to medium-grained rocks, with angular particles mainly composed of quartz, which is consistent with a sialic continental block affinity. However, more definitive details are missing and waiting for new provenance research.

4.3. Detrital Zircon Geochronology

The results of four new detrital zircon U–Pb analyses are presented and compared with previously published geochronological data to complement the sedimentary provenance of the

Lower Cretaceous units exposed in both the western and eastern flanks of the Central Cordillera. We report the maximum accumulation age based on the three youngest overlapping grains approach of Dickinson & Gehrels (2009), but only when it is close to the stratigraphic age previously suggested by the fossil content, since older ages are meaningless for the purpose of analyzing accumulation ages. Single- or two-grain ages are also noted when necessary, although we are aware that such types of ages are not statistically robust (Dickinson & Gehrels, 2009).

One sample collected from the Quebradagrande Complex exposed northwest of the city of Medellín (Figures 1, 2) yielded only seven individual zircon U–Pb ages clustered at approximately 190 Ma, with additional Early Cretaceous, Paleozoic, and Neoproterozoic ages (Figure 6).

Two samples were analyzed from the Abejorral Formation and the Quebradagrande Complex (eastern and western intervals in the sense of Gómez-Cruz et al., 1995) exposed in the western flank of the Central Cordillera near the city of Manizales (Figures 1, 2). A total of 95 individual zircon grains were dated from the eastern interval (Abejorral Formation equivalent). The sample is characterized by major age peaks in the Permian – Triassic (240–296 Ma), early Paleozoic (340–530 Ma), and Proterozoic (ca. 630–1400 Ma). Thirty-six individual grains were analyzed from a sample from the western interval. This sample has a major Early Cretaceous peak (ca. 105 Ma) with additional Permian – Triassic, Paleozoic, and Proterozoic

zircon ages and a well-defined maximum accumulation age of 103.4 ± 1.1 Ma (Figure 6).

One hundred and twenty-seven individual zircon U–Pb ages were also obtained from one sample collected from the San Luis Sedimentites close to the town of San Luis (Figure 6). The sample is characterized by Late Jurassic (145–150 Ma), Permian – Triassic (ca. 220–270 Ma), Paleozoic (ca. 340–540 Ma), and Proterozoic ages (ca. 560–1800 Ma). Although this sample also includes minor Early Cretaceous ages of ca. 120–127 Ma and 136–137 Ma, the three youngest overlapping grains suggest a maximum accumulation age of 146.1 ± 2.0 Ma.

4.4. Zircon Geochronology of Magmatic Rocks

Early Cretaceous magmatic rocks from the Central Cordillera have yielded ca. 129 Ma U–Pb crystallization ages obtained from stock-sized plutons in the eastern flank of the cordillera, which intrude Jurassic metamorphic rocks of the Cajamarca Complex (Bustamante *et al.*, 2016) and are exposed immediately to the south of the San Luis and Berlin Sedimentites.

Cretaceous magmatism in the Central Cordillera of Colombia includes both plutonic and volcanic units. The plutonic record is widely exposed in a ca. 8000 km² trapezoidal body that has been defined as the Antioquian Batholith (Figures 1, 2; Feininger & Botero, 1982). Compositionally, it varies between gabbro and monzogranite, although it is mainly composed of medium- to coarse-grained tonalite and granodiorite facies. The mafic minerals are hornblende and biotite, which are typical of hydrated sources for magmas generated at convergent margins. These plutons intrude Triassic and older metamorphic rocks of the Cajamarca Complex as well as the Lower Cretaceous sedimentary rocks, forming well-defined contact aureoles (Botero, 1963; Feininger *et al.*, 1972; González, 2001). Different small bodies with similar tonalite, granodiorite, and gabbro compositions include the La Union, La Culebra, Ovejas, Belmira, San Diego, and Altavista Stocks, which have also been interpreted as associated with the different pulses that formed the Antioquian Batholith.

Available U–Pb zircon crystallization ages obtained by multigrain TIMS and single grain LA–ICP–MS analyses have yielded ages between 95 and 59 Ma (Correa *et al.*, 2006; Ibañez–Mejía *et al.*, 2007; Restrepo–Moreno *et al.*, 2007; Leal–Mejía, 2011; Villagómez *et al.*, 2011), without any particular spatial trend. Although areas of this broad plutonic province remain to be analyzed, available whole-rock geochemical data have indicated a typical convergent margin setting for its origin with a well-defined calc–alkaline signature and Nb–Ti anomalies that suggest a magmatic arc affinity (Leal–Mejía, 2011; Villagómez *et al.*, 2011). Farther to the south, Leal–Mejía (2011) described ca. 90 Ma plutonic rocks that intrude the Lower Cretaceous rocks of the Mariquita Stock (Bustamante *et*

al., 2016) and therefore extend the latitudinal distribution of the Late Cretaceous magmatism.

Volcanic rocks are exposed in the western flank of the Central Cordillera, forming a quasi-continuous and highly deformed belt that has been grouped as the Quebradagrande Complex (Maya & González, 1995). This unit is within the San Jerónimo Fault system that separates it from the eastern Lower Cretaceous and Triassic metamorphic rocks of the cordillera and is also in fault contact with ultrabasic units. Its lithostratigraphy includes basaltic to andesitic lavas and pyroclastic rocks with intercalated mudstones and fine-grained sandstones (Nivia *et al.*, 2006; Villagómez *et al.*, 2011; Jaramillo *et al.*, 2017). A coarser siliciclastic sequence, including sandstones and conglomerates, has also been reported (González, 1980). This unit is in fault contact to the west with Lower Cretaceous greenschist- to amphibolite-facies metamorphic rocks included in the Arquía Complex (Maya & González, 1995), as well as Triassic meta-igneous bodies and metasedimentary rocks that resemble those found to the east in the Central Cordillera (Vinasco *et al.*, 2006; Cochrane *et al.*, 2014a).

Published geochemical data suggest the existence of multiple compositional groups within the Quebradagrande Complex. A MORB to E–MORB character (Nivia *et al.*, 2006; Villagómez *et al.*, 2011; Rodríguez & Cetina, 2016) and an arc-like signature are represented by lavas and pyroclastic rocks (review in Jaramillo *et al.*, 2017). These geochemical patterns have been interpreted in terms of the evolution of a single back-arc system that might have resulted from the progressive reduction of the supra-subduction zone mantle signature (Nivia *et al.*, 2006). Nevertheless, Jaramillo *et al.* (2017) suggested that the compositional evolution followed a trend from MORB-like signatures toward arc-related signatures as a consequence of ongoing crustal thickening.

Available temporal constraints for the magmatic units of the Quebradagrande Complex include local stratigraphic relations with Aptian – Albian mudstone levels (Grosse, 1926; Botero, 1963; González, 1980; Botero & González, 1983; Arévalo *et al.*, 2001), in which basaltic volcanic rocks intrude and are deposited over the fossiliferous strata (Grosse, 1926; Botero, 1963; Arévalo *et al.*, 2001). Zircon U–Pb ages from diorite and tuff samples have yielded ages between 112 Ma and 114 Ma (Villagómez *et al.*, 2011; Cochrane *et al.*, 2014b). Zapata *et al.* (2018) also documented U–Pb crystallization ages between 103 Ma and 115 Ma in different tuffs and andesitic bodies that are related to the Abejorral Formation and the Quebradagrande Complex. Although a more extensive discussion is beyond the scope of this contribution, it is arguable that the Aptian – Albian volcanic and sedimentary records exposed in the western flank of the Central Cordillera (Quebradagrande Complex and Abejorral Formation) are part of a continuous Aptian – Albian domain.

Elsewhere, Upper Cretaceous fossil content has been recognized in two localities where a sequence of interlayered pyroclastic rocks and mudstones associated with the Que-

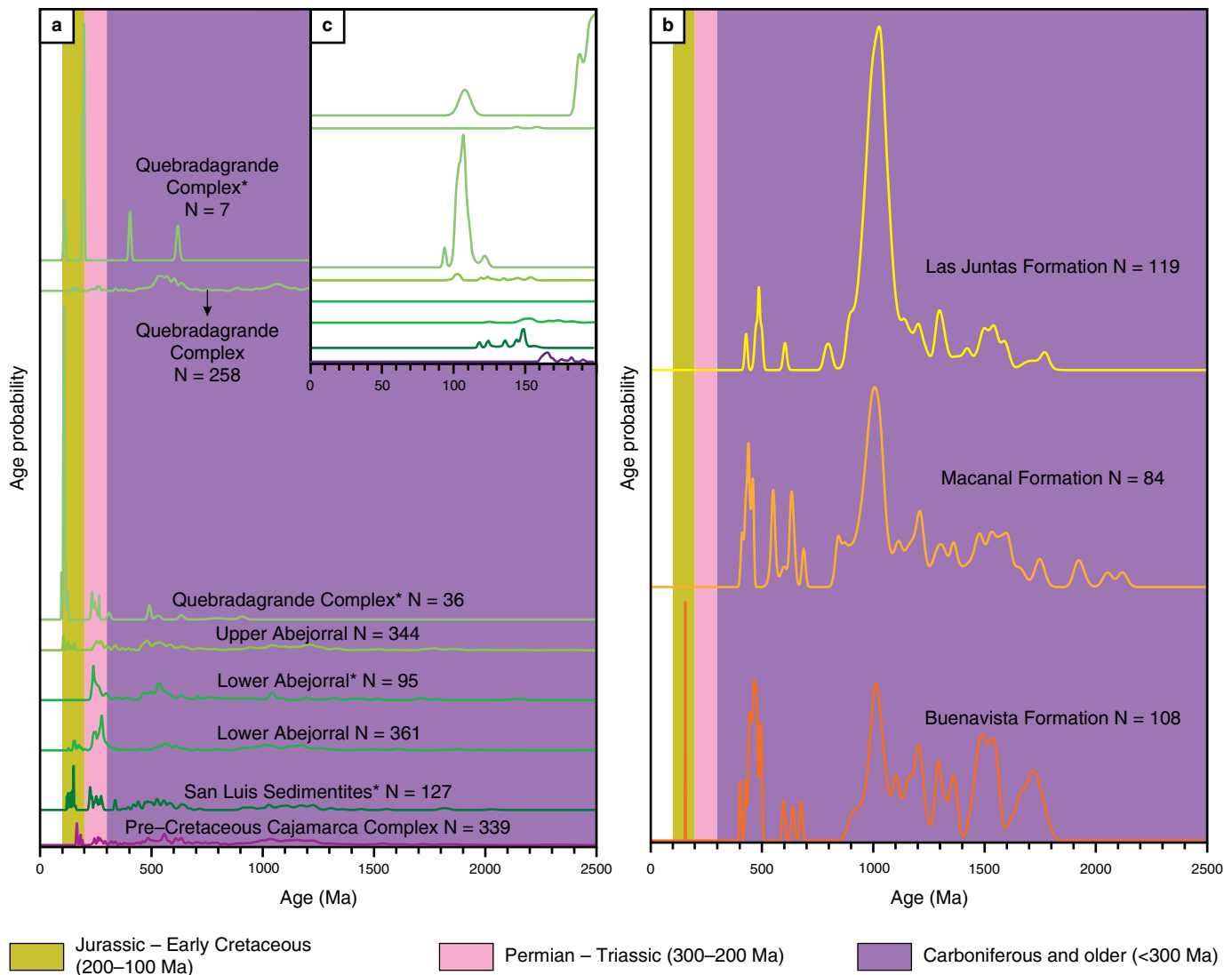


Figure 6. (a) U–Pb zircon geochronology of detrital samples from the Abejorral Formation, Quebradagrande Complex, and San Luis Sedimentites. (b) Published results from the same units and the Eastern Cordillera are also included (see text for references). (c) Expanded view of panel a showing the distribution of detrital ages between 0 and 200 Ma. *New data presented in this contribution.

Quebradagrande Complex is found (Botero & González, 1983; Gómez-Cruz et al., 2002). Although these rocks are not extensively discussed, Cochrane (2013) reported U–Pb zircon ages of 80.2 ± 0.7 Ma and 82.1 ± 0.7 Ma from deformed agglomerates near the city of Manizales. These agglomerates are also associated with cherts that include *Hastigerinoides watersi* Cushman, foraminifera characteristic of the Turonian – Campanian (Hall et al., 1972). Similarly, Zapata et al. (2018) documented the existence of ca. 80 Ma volcanic rocks overlying the Early Cretaceous volcano–sedimentary sequence.

Several plutonic bodies of tonalitic and gabbroic compositions with an arc–related geochemical affinity and intrusive relations with volcanic rocks of the Quebradagrande Complex have yielded U–Pb zircon crystallization ages of ca. 80 Ma and 90 Ma (Villagómez et al., 2011; Jaramillo et al., 2017).

It is therefore concluded that the magmatic record of the Quebradagrande Complex represents long–term Cretaceous magmatic evolution between 114 Ma and 80 Ma, which likely occurred through different tectonic scenarios.

Although scarcely studied, in the northern axial zone of the Central Cordillera, in association with the La Soledad Formation, two different volcanic units have been reported: an eastern basaltic unit interlayered with the upper levels of the siliciclastic rocks (Hall et al., 1972) and a prominent pyroclastic unit that includes agglomerates and tuffs, as well as several porphyritic intrusive rocks. The latter is located west of La Soledad Formation, is limited to the west by ultramafic bodies and apparently Triassic gneisses and has been correlated with the Quebradagrande Complex and tentatively assigned to the Late Cretaceous (Hall et al., 1972).

4.5. New U–Pb Zircon Geochronology of Plutonic Rocks

U–Pb LA–ICP–MS ages were obtained from four samples that intruded the Cajamarca Complex (2 samples) and the Lower Cretaceous sedimentary rocks exposed in the western and eastern flank of the Central Cordillera (2 samples; see red triangles in Figure 2). We attempted to refine the timing of the Cretaceous magmatic history and test the temporal relations among magmatism, sedimentation, and deformation.

4.5.1. San Diego Gabbro and Altavista Stock

Both units crop out on the western flank of the Central Cordillera in the city of Medellín (Figures 1, 2). The Altavista Stock intrudes micaceous schists with graphite, biotitic gneisses, and amphibolites, which are part of the pre–Cretaceous Cajamarca Complex (Rodríguez & Montoya, 1993), whereas the San Diego Gabbro intrudes only Triassic gneisses (Rendón, 1999).

In the sampled area, two different facies are recognized in the Altavista Stock; one facies has a predominantly medium–grained granodioritic composition represented by andesine plagioclase (40%), quartz (20%), K–feldspar (15%), hornblende (15%), and biotite (8%), with accessory minerals including apatite, zircon, titanite, and opaque minerals. A second and more mafic diorite facies commonly found as enclaves within the felsic facies is characterized by intermediate plagioclase (40%), quartz (10%), amphibole (40%), biotite (10%), and ~3% accessory minerals including titanite, opaque minerals, and apatite.

The San Diego Gabbro is characteristically a medium–grained, highly altered rock that includes saussuritized plagioclase (50%), hornblende altered to actinolite (45%), and quartz (2%) with titanite, apatite, and opaque minerals as accessory minerals.

Twenty zircon crystals in a granodiorite sample from the Altavista Stock (JCA–045) and twenty more in a diorite sample from the San Diego Gabbro (JCA–046) were analyzed. Crystal sizes vary between 40 and 200 μm and exhibit prismatic habits with (length:width) L:W ratios of 3:1 and 2:1. Cathodoluminescence images are characterized by a single oscillatory zoning pattern that is characteristic of igneous–related zircons (Vavra *et al.*, 1999). The Th/U ratio varies between 0.91 and 5.05 and can also be related to zircons with a magmatic origin (Rubatto, 2002). U–Pb zircon crystallization ages from the two stocks are strongly similar, with weighted mean ages of 97.0 ± 1.4 Ma and 98.2 ± 1.4 Ma, Altavista Stock and San Diego Gabbro, respectively (Figure 7). Previously published multigrain TIMS analyses yield ages of 96 ± 0.4 Ma and 87 ± 0.5 Ma for a mafic and a felsic facies, respectively, of the Altavista Stock and 94 ± 0.9 Ma for the San Diego Gabbro (Correa *et al.*, 2006). Whereas the older TIMS ages for the Altavista Stock overlap with our

new results, the other two ages are younger and may reflect a protracted magmatic history.

4.5.2. Aguadas Porphyritic Andesite

Thirty–one zircons were analyzed from a porphyritic andesite with hornblende phenocrysts that intrudes a sequence of interlayered gray and black mudstones from the Abejorral Formation (sample DM–056), located farther to the south of the Altavista Stock and San Diego Gabbro. Zircon crystal sizes range between 60 and 300 μm and show prismatic shapes with L:W of 3:1. Cathodoluminescence images show single oscillatory zoning patterns characteristic of igneous zircons (Vavra *et al.*, 1999). The Th/U ratio varies between 0.4 and 1.6, consistent with a magmatic character for the analyzed zircons (Rubatto, 2002). The analyzed individual grains yield a weighted mean age of 97.3 ± 1.3 Ma (Figure 7), which is related to the magmatic crystallization. No previous geochronological data are available for this porphyritic unit, which has been related to the Sonsón Batholith, considered Eocene in age based on U–Pb zircon geochronology (Ordóñez–Carmona *et al.*, 2001; Leal–Mejía, 2011).

4.5.3. Antioquian Batholith

We analyzed the zircon U–Pb geochronology of a quartz diorite sample with hornblende and biotite from the Antioquian Batholith near the Samaná River (AG–01), where it intrudes the Lower Cretaceous San Luis Sedimentites and the Triassic Samaná Gneiss. The twenty analyzed zircon crystals range from 75 to 200 μm in size and have a L:W ratio of 2:1. Cathodoluminescence images show a single oscillatory zoning pattern characteristic of igneous zircons (Vavra *et al.*, 1999). The Th/U ratio varies between 0.91 and 3.67, which may suggest a magmatic character for the analyzed grains (Rubatto, 2002). Zircons yield a weighted average age of 89.7 ± 1.3 Ma (Figure 7), which is related to the magmatic crystallization. Three U–Pb ages between 84.5 Ma and 93.5 Ma have previously been obtained by single–grain LA–ICP–MS and multigrain TIMS within the same region and are consistent with the new results presented in this contribution (Ibañez–Mejía *et al.*, 2007; Villagómez *et al.*, 2011).

4.6. Whole–Rock Geochemistry from Plutonic Rocks: New and Published Data

Four whole–rock geochemical analyses were conducted on three samples from the Altavista Stock and one from the San Diego Gabbro. SiO_2 varies between 54.6 and 67.4 wt %; total alkalis ($\text{Na}_2\text{O} + \text{K}_2\text{O}$), between 3.79 and 8.1 wt %; and CaO and MgO, from 2.87 to 9.36 wt % and 0.83 to 5.93 wt %, respectively. Al_2O_3 and Fe_2O_3 range from 15.6 to 16.8 wt % and 4.12

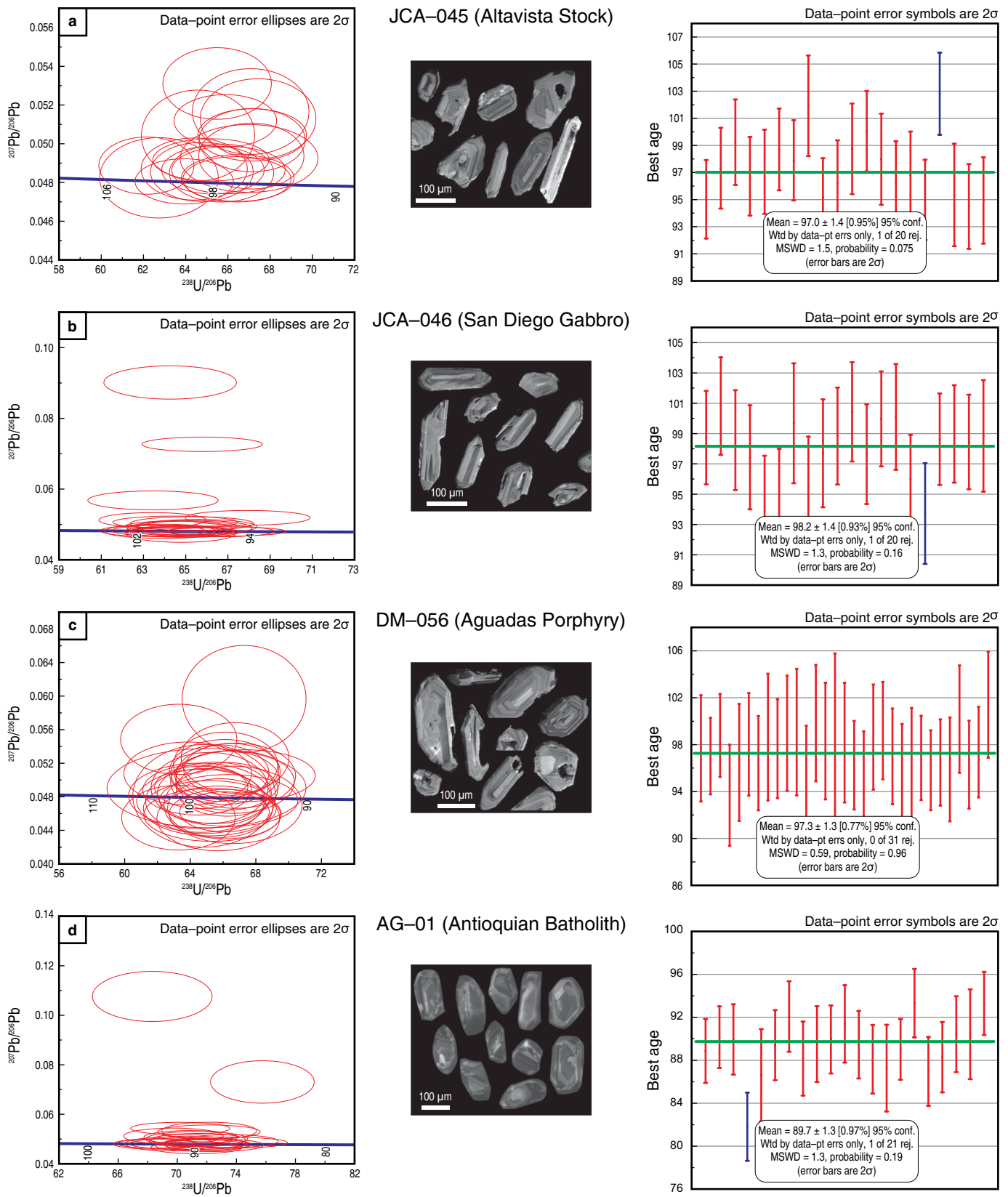


Figure 7. U-Pb zircon geochronology and cathodoluminescence images for: **(a)** Altavista Stock, **(b)** San Diego Gabbro, **(c)** porphyritic rock near Aguadas, and **(d)** Antioquian Batholith.

to 7.19 wt %, respectively, and these values are characteristic of basic to acidic compositions, which allows the classification of these rocks as diorite–gabbro to quartz monzonite (Figure 8a; TAS diagram after Middlemost, 1994), associated with the calc–alkaline magmatic series (Figure 8b, 8c; AFM diagram after Irvine & Baragar, 1971).

REE patterns normalized to the chondrite composition of Nakamura (1974) are characterized by enrichments in light rare earth elements (LREE), with $(La/Sm)_N$ ratios between 1.64 and 3.29, $(La/Yb)_N$ between 2.06 and 4.79, and a flat trend in the heavy rare earth elements (Figure 9; HREE). Only one sample presents a negative Eu anomaly with a Eu/Eu^* value of 0.71, while the other three samples show flat trends in the MREE and HREE with Eu/Eu^* between 0.92 and 1.08.

Multielemental patterns, normalized to the N–MORB composition of Sun & McDonough (1989), are characterized by negative anomalies in some high field strength elements (HFSE) such as Nb and Ti and enrichments in large ion lithophile elements (LILE), such as Cs, Ba, Th, and K, which may be correlated to subduction–related magmas (Figure 9; Pearce *et al.*, 1984).

The available geochemical data for the Antioquian Batholith show that this body ranges in composition between gabbro and granite (Figure 8; TAS diagram after Middlemost, 1994) and exhibits a typical calc–alkaline affinity (Figure 8; AFM diagram after Irvine & Baragar, 1971). REE patterns normalized to the chondrite composition of Nakamura (1974) are characterized by a well–defined enrichments in LREE and depletions in HREE with both negative and positive Eu anomalies, which could be related to plagioclase fractionation (Figure 9). Multielemental patterns normalized to N–MORB (Sun & McDonough, 1989) show negative anomalies in some HFSE such as Nb and Ti, together with enrichments in LILE such as Cs, Rb, Ba, Th, and K, which suggest the geochemical signature of a magmatic arc (Figure 9; Pearce *et al.*, 1984).

It is noteworthy that the Altavista Stock and San Diego Gabbro, when compared with samples from the Antioquian Batholith, show flatter HREE patterns and more limited enrichments in LREE and Th (Figure 9).

In the tectonic discrimination diagrams, all samples plot in the arc–related pluton field (Figure 10; Pearce *et al.*, 1984). The Th/Yb and Nb/Yb relations also suggest a continental magmatic arc setting. However, the older plutons, including Altavista and San Diego, show relatively less Th enrichment (Figure 10).

4.7. Isotopic Constraints

Isotopic analyses of plutonic rocks from the Cretaceous magmatism are still scarce (Ordóñez–Carmona & Pimentel, 2001; Correa *et al.*, 2006; Leal–Mejía, 2011); however, with the available data, some general observations are possible regarding the temporal changes in isotopic fingerprints and their potential relations with changes in tectonic scenarios.

We have considered data from those samples whose crystallization ages are within the ca. 90–100 Ma time span in order to avoid those that could be related to younger magmatic phases, which are preferentially exposed along the northwestern and northeastern flanks of the Central Cordillera (Jaramillo *et al.*, 2017).

Published Nd–Sr results from the Altavista Stock at 98 Ma are characterized by $\epsilon Nd_{(98\text{ Ma})}$ values between +7.4 and +9.8 and initial $^{87}\text{Sr}/^{86}\text{Sr}$ values ranging from 0.70402 to 0.70456, whereas the values for the San Diego Gabbro vary between +2.8 and +6.2 and 0.70326–0.70331, respectively (Ordóñez–Carmona & Pimentel, 2001; Correa *et al.*, 2006). Conversely, available data from younger samples (ca. 90 Ma) of the Antioquian Batholith on the western and eastern flanks of the cordillera, including samples near the San Diego and Altavista Plutons, yield more radiogenic values with $\epsilon Nd_{(90\text{ Ma})}$ varying between –2.47 and +2.6 and initial $^{87}\text{Sr}/^{86}\text{Sr}$ between 0.70405 and 0.70734 (Ordóñez–Carmona *et al.*, 2001; Leal–Mejía, 2011).

We obtained zircon Hf isotope data from the above–described porphyritic andesite sample that intrudes the Abejorral Formation (DM–056), which yield a U–Pb crystallization age of ca. 97 Ma. The initial $^{176}\text{Hf}/^{177}\text{Hf}$ ratios in thirteen zircons range from 0.282989 to 0.283067, with positive values of initial $\epsilon Hf_{(97\text{ Ma})}$ ranging from 9.0 to 12.2 (Figure 11).

As Hf and Nd isotopes behave in a similar fashion, we can use them for the same petrogenetic considerations (Chapman *et al.*, 2017). Therefore, older plutons (ca. 98 Ma) are characterized by a more depleted mantle source and differ from the younger Upper Cretaceous magmatic units, which are more radiogenic and may include additional older crustal input.

4.8. Oxygen Isotopes

Oxygen isotope analyses were conducted on zircons from the samples of the Altavista Stock, San Diego Gabbro (98 Ma), and the Antioquian Batholith (90 Ma) dated by U–Pb LA–ICP–MS geochronology. The $\delta^{18}\text{O}$ values for the Altavista Stock (24 magmatic crystals) range between 4.9‰ and 6.1‰, and those for the San Diego Gabbro (24 magmatic crystals) show similar values between 5.0‰ and 5.9‰, with mean values of 5.6‰ and 5.5‰, respectively. In the case of the Antioquian Batholith, the 13 analyzed crystals have $\delta^{18}\text{O}$ values between 6.8‰ and 7.9‰ (Table 6). These results show that the older plutons have values characteristic of mantle–derived oxygen isotope compositions, whereas a stronger crustal signature characterizes the younger Antioquian Batholith (Figure 12), buttressing the considerations drawn from the radiogenic isotopes.

5. Discussion

The Jurassic to Early Cretaceous tectonic evolution of the northwestern margin of South America has been related to

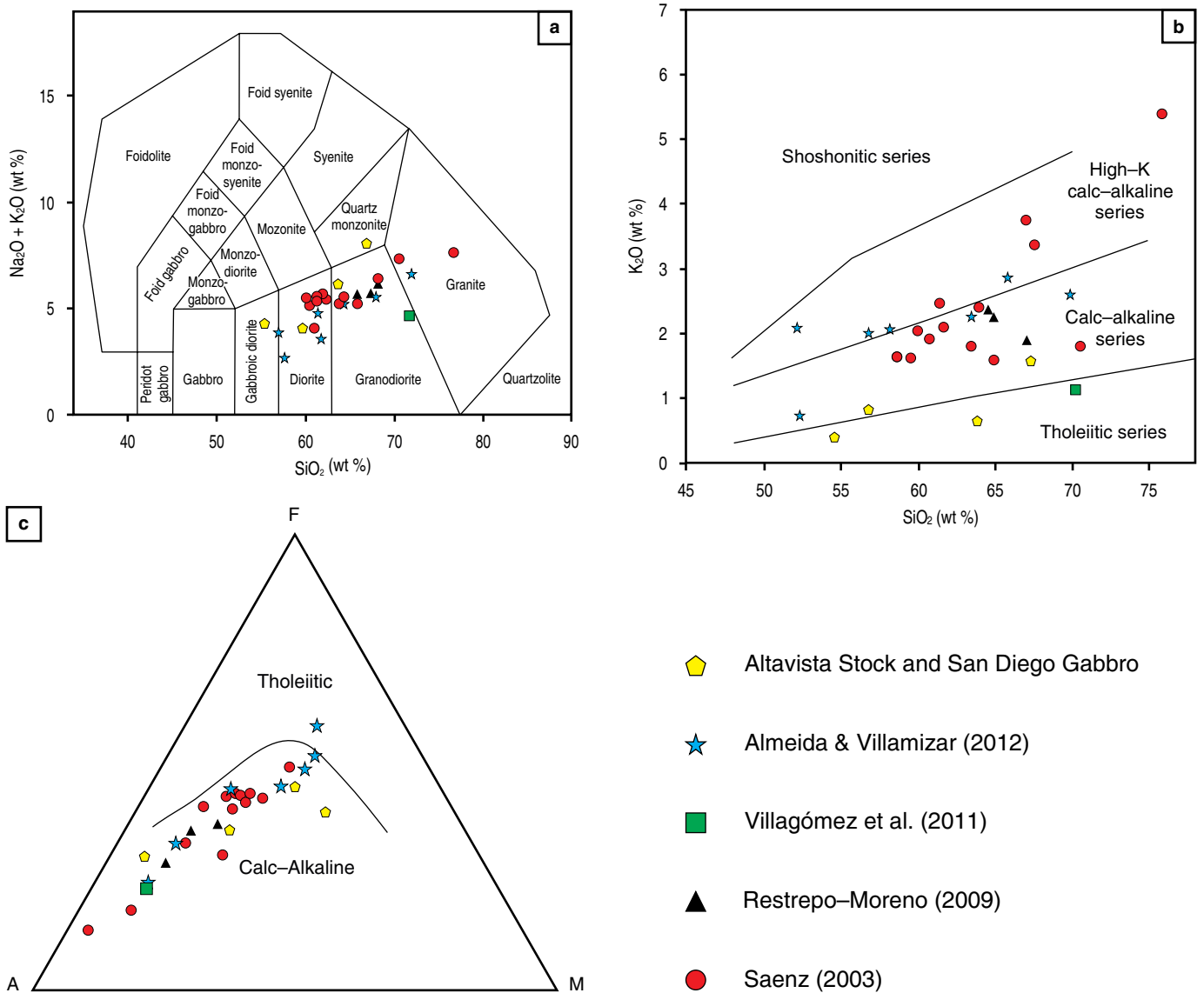


Figure 8. Whole-rock geochemical results from the Altavista Stock and San Diego Gabbro compared with published data from the Antioquian Batholith (see text for references). **(a)** TAS classification diagram (Middlemost, 1994). **(b)** Alkaline series (Peccerillo & Taylor, 1976), **(c)** AFM diagram (Irvine & Baragar, 1971).

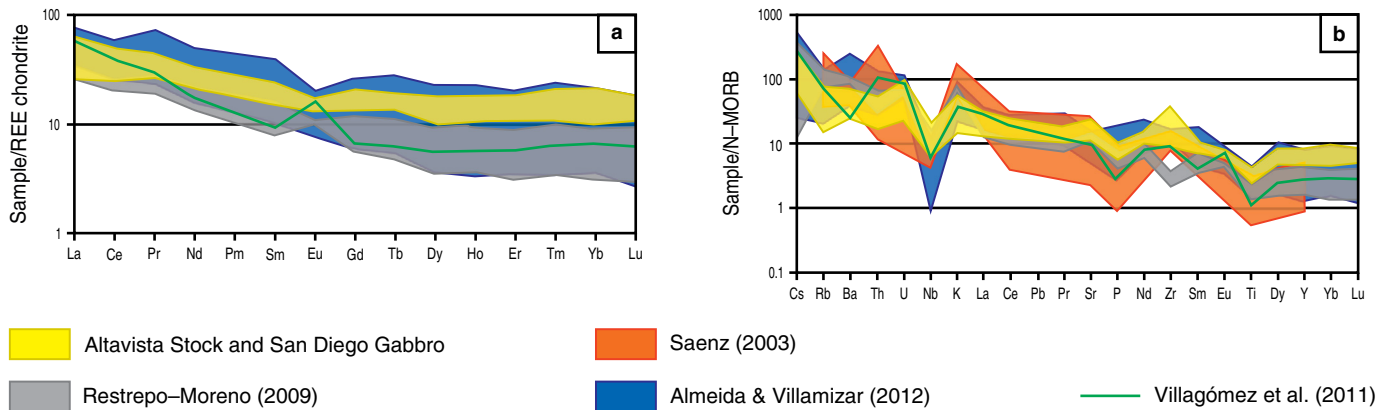


Figure 9. Trace element patterns from the Altavista Stock and San Diego Gabbro compared with published data from the Antioquian Batholith (see text for references). **(a)** REE diagram normalized to chondrites (Nakamura, 1974). **(b)** Multielemental patterns normalized to N-MORB (Sun & McDonough, 1989).

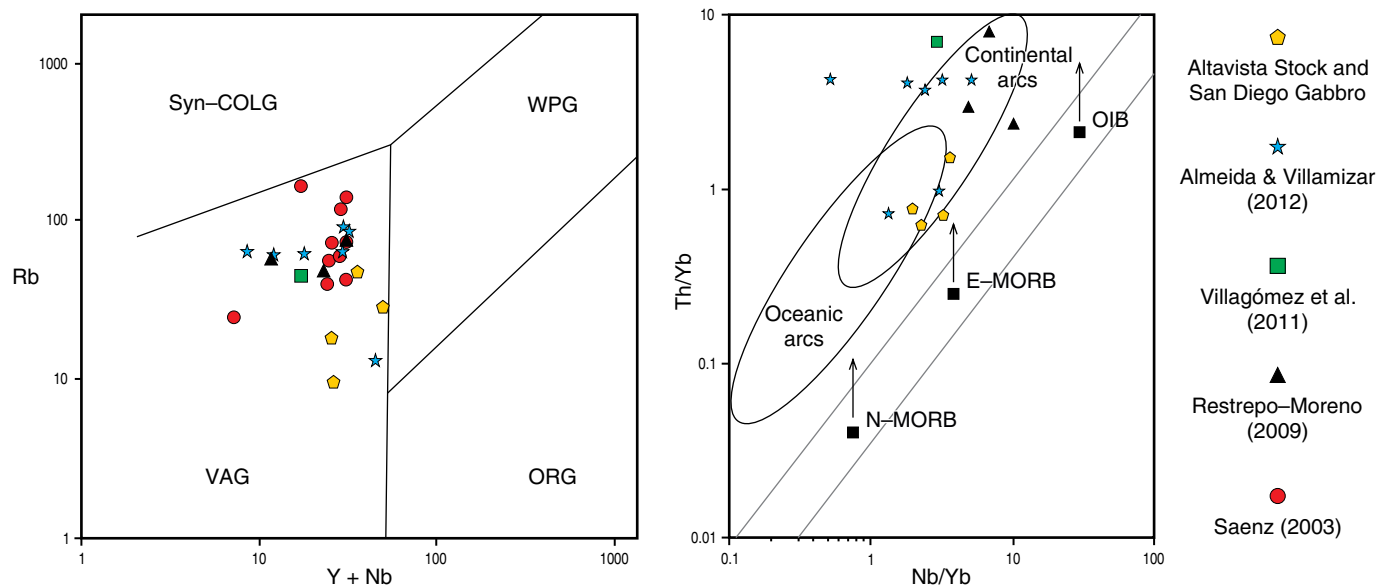


Figure 10. Geotectonic discrimination diagrams from the Altavista Stock and San Diego Gabbro compared with published data from the Antioquian Batholith (see text for references). **(a)** Granitoid discrimination diagram after Pearce et al. (1984). **(b)** Th/Yb vs. Nb/Yb discrimination diagram for subduction input and mantle reservoirs after Pearce (2008). (Syn-COLG) Syn-collisional granite; (WPG) Within-plate granite; (ORG) Ocean ridge granite; (VAG) Volcanic arc granite.

the growth of a series of magmatic arcs, which record major spatial and compositional changes related to modifications in the obliquity of plate convergence as well as in the subduction angle (recent reviews in Spikings et al., 2015; van der Lelij et al., 2016; Bustamante et al., 2017). During this time interval and until the Early Cretaceous, along-strike translation of Jurassic arc-related units from southern latitudes toward the Colombian margin has also been suggested by paleomagnetic data (Bayona et al., 2006, 2010). Conversely, metamorphic rocks included within the Cajamarca and Arquía Complexes on both flanks of the Central Cordillera have been related to different accretionary events at ca. 157–146 Ma (Blanco-Quintero et al., 2014) and between 137 and 112 Ma (Toussaint, 1996; Villagómez et al., 2011). Although we are aware that the Jurassic magmatic evolution and the Early Cretaceous metamorphic record of the Arquía Complex must have influenced the younger magmatic and sedimentary record presented in this contribution, in the next paragraphs, we consider them as already incorporated into a common domain that formed part of the Central Cordillera when the units discussed in this contribution were forming.

5.1. Early Cretaceous Sedimentary Provenance and Tectonostratigraphic Implications

Although more stratigraphic constraints are still necessary, the Early Cretaceous siliciclastic record found in the different belts exposed along the Central Cordillera is characterized by a well-defined fining-upward trend with interlayered chert levels

that implies a basin-deepening pattern. The fossiliferous record extends from the Berriasian to the Aptian for these sedimentary successions, which are characterized by initial coarse-grained sequences that most likely accumulated in fluvial-deltaic environments (particularly well defined on the western flank). A major environmental change is registered upward in the sequence when sedimentation began to reflect marine turbiditic settings (Feininger et al., 1972; Hall et al., 1972; Etayo-Serna, 1985; Rodríguez & Rojas, 1985; Gómez-Cruz et al., 1995; González, 2001; Gómez-Cruz et al., 2002; Quiroz, 2005) and may include relatively distal subenvironments, as suggested by the presence of interlayered chert levels.

Although sedimentation may be as old as the Berriasian, the most abundant paleontological record, the estimated maximum accumulation ages from zircon U–Pb data, and geochronological constraints from associated volcanism (see former temporal considerations), coincide between the Aptian and Albian (126.3 to 100.5 Ma after Gradstein et al., 2012), and we therefore consider this time interval for the main Early Cretaceous tectonostratigraphic evolution of the transgressive basin discussed in this contribution.

Petrographic constraints from different sandstone levels are characterized by significant textural immaturity and dominantly quartz-rich compositions. Lithic fragments are mostly metamorphic (schists) with minor sedimentary (sandstones and mudstones) rocks. Such components can be related to proximal depocenters adjacent to first-cycle crystalline metamorphic rocks as well as siliciclastic sedimentary sources that were being eroded and rapidly buried.

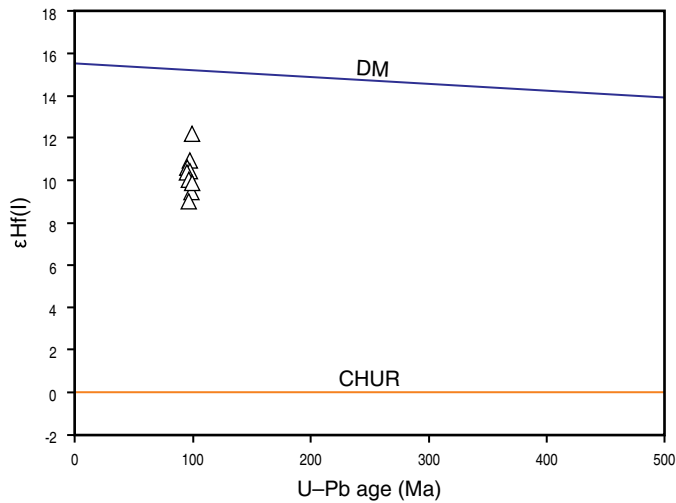


Figure 11. Hf isotope data for zircons from the Aguadas porphyritic body.

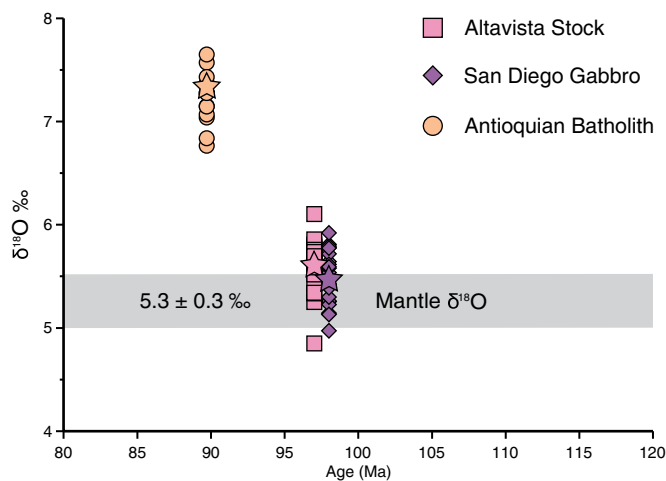


Figure 12. Oxygen isotope data for zircons from the Altavista Stock, San Diego Gabbro, and Antioquian Batholith (after Lackey et al., 2005). The stars are the weight average for each sample.

The origin of quartz-rich compositions in sandstones is commonly a consequence of multiple parameters (Dott, 2003; Smyth et al., 2008), as it may reflect sedimentary recycling in the source area, intense chemical weathering conditions, diagenetic modifications, or strong eolian or littoral derivation. In the case of the Cretaceous sandstones from the Central Cordillera, diagenetic and environmental controls on composition are discarded since petrographic evidence of intense cementation, mineral replacement, or extreme roundness is not observed. Therefore, some recycling (as suggested by the sedimentary lithic fragments) and particularly relatively high weathering rates in the source areas are considered the major controls for

the observed quartz enrichment. Similar high quartz contents have been documented in the eastern basins of Colombia within the Upper Magdalena Valley and the Eastern Cordillera (Figure 13; Moreno, 1990, 1991; Duarte et al., 2018), as well as in several deformed Cretaceous siliciclastic units from the Cordillera Real of Ecuador (Litherland et al., 1994), which may be temporally and geologically related (Spikings et al., 2015). Chemical and fossil data have shown that during the Early Cretaceous, particularly the Aptian – Albian, climate conditions in some of the eastern Colombian basins were characterized by high humidity (Campos-Álvarez & Roser, 2007; Suárez et al., 2010; Mejía-Velásquez et al., 2012), which favored strong chemical weathering that facilitated the formation of stable quartzose sediments, as discussed for the origin of high quartz contents in the northern Andean basins.

A comparison shows that the detrital geochronological signatures of the San Luis Sedimentites, the Abejorral Formation, and the Quebradagrande Complex are characterized by similar pre-Jurassic zircon U–Pb age distributions (Figure 6; Cochrane et al., 2014b; Jaramillo et al., 2017), which suggests that they probably shared common regional source areas and could have been part of the same crustal domain. Published zircon U–Pb geochronological data from metasedimentary rocks of the Cajamarca Complex are included in Figure 6 to test whether they could be considered the main source areas (Martens et al., 2012; Cochrane et al., 2014a; Bustamante et al., 2017; Jaramillo et al., 2017).

The Permian – Triassic detrital zircon age peaks found in the Early Cretaceous sedimentites resemble those yielded by the meta-igneous basement of the Central Cordillera (Cajamarca Complex; Vinasco et al., 2006; Restrepo et al., 2011; Villagómez et al., 2011; Bustamante et al., 2017), which borders the basins at present. Likewise, the older Paleozoic and Proterozoic detrital ages are also associated with the erosion of both gneissic and metasedimentary units of the same complex (Cochrane et al., 2014a; Martens et al., 2014; Jaramillo et al., 2017).

The Middle and Upper Jurassic detrital ages are likely derived either from a long-lived magmatic arc exposed along the axis and the eastern flank of the Central Cordillera (i.e., Ibagué Batholith, Mariquita Stock; Villagómez et al., 2011; Rodríguez et al., 2018; Bustamante et al., 2016 and references therein) or from the recently identified Jurassic metavolcano-sedimentary belt and hidden arc, which crop out in the core of the Central Cordillera (Blanco-Quintero et al., 2014; Bustamante et al., 2017).

The Early Cretaceous detrital ages between 127 Ma and 105 Ma identified in sandstones from the Abejorral Formation and the Quebradagrande Complex (Cochrane et al., 2014b; Zapata et al., 2018; this contribution) suggest that active magmatism accompanied basin filling. Stratigraphic relationships in the Abejorral Formation (Quiroz, 2005; Zapata et al., 2018), the Quebradagrande Complex (Arévalo et al., 2001), and the San Pablo Formation (Hall et al., 1972; Rodríguez & Celada-Arango, 2018) show that volcanic rocks with Early

Table 6. Oxygen isotope results for zircons from the Altavista, San Diego, and Antioquia plutonic units.

Sample	¹⁶ O	¹⁸ O	¹⁸ O/ ¹⁶ O Raw	¹⁸ O/ ¹⁶ O Raw 1σ	¹⁸ O/ ¹⁶ O Corr	¹⁸ O/ ¹⁶ O Corr 1σ	δ ¹⁸ O	δ ¹⁸ O 1σ (internal)	δ ¹⁸ O 1σ (external)	Age (Ma)
Altavista Stock										
Altavista_1	3688114048	7449863.765	0.002019966	1.02055E-07	0.002016377	1.01874E-07	5.574058437	0.050523335	0.145198714	97
Altavista_2	3664205016	7402418.776	0.002020198	1.00256E-07	0.002016609	1.00078E-07	5.689597941	0.049626932	0.145198714	97
Altavista_3	3682975462	7440542.502	0.002020253	8.3584E-08	0.002016664	8.34355E-08	5.717133239	0.041373026	0.145198714	97
Altavista_4	3654928559	7382951.554	0.002019999	1.01673E-07	0.00201641	1.01493E-07	5.59058503	0.050333378	0.145198714	97
Altavista_5	3651019532	7372580.95	0.002019321	8.60402E-08	0.002015734	8.58874E-08	5.253203371	0.042608494	0.145198714	97
Altavista_6	3684495700	7444167.771	0.002020403	9.55637E-08	0.002016814	9.5394E-08	5.791985504	0.047299339	0.145198714	97
Altavista_7	3666162780	7404152.036	0.002019592	1.03906E-07	0.002015902	1.03717E-07	5.337225934	0.051449243	0.145198714	97
Altavista_8	3559797233	7189990.625	0.002019775	8.61823E-08	0.002016085	8.60249E-08	5.428619019	0.042669253	0.145198714	97
Altavista_9	3779521491	7636316.983	0.002020445	9.07805E-08	0.002016754	9.06147E-08	5.762198472	0.044930934	0.145198714	97
Altavista_10	3677779704	7428959.815	0.002019958	1.10197E-07	0.002016268	1.09996E-07	5.519454125	0.054554033	0.145198714	97
Altavista_11	3766601349	7610365.013	0.002020486	1.07642E-07	0.002016795	1.07445E-07	5.782349073	0.053275372	0.145198714	97
Altavista_12	3616035500	7302963.015	0.002019605	8.24489E-08	0.002015915	8.22982E-08	5.343781496	0.040824248	0.145198714	97
Altavista_13	3647100442	7370919.576	0.002021036	8.18711E-08	0.002017445	8.17256E-08	6.10637449	0.040509483	0.145198714	97
Altavista_14	3733251978	7541150.441	0.002019995	1.007E-07	0.002016406	1.00521E-07	5.588237328	0.049851515	0.145198714	97
Altavista_15	3642221912	7358367.421	0.002020296	1.13869E-07	0.002016706	1.13666E-07	5.73821049	0.056362361	0.145198714	97
Altavista_16	3651394559	7376470.8	0.002020179	1.19009E-07	0.002016589	1.18798E-07	5.679846786	0.058910187	0.145198714	97
Altavista_17	3682717208	7439367.36	0.002020076	7.37248E-08	0.002016486	7.35938E-08	5.628529859	0.036496049	0.145198714	97
Altavista_18	3656727727	7388212.236	0.002020444	9.40272E-08	0.002016854	9.38601E-08	5.811715483	0.04653789	0.145198714	97
Altavista_19	3704404268	7477398.233	0.002018516	9.78316E-08	0.002014929	9.76578E-08	4.851967357	0.048467115	0.145198714	97
Altavista_20	3683194245	7442038.138	0.002020539	1.30672E-07	0.002016949	1.3044E-07	5.859263637	0.064671709	0.145198714	97
Altavista_21	3623706784	7321114.318	0.002020338	8.93737E-08	0.002016749	8.92149E-08	5.759379322	0.044237004	0.145198714	97
Altavista_22	3643404245	7360750.653	0.002020295	9.66362E-08	0.002016705	9.64645E-08	5.737468393	0.047832709	0.145198714	97
Altavista_23	3734672516	7544317.434	0.002020075	9.61603E-08	0.002016485	9.59894E-08	5.627894597	0.047602352	0.145198714	97
Altavista_24	3693810456	7462291.118	0.002020215	8.2551E-08	0.002016625	8.24043E-08	5.69771896	0.040862491	0.145198714	97
San Diego Gabbro										
SanDiego_1	3650642115	7372414.213	0.002019484	8.98598E-08	0.002016082	8.97084E-08	5.426775849	0.044496419	0.145198714	98
SanDiego_2	3634562415	7340497.673	0.002019637	1.05268E-07	0.002016015	1.05079E-07	5.39360339	0.052122045	0.145198714	98
SanDiego_3	3646294898	7363187.8	0.002019362	8.98188E-08	0.00201574	8.96577E-08	5.256364219	0.044478816	0.145198714	98
SanDiego_4	3632609938	7337608.241	0.002019927	1.04179E-07	0.002016305	1.03992E-07	5.538023628	0.05157555	0.145198714	98
SanDiego_5	3679460339	7430391.551	0.002019424	6.88846E-08	0.002016022	6.87685E-08	5.396925428	0.034111011	0.145198714	98
SanDiego_6	3644024017	7359343.877	0.002019565	1.14924E-07	0.002016163	1.1473E-07	5.467053992	0.056905228	0.145198714	98
SanDiego_7	3676308415	7427076.792	0.002020254	8.86218E-08	0.00201685	8.84725E-08	5.810012987	0.04386668	0.145198714	98
SanDiego_8	3671901676	7417947.225	0.002020192	1.15873E-07	0.002016789	1.15678E-07	5.779257241	0.057357541	0.145198714	98
SanDiego_9	3664735153	7403568.957	0.002020219	9.3783E-08	0.002016816	9.3625E-08	5.792772709	0.046422186	0.145198714	98
SanDiego_10	3628969778	7329395.226	0.00201969	9.11728E-08	0.002016068	9.10093E-08	5.420030348	0.045141967	0.145198714	98
SanDiego_11	3664209716	7399398.551	0.002019371	1.00423E-07	0.002015749	1.00242E-07	5.261018193	0.049729639	0.145198714	98
SanDiego_12	3675246379	7424036.598	0.002020011	1.04105E-07	0.002016388	1.03918E-07	5.579449645	0.051536869	0.145198714	98
SanDiego_13	3593837725	7255573.938	0.002018893	7.50014E-08	0.002015514	7.48759E-08	5.143402247	0.037149788	0.145198714	98
SanDiego_14	3629458641	7328088.292	0.002019058	7.67725E-08	0.002015683	7.66442E-08	5.227903504	0.038023917	0.145198714	98
SanDiego_15	3580149828	7227834.793	0.002018864	1.40919E-07	0.002015489	1.40684E-07	5.131096342	0.069801207	0.145198714	98
SanDiego_16	3614330705	7298068.753	0.002019203	1.14343E-07	0.002015828	1.14151E-07	5.300172878	0.056627566	0.145198714	98
SanDiego_17	3607217243	7286212.498	0.002019898	7.39302E-08	0.002016517	7.38065E-08	5.643966011	0.036600952	0.145198714	98
SanDiego_18	3702243622	7473173.912	0.002018553	1.10825E-07	0.002015174	1.10639E-07	4.97396946	0.054902959	0.145198714	98
SanDiego_19	3644848397	7362778.447	0.002020051	1.19558E-07	0.002016669	1.19358E-07	5.719754622	0.059185539	0.145198714	98
SanDiego_20	3658102880	7391030.78	0.002020455	1.40003E-07	0.002017073	1.39769E-07	5.920856995	0.069292906	0.145198714	98

Table 6. Oxygen isotope results for zircons from the Altavista, San Diego, and Antioquia plutonic units (*continued*).

Sample	^{16}O	^{18}O	$^{18}\text{O}/^{16}\text{O}$ Raw	$^{18}\text{O}/^{16}\text{O}$ Raw 1σ	$^{18}\text{O}/^{16}\text{O}$ Corr	$^{18}\text{O}/^{16}\text{O}$ Corr 1σ	$\delta^{18}\text{O}$	$\delta^{18}\text{O}$ 1σ (internal)	$\delta^{18}\text{O}$ 1σ (external)	Age (Ma)
SanDiego_21	3613283980	7296616.05	0.002019386	9.77497E-08	0.002016006	9.75861E-08	5.388969282	0.048405652	0.145198714	98
SanDiego_22	3633779270	7339641.028	0.002019837	9.81263E-08	0.00201646	9.79623E-08	5.615527566	0.048581299	0.145198714	98
SanDiego_23	3646412845	7366328.834	0.002020158	7.59605E-08	0.002016781	7.58335E-08	5.775282021	0.037601279	0.145198714	98
SanDiego_24	3613042799	7297587.514	0.00201979	1.07292E-07	0.002016413	1.07113E-07	5.592208601	0.053120614	0.145198714	98
Antioquian Batholith										
Antioquia_1	3632822808	7363514.284	0.00202694	1.01491E-07	0.002023144	1.01301E-07	8.94877152	0.050070925	0.145198714	89.7
Antioquia_2	3285597305	6650625.361	0.002024175	9.42455E-08	0.002020385	9.4069E-08	7.572598937	0.046559929	0.145198714	89.7
Antioquia_3	1828915444	3700092.154	0.002023107	1.85592E-07	0.002019318	1.85244E-07	7.040904134	0.091735979	0.145198714	89.7
Antioquia_4	3224101918	6520936.4	0.002022559	1.24489E-07	0.002018771	1.24256E-07	6.767993465	0.061550385	0.145198714	89.7
Antioquia_5	3312559147	6700331.775	0.002022706	1.07826E-07	0.002018917	1.07624E-07	6.840934748	0.053307695	0.145198714	89.7
Antioquia_6	3390186708	6858919.049	0.002023169	1.05978E-07	0.00201938	1.0578E-07	7.07138988	0.052382315	0.145198714	89.7
Antioquia_7	3353470156	6784748.313	0.002023202	9.8269E-08	0.002019799	9.81037E-08	7.280617887	0.048571027	0.145198714	89.7
Antioquia_8	3354500943	6787460.026	0.002023389	1.0839E-07	0.002019985	1.08207E-07	7.373559824	0.053568451	0.145198714	89.7
Antioquia_9	3340687423	6758026.56	0.002022945	1.09166E-07	0.002019542	1.08982E-07	7.152496341	0.053963836	0.145198714	89.7
Antioquia_10	3359762175	6799979.233	0.002023947	9.35875E-08	0.002020542	9.34301E-08	7.651211355	0.046240102	0.145198714	89.7
Antioquia_11	3367941785	6813126.447	0.002022935	9.02515E-08	0.002019532	9.00997E-08	7.147442904	0.044614147	0.145198714	89.7
Antioquia_12	3326712333	6731638.28	0.002023511	8.66576E-08	0.002020107	8.65118E-08	7.434233581	0.042825362	0.145198714	89.7
Antioquia_13	3330684484	6738635.218	0.002023198	1.2408E-07	0.002019795	1.23871E-07	7.278663753	0.061328642	0.145198714	89.7

Cretaceous ages are interspersed and overlying the coeval siliciclastic rocks, confirming the appearance of volcanic activity in the history of the basin. Several discontinuous segments of predominantly volcanic rocks, which are locally associated with gabbros and/or serpentized peridotite lenses, present different calc-alkaline, MORB, and E-MORB geochemical signatures (Nivia et al., 2006; Villagómez et al., 2011; Rodríguez & Cetina, 2016; Rodríguez & Celada-Arango, 2018; Zapata et al., 2018). Although precise geochronological constraints for each of the geochemical units are still lacking, by assuming probable Cretaceous ages, heterogeneous geochemical fingerprints, the existence of ophiolite-type associations, and the discussed transgressive nature of the Aptian – Albian sedimentation, it is possible to interpret a tectonic setting in which a magmatic arc was affected by a major extensional episode with associated back-arc basin formation (Figure 14a, 14b; Nivia et al., 2006; Cochrane et al., 2014b; Zapata et al., 2018). The presence of pre-Cretaceous detrital zircons in the Quebradagrande Complex suggests that this arc formed adjacent to a continental basement as part of a fringing arc that records the Early Cretaceous back-arc formation (Nivia et al., 2006; Cochrane et al., 2014b; Spikings et al., 2015; Jaramillo et al., 2017), eliminating its origin as an allochthonous oceanic arc.

Several authors have argued that the lack of volcanic material of the Abejorral Formation precludes its relation to the magmatism associated with the Quebradagrande Complex (Toussaint, 1996; Moreno-Sánchez et al., 2008; Restrepo et

al., 2009). However, we suggest that such an interpretation was biased by the observed stratigraphic sections and samples. The observations presented by Quiroz (2005) have shown that whereas the lower segment of the Abejorral Formation is in fact highly quartzose and lacks related magmatism, toward the top, intercalations of volcanic rocks are remarkably common, similar to what is reported for the La Soledad Formation (Hall et al., 1972).

Plutonic activity at ca. 98 Ma, such as that recorded by the three analyzed plutons (Altavista Stock, San Diego Gabbro, and Aguadas porphyritic andesite), is characterized by a significant juvenile mantle isotopic fingerprint, which is compatible with the existence of a thinned lithosphere associated with the extensional setting discussed above.

An extension-dominated tectonic setting that temporally extended until the Albian suggests that models of back-arc basin closure and compression by 114 Ma (Cediél et al., 2003; Villagómez & Spikings, 2013; Cochrane et al., 2014a; Spikings et al., 2015) are not sustainable.

Extension-controlled sedimentation and tectonics have also been reported in the stratigraphic record of the Eastern Cordillera, the Middle and Upper Magdalena Valley, and the Putumayo region, as well as in Ecuador (Sarmiento-Rojas et al., 2006; Baby et al., 2013). In the Eastern Cordillera, magmatism is restricted to minor gabbroic bodies (Vásquez et al., 2010) and distal volcanism represented by a series of lapilli tuffs altered to clay, which have been reported in the post-Hauterivian sedimentites (Sarmiento-Rojas et al., 2006).

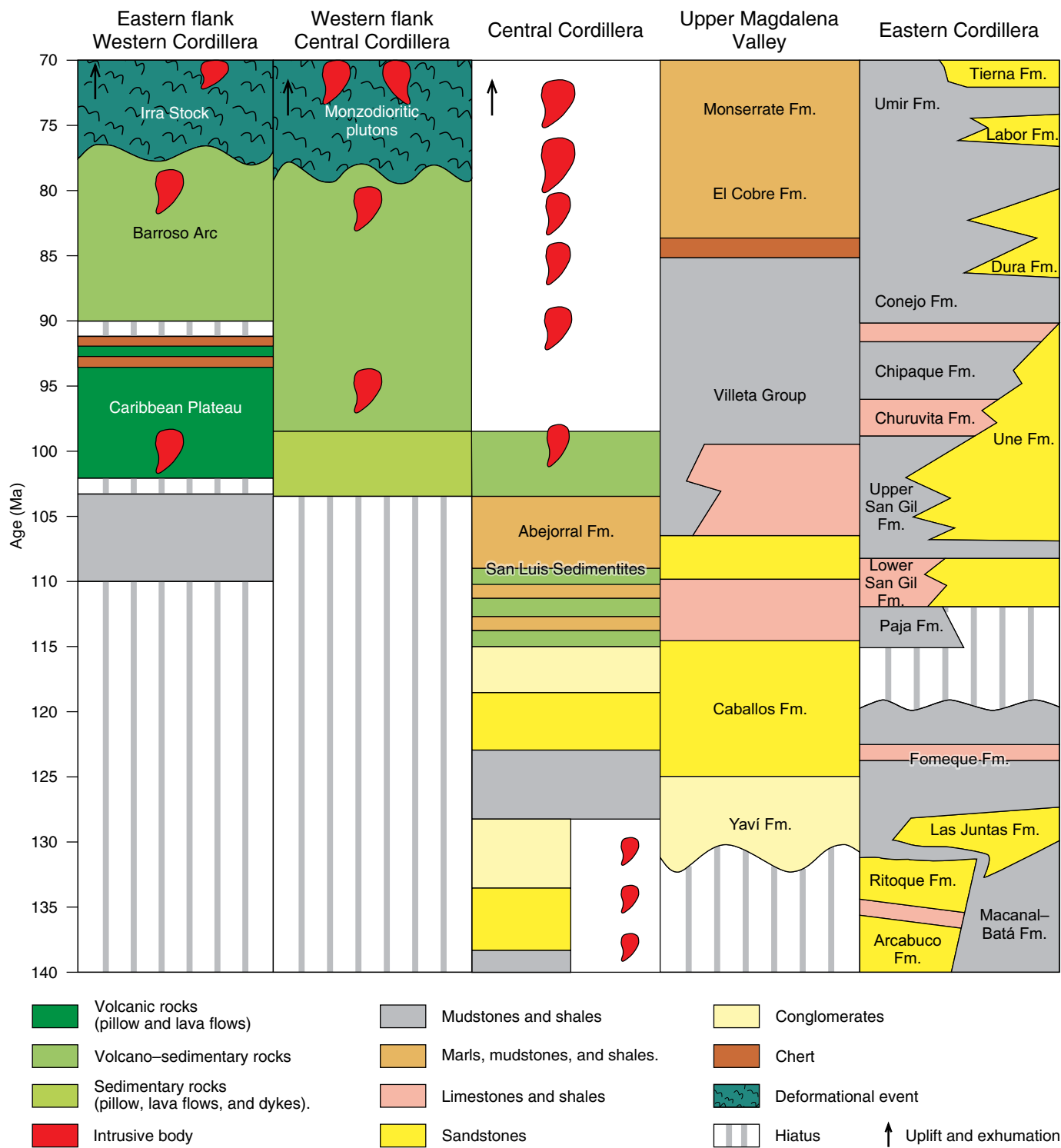
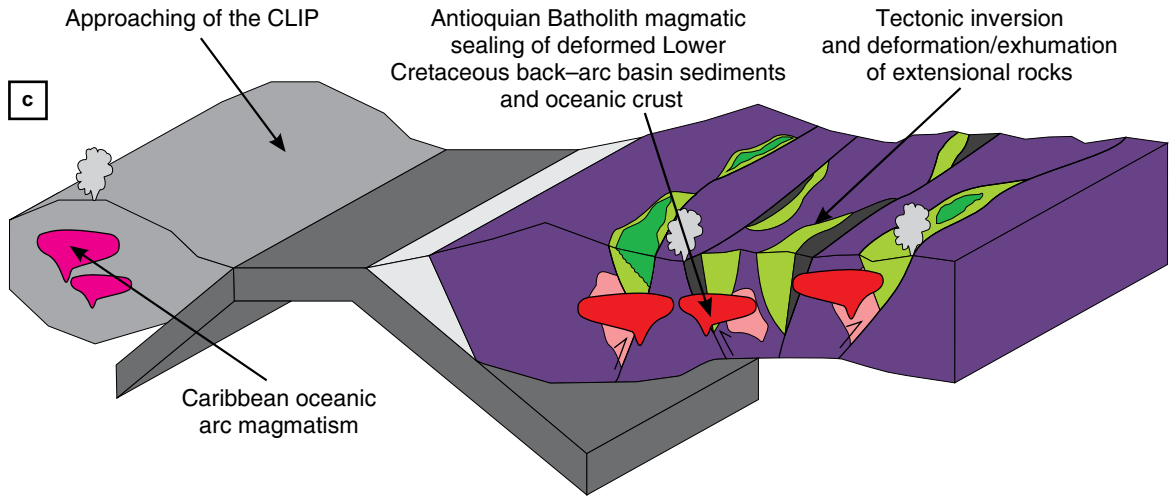


Figure 13. Simplified chronostratigraphic chart of Cretaceous events (after Sarmiento-Rojas et al., 2006; Barrero et al., 2007; Jaramillo et al., 2017). (Fm.) Formation.

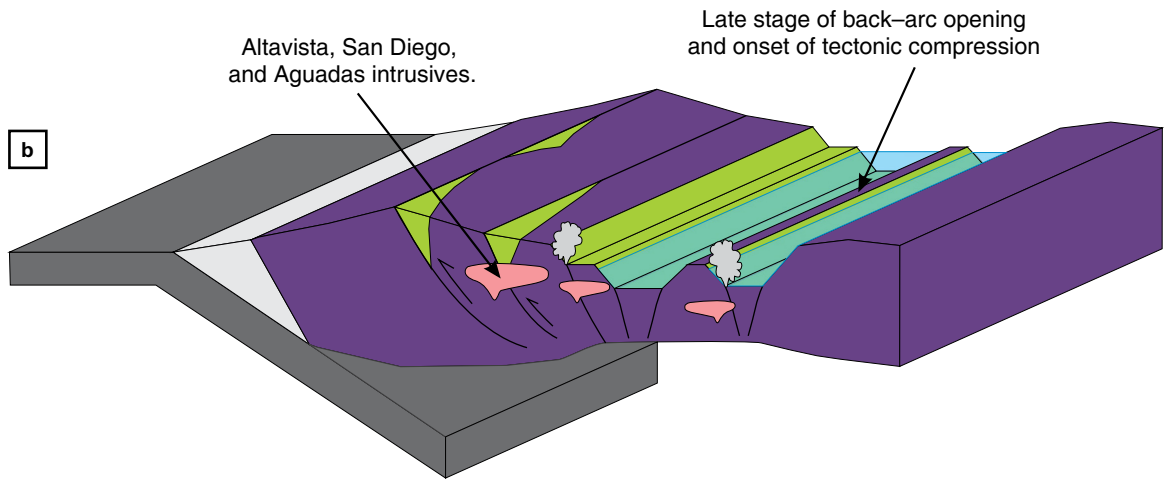
Published detrital zircon geochronological data from the Lower Cretaceous units of the Eastern Cordillera (Horton et al., 2010) show a well-defined dominance of Paleozoic and older sources (>400 Ma), with a prominent Grenvillian age peak (ca. 1000 Ma) and only one individual age from the Early

Cretaceous yielded by the Buenavista Formation (Figure 6). Paleozoic and older zircon U-Pb ages found in the Lower Cretaceous units of the Eastern Cordillera were probably sourced from magmatic and metasedimentary units included as part of the continental basement of eastern Colombia, which is exposed

93–80 Ma



100–93 Ma



125–100 Ma

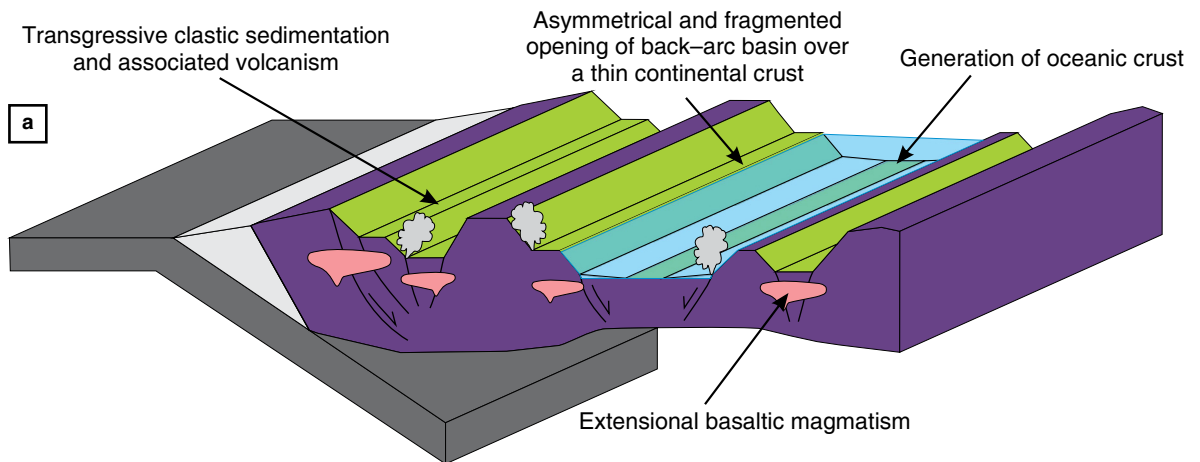


Figure 14. Proposed Cretaceous tectonic scenarios and paleogeography (this contribution; and modifications from Jaramillo et al. (2017) and Zapata et al. (2018)). (CLIP) Caribbean Large Igneous Province.

in the Floresta, Santander, and Quetame Massifs (Horton *et al.*, 2010; Cardona *et al.*, 2016). The diachronic Early Cretaceous opening of basins in the central and eastern Colombian sedimentary systems, together with the remarkable differences in the detrital zircon age populations of the two domains, suggests that these basins were not connected and may represent independent depocenters formed by regional-scale upper-plate asymmetric extension.

Generally, the extensional record of the northern Andes is represented by characteristic marine sedimentation and the quartz-rich compositions of sandstones, which may reflect strong weathering in which not only the climate but also the lack of strong relief and the proximity to the sea level must play major roles.

The formation of extensional basins related to mafic volcanism and ophiolite associations in the Central Cordillera record both intra-arc extension (San Pablo Formation along the axis of the cordillera) and back-arc basin formation (Quebradagrande Complex – Abejorral Formation on the western flank). As the basin opened, a remnant arc was probably left to the east, as suggested by the ca. 129–143 Ma plutons exposed on the eastern flank of the Central Cordillera (Bustamante *et al.*, 2017) and by the detrital geochronology of the Abejorral and San Luis Sedimentites discussed above. The existence of fragments of a western Jurassic remnant arc remains to be discovered.

Similar back-arc scenarios have been proposed from the Upper Jurassic to Lower Cretaceous volcano-sedimentary record of the Cordillera Real of Ecuador (Litherland *et al.*, 1994; Cochrane *et al.*, 2014b; Spikings *et al.*, 2015), as well as from the thermal histories recorded in the Triassic basements of Colombia and Ecuador (Paul *et al.*, 2018). Such correlations suggest that a regional-scale extensional back-arc system was common in the northern Andes during the Early Cretaceous.

Early Cretaceous extensional basins have also been recognized along the entire Andean chain, including the Celica-Lancones and Casma Basins in Perú (Jaillard *et al.*, 1999) as well as other basins in central and southern Chile (Fildani & Hessler, 2005; Ramos, 2010).

The existence of regional-scale back-arc basins, which characterized a Cenozoic Mariana-type style of subduction in the Pacific (Uyeda & Kanamori, 1979), can be related to upper plate motions that favor trench rollback (reviews in Ramos, 2010), the subduction of old oceanic plates, or lateral variations in the buoyancy of the subducted slab (Sdrolias & Müller, 2006; Seton *et al.*, 2016).

In the Andean case, it has been suggested that this tectonic regime is likely related to upper plate kinematic changes associated with the opening of the Atlantic during the Early Cretaceous (Torsvik *et al.*, 2009; Moulin *et al.*, 2010; Ramos, 2010).

5.2. Late Cretaceous Magmatism and Deformation

Both along the axis and on the eastern flank of the Central Cordillera, the Lower Cretaceous siliciclastic rocks from the San Luis Sedimentites, the San Pablo Formation, and the Berlin Sedimentites are folded and affected by low-grade metamorphism with associated neofabrication of mica and are also intruded by the Antioquian Batholith with ages of ca. 90–93 Ma (Leal-Mejía, 2011; Villagómez *et al.*, 2011; this contribution). Such intrusive activity has left a clear contact metamorphic imprint, as evidenced by the growth of metamorphic minerals (e.g., andalusite) lacking any preferentially oriented texture that is imposed over a previously existing foliated fabric. Such cross-cutting relationships clearly constrain a major deformational event that occurred between ca. 100 Ma (Aptian age of sedimentation) and 93 Ma, i.e., the age of the intrusive bodies that cut these units (Figure 14c). As already discussed, there are clear and distinct geochemical and isotopic signals from the older (ca. 98 Ma) plutonic units compared with the youngest <93 Ma granitoid pulses, with the latter showing increased enrichment in the LREE and Th, together with more radiogenic Nd–Sr and $\delta^{18}\text{O}$ values of zircons. This compositional trend reflects more extensive interaction with the older continental basement, which may be in part related to increased crustal thickness caused by the deformational event, as also suggested by relatively steeper La/Yb_N values in the younger rocks. Arc-related volcanism and plutonism continued in the axis and western flank of the Central Cordillera, intruding or overlying rocks from the Quebradagrande Complex between 93 Ma and 78 Ma (Villagómez *et al.*, 2011; Jaramillo *et al.*, 2017; Zapata *et al.*, 2018), and may also have been related to the protracted compressional event that affected former extensional domains.

Although some authors have considered the Late Cretaceous magmatism in the Central Cordillera to represent the record of subduction initiation (Pindell & Kennan, 2009) or to be related to a plume (Whattam & Stern, 2015), the long-term arc-related Cretaceous units discussed here, as well as the continental nature of the host rocks, refute both hypotheses and suggest that an east-vergent subduction zone was active in the northern Andean margin during this time.

5.2.1. On the Discussion of Plausible Tectonic Mechanisms

To date, two different models have been proposed to explain the tectonic mechanisms responsible for this post-Albian event in the Central Cordillera. One model involves the collision of an oceanic arc terrane (Quebradagrande Complex) during which the obduction of a major ophiolitic complex that is currently exposed on the western flank and along the axis of the Cen-

tral Cordillera took place, consequently deforming the Lower Cretaceous siliciclastic sequences (reviews in Toussaint, 1996). The other model suggests that an Early Cretaceous back-arc basin was closed by 114 Ma (Villagómez et al., 2011; Spikings et al., 2015) and was followed by the occurrence of minor magmatism along the continental margin during the Late Cretaceous (Pindell & Kennan, 2009; Spikings et al., 2015).

The results presented in this contribution and the review of published geological, geochemical, and geochronological data favor a model of back-arc basin closure, in which the related ophiolitic bodies represent oceanic crust formed in a supra-subduction zone environment during the back-arc and intra-arc extension. Nevertheless, our interpretation differs in timing from the previously proposed models because in the light of the new data presented here, the time may have been later than ca. 100 Ma, as suggested by the presence of Albian detrital and magmatic zircon U–Pb ages (Cochrane et al., 2014b; Zapata et al., 2018; this contribution). It is also suggested that basin closure caused folding and thickening of the crust, as recorded in the Aptian – Albian sedimentary units, and could also have been responsible for the ca. 100 Ma metamorphism identified on the western flank of the Central Cordillera near the city of Medellín (Restrepo et al., 2012; Rodríguez & Correa-Martínez, 2015).

Similar to the Early Cretaceous event, the Late Cretaceous compressional event in the northern Andes left evidence of its regional-scale nature in the Upper Magdalena Valley of Colombia, where Albian to Cenomanian deformation has been documented by seismic lines (Jaimes & De Freitas, 2006). In addition, in the Ecuadorian Andes, including the eastern Amazon region (Ruiz et al., 2007; Jaillard et al., 2008; Baby et al., 2013), and in Perú and Chile, former extensional and back-arc basins were closed (Atherton & Aguirre, 1992; Fildani et al., 2003).

Geochronological data from the Cretaceous plutonic rocks of the Central Cordillera (Leal-Mejía, 2011; Villagómez et al., 2011; this contribution) as well as the distal pyroclastic record found in the eastern basins of Colombia (Figure 13; Villamil, 1999) suggest that Late Cretaceous (ca. 94–75 Ma) arc magmatism, which ended the ca. 100 Ma deformational episode, was significant in the evolution of the margin. This deformational event and the reinstallation of a productive magmatic arc have been recognized along most of the 85–100 Ma Andean record (Tunik et al., 2010) and may also have resulted from regional-scale plate kinematic modifications, including changes in upper plate velocity, increases in the subduction rates, and changes to more orthogonal convergence between the South American and Caribbean Plates (Ramos, 2010; Matthews et al., 2012; Seton et al., 2012).

The 100–90 Ma subduction initiation along the margins of the Caribbean oceanic plateau, which was part of the Pacific Plate (Whattam & Stern, 2015), must have also changed the mantle flow associated with eastward subduction underneath

South America, which likely prompted plate coupling and deformation in the northern Andes.

Finally, another younger compressional episode in the northern Andes has been related to the ca. 75–70 Ma collision of an allochthonous oceanic terrane against the continental margin (Figure 13; Villagómez & Spikings, 2013; Jaramillo et al., 2017). This exotic oceanic domain includes a Lower to Upper Cretaceous plateau and an associated island arc, which were formed in southern latitudes (Figure 14c; reviews in Zapata et al., 2017; Hincapié-Gómez et al., 2018).

5.3. Paleogeographic Restrictions

Paleogeographic reconstructions of the multiple Cretaceous tectonostratigraphic domains of the northern Andes remain an exciting field of discussion, as the oblique nature of the convergence through the Mesozoic and Cenozoic, including the collision with the Caribbean Plate, provides the possibility of dextral terrane translation along the continental margin (Toussaint, 1996; Pindell et al., 2005; Bayona et al., 2006, 2010; Pindell & Kennan, 2009).

Although specific palinspastic restorations, including the amounts of displacement during the Cretaceous and Cenozoic, have not been precisely quantified, several considerations can constrain the margin-scale configuration.

The Cretaceous oceanic terranes that constitute most of the Western Cordillera were in southwestern positions until ca. 89 Ma, as suggested by their intra-oceanic plateau and arc-related origin as well as some of the available paleomagnetic constraints (reviews in Hincapié-Gómez et al., 2018).

Provenance constraints from the Cretaceous units of the Central Cordillera, including those associated with the Quebradagrande Complex, have shown that these units were associated with a continental domain having a pre-Cretaceous basement similar to that exposed in the cordillera (Nivia et al., 2006; Villagómez et al., 2011; Cochrane et al., 2014b; Jaramillo et al., 2017; Zapata et al., 2018). Moreover, the Cretaceous and older records of the Central Cordillera show remarkable similarities with those of the Cordillera Real in Ecuador (Litherland et al., 1994; Toussaint, 1996; Cochrane et al., 2014b; Spikings et al., 2015).

Therefore, Cretaceous domains in the Central Cordillera would have been located in southern positions (Toussaint, 1996; Pindell & Kennan, 2009), and both the back-arc opening and closure and the subsequent Cenozoic tectonic movements would have contributed to their northward displacements.

6. Conclusions

The integration of new and published data from the Cretaceous record of the Central Cordillera of Colombia provides insights into the feasible regional tectonic scenarios responsible for the

geological evolution of this segment of the northern Colombian Andes during this time. Nevertheless, as one of the main goals of this contribution, specific areas are also identified where the acquisition of more geological data is required in order to test the tectonic evolution discussed here.

Major conclusions that can be reached following the discussion of the results presented in this work are as follows:

- Lithostratigraphic trends and provenance characteristics of the Early Cretaceous siliciclastic units of the Central Cordillera record transgressive basin filling and the erosion of the adjacent metamorphic basement. The high quartz contents of the sandstones are most likely related to intense chemical weathering in the source areas and some sedimentary recycling.
- Detrital zircons and stratigraphic relationships between magmatic and sedimentary rocks of the described units suggest that volcanic activity became significant at the top of the sequence.
- The basin–deepening trend, the geochemical heterogeneity of associated magmatic rocks (arc–like, MORB, and E–MORB signatures), and the relation with ophiolite remnants are interpreted as records of back–arc basin formation.
- The Early Cretaceous arc and back–arc basin system was subsequently deformed and intruded by ca. 90 Ma undeformed arc–related granitoids.
- Similar Early Cretaceous upper–plate basin formation and subsequent Late Cretaceous closure and deformation are documented in eastern Colombia and along most of the entire Andean margin, suggesting regional–scale plate kinematic control for the switch from Mariana– to Andean–style tectonics.

Acknowledgments

We acknowledge the Fundación para la Promoción de la Investigación y la Tecnología del Banco de la República de Colombia project 3451 and the Sistema de Investigación (Hermes) from the Universidad Nacional de Colombia projects 30362 and 25452. The HIP facility at Heidelberg University is operated under the auspices of the DFG Scientific Instrumentation and Information Technology program. Students and researchers associated with EGEO between 2014 and 2018 are especially thanked for fruitful discussions and help during fieldwork. Thoughtful and key reviews and comments from the editor, Victor A. RAMOS, and Robert J. STERN are gratefully acknowledged.

References

- Almeida, J. J. & Villamizar, F. 2012. Petrografía y geoquímica del Batolito Antioqueño en un sector del municipio Santa Rosa de Osos, Antioquia. Bachelor thesis, Universidad Industrial de Santander, 88 p. Bucaramanga.
- Álvarez, J. 1987. Geología del Complejo Ofiolítico de Pácora y secuencias relacionadas de arco de islas (Complejo Quebradagrande), Colombia. Ingeominas, Internal report 2027, 81 p. Medellín.
- Álvarez, J., Rico, H., Vásquez, H., Hall, R. & Blade, L. 1975. Geologic map of the Yarumal quadrangle (H–8) and part of the Ituango quadrangle (H–7), Colombia. Scale 1:100 000. Ingeominas & U.S. Geological Survey. <https://doi.org/10.3133/i842>
- Amelin, Y., Krot, A.N., Hutcheon, I.D. & Ulyanov, A.A. 2002. Lead isotopic ages of chondrules and calcium–aluminum–rich inclusions. *Science*, 297(5587): 1678–1683. <https://doi.org/10.1126/science.1073950>
- Arévalo, O.J., Mojica, J. & Patarroyo, P. 2001. Sedimentitas del Aptiano tardío al sur de Pijao, quebrada La Maizena, flanco occidental de la cordillera Central, departamento del Quindío, Colombia. *Geología Colombiana*, 26: 29–43.
- Atherton, M. & Aguirre, L. 1992. Thermal and geotectonic setting of Cretaceous volcanic rocks near Ica, Perú, in relation to Andean crustal thinning. *Journal of South American Earth Sciences*, 5(1): 47–69. [https://doi.org/10.1016/0895-9811\(92\)90059-8](https://doi.org/10.1016/0895-9811(92)90059-8)
- Baby, P., Rivadeneira, M., Barragan, R. & Christophoul, F. 2013. Thick–skinned tectonics in the Oriente foreland basin of Ecuador. In: Nemčok, M., Mora, A. & Cosgrove, J.W. (editors), Thick–skinned–dominated orogens: From initial inversion to full accretion. Geological Society of London, Special Publication 377, p. 59–76. <https://doi.org/10.1144/SP377.1>
- Baertschi, P. 1976. Absolute ¹⁸O content of standard mean ocean water. *Earth and Planetary Science Letters*, 31(3): 341–344. [https://doi.org/10.1016/0012-821X\(76\)90115-1](https://doi.org/10.1016/0012-821X(76)90115-1)
- Barrero, D. & Vesga, C.J. 1976. Mapa geológico del cuadrángulo K–9 Armero y mitad sur del J–9 La Dorada. Scale 1:100 000. Ingeominas. Bogotá.
- Barrero, D., Pardo, A., Vargas, C. A., & Martínez, J. F. 2007. Colombian sedimentary basins: Nomenclature, boundaries and petroleum geology, a new proposal. *Agencia Nacional de Hidrocarburos*, 92 p. Bogotá.
- Bayona, G., Rapalini, A. & Costanzo–Álvarez, V. 2006. Paleomagnetism in Mesozoic rocks of the northern Andes and its implications in Mesozoic tectonics of northwestern South America. *Earth, Planets and Space*, 58(10): 1255–1272. <https://doi.org/10.1186/BF03352621>
- Bayona, G., Jiménez, G., Silva, C., Cardona, A., Montes, C., Roncancio, J. & Cordani, U. 2010. Paleomagnetic data and K–Ar ages from Mesozoic units of the Santa Marta massif: A preliminary interpretation for block rotation and translations. *Journal of South American Earth Sciences*, 29(4): 817–831. <https://doi.org/10.1016/j.jsames.2009.10.005>
- Blanco–Quintero, I.F., García–Casco, A., Toro–Toro, L.M., Moreno, M., Ruiz, E.C., Vinasco, C.J., Cardona, A., Lázaro, C. & Morata, D. 2014. Late Jurassic terrane collision in the northwestern margin of Gondwana (Cajamarca Complex, eastern flank of the Central Cordillera, Colombia). *International Geology*

- Review, 56(15): 1852–1872. <https://doi.org/10.1080/00206814.2014.963710>
- Botero, G. 1963. Contribución al conocimiento de la geología de la zona central de Antioquia. Universidad Nacional de Colombia, Anales de la Facultad de Minas, 57, 101 p. Medellín.
- Botero, G. & González, H. 1983. Algunas localidades fosilíferas cretáceas de la cordillera Central, Antioquia y Caldas, Colombia. *Geología Norandina*, (7): 15–28.
- Busby, C.J. 2012. Extensional and transtensional continental ARC basins: Case studies from the southwestern United States. In: Busby, C. & Azor, A. (editors), *Tectonics of sedimentary basins: Recent advances*. Wiley–Blackwell, p. 382–404. <https://doi.org/10.1002/9781444347166.ch19>
- Bustamante, A., Juliani, C.M., Hall, C.M. & Essene, E.J. 2011. $^{40}\text{Ar}/^{39}\text{Ar}$ ages from blueschists of the Jambaló region, Central Cordillera of Colombia: Implications on the styles of accretion in the Northern Andes. *Geologica Acta*, 9(3–4): 351–362. <http://dx.doi.org/10.1344/105.000001697>
- Bustamante, C., Archanjo, C.J., Cardona, A. & Vervoort, J.D. 2016. Late Jurassic to Early Cretaceous plutonism in the Colombian Andes: A record of long-term arc maturity. *Geological Society of America Bulletin*, 128(11–12): 1762–1779. <https://doi.org/10.1130/B31307.1>
- Bustamante, C., Archanjo, C.J., Cardona, A., Bustamante, A. & Valencia, V. 2017. U–Pb ages and Hf isotopes in zircons from parautochthonous Mesozoic terranes in the western margin of Pangea: Implications for the terrane configurations in the northern Andes. *The Journal of Geology*, 125(5): 487–500. <https://doi.org/10.1086/693014>
- Campos–Álvarez, N.O. & Roser, B.P. 2007. Geochemistry of black shales from the Lower Cretaceous Paja Formation, Eastern Cordillera, Colombia: Source weathering, provenance, and tectonic setting. *Journal of South American Earth Sciences*, 23(4): 271–289. <https://doi.org/10.1016/j.jsames.2007.02.003>
- Cardona, A., Valencia, V.A., Lotero, A., Villafañez, Y. & Bayona, G. 2016. Provenance of middle to late Palaeozoic sediments in the northeastern Colombian Andes: Implications for Pangea reconstruction. *International Geology Review*, 58(15): 1914–1939. <https://doi.org/10.1080/00206814.2016.1190948>
- Cawood, P.A., Kröner, A., Collins, W.J., Kusky, T.M., Mooney, W.D. & Windley, B.F. 2009. Accretionary orogens through Earth history. In: Cawood, P.A. & Kröner, A. (editors), *Earth Accretionary Systems in Space and Time*. Geological Society of London, Special Publication 318, p. 1–36. <https://doi.org/10.1144/SP318.1>
- Cediel, F., Shaw, R.P. & Cáceres, C. 2003. Tectonic assembly of the northern Andean block. In: Bartolini, C., Buffer, R.T. & Blickwede, J. (editors), *The circum-Gulf of Mexico and the Caribbean: Hydrocarbon habitats, basin formation, and plate tectonics*. American Association of Petroleum Geologists, Memoir 79, 815–848. Tulsa, USA.
- Chang, Z., Vervoort, J.D., McClelland, W.C. & Knaack, C. 2006. U–Pb dating of zircon by LA–ICP–MS. *Geochemistry, Geophysics, Geosystems*, 7(5): 1–14. <https://doi.org/10.1029/2005GC001100>
- Chapman, J.B., Ducea, M.N., Kapp, P., Gehrels, G.E. & DeCelles, P.G. 2017. Spatial and temporal radiogenic isotopic trends of magmatism in Cordilleran orogens. *Gondwana Research*, 48: 189–204. <https://doi.org/10.1016/j.gr.2017.04.019>
- Cochrane, R. 2013. U–Pb thermochronology, geochronology and geochemistry of NW South America: Rift to drift transition, active margin dynamics and implications for the volume balance of continents. Doctoral thesis, University of Geneva, 118 p. Geneva.
- Cochrane, R., Spikings, R., Gerdes, A., Ulianov, A., Mora, A., Villagómez, D., Putlitz, B. & Chiaradia, M. 2014a. Permo–Triassic anatexis, continental rifting and the disassembly of western Pangea. *Lithos*, 190–191: 383–402. <https://doi.org/10.1016/j.lithos.2013.12.020>
- Cochrane, R., Spikings, R., Gerdes, A., Winkler, W., Ulianov, A., Mora, A. & Chiaradia, M. 2014b. Distinguishing between in-situ and accretionary growth of continents along active margins. *Lithos*, 202–203: 382–394. <https://doi.org/10.1016/j.lithos.2014.05.031>
- Correa, A.M., Pimentel, M., Restrepo, J.J., Nilson, A., Ordoñez, O., Martens, U., Laux, J.E. & Junges, S. 2006. U–Pb zircon ages and Nd–Sr isotopes of the Altavista Stock and the San Diego Gabbro: New insights on Cretaceous arc magmatism in the Colombian Andes. V South American Symposium on Isotope Geology. *Memoirs*, p. 84–86. Punta del Este, Uruguay.
- DeGraaff–Surpless, K., Graham, S.A., Wooden, J.L. & McWilliams, M.O. 2002. Detrital zircon provenance analysis of the Great Valley Group, California: Evolution of an arc–forearc system. *Geological Society of America Bulletin*, 114(12): 1564–1580. [https://doi.org/10.1130/0016-7606\(2002\)114<1564:DZ-PAOT>2.0.CO;2](https://doi.org/10.1130/0016-7606(2002)114<1564:DZ-PAOT>2.0.CO;2)
- Dickinson, W.R. & Gehrels, G.E. 2009. Use of U–Pb ages of detrital zircons to infer maximum depositional ages of strata: A test against a Colorado Plateau Mesozoic database. *Earth and Planetary Science Letters*, 288(1–2): 115–125. <https://doi.org/10.1016/j.epsl.2009.09.013>
- Dott Jr., R.H. 2003. The importance of eolian abrasion in supermature quartz sandstone and the paradox of weathering on vegetation-free landscapes. *The Journal of Geology*, 111(4): 387–405. <https://doi.org/10.1086/375286>
- Duarte, E., Cardona, A., Lopera, S., Valencia, V. & Estupiñan, H., 2018. Provenance and diagenesis from two stratigraphic sections of the Lower Cretaceous Caballos Formation in the Upper Magdalena Valley: Geological and reservoir quality implications. *Ciencia, Tectonología y Futuro*, 8 (1): 5–29.
- Dufrane, S.A., Vervoort, J.D. & Hart, G.L. 2007. Uncertainty of Hf isotope analysis in zircon using LA–MC–ICPMS techniques: Full disclosure. 17th Annual V.M. Goldschmidt Conference, Cologne, Germany. *Geochimica et Cosmochimica Acta*, 71(15): 241.

- Duque-Trujillo, J., Bustamante, C., Solari, L., Gómez-Mafla, Á., Toro-Villegas, G., & Hoyos, S. 2018. Reviewing the Antioquia Batholith and satellite bodies: A record of Late Cretaceous to Eocene syn- to post-collisional arc magmatism in the Central Cordillera of Colombia: *Andean Geology*, 46(1): 82–101. <http://dx.doi.org/10.5027/andgeoV46n1-3120>
- Etayo-Serna, F. 1985. Documentación paleontológica del Infracretácico de San Felix y Valle Alto, cordillera Central. In: Etayo-Serna, F. & Laverde, F. (editors), *Proyecto Cretácico: Contribuciones. Publicaciones Geológicas Especiales del Ingeominas 16*, p. XXV–1–XXV–7. Bogotá.
- Etayo-Serna, F., Renzoni, G. & Barrero, D. 1969. Contornos sucesivos del mar cretáceo en Colombia. *Primer Congreso Colombiano de Geología. Memoirs*, p. 217–252. Bogotá.
- Feininger, T. & Botero, G. 1982. The Antioquian Batholith, Colombia. *Publicaciones Geológicas Especiales del Ingeominas 12*, p. 1–50. Bogotá.
- Feininger, T., Barrero, D. & Castro, N. 1972. Geología de parte de los departamentos de Antioquia y Caldas (sub-zona II–B). *Boletín Geológico*, 20(2): 1–173.
- Fildani, A. & Hessler, A.M. 2005. Stratigraphic record across a retroarc basin inversion: Rocas Verdes–Magallanes Basin, Patagonian Andes, Chile. *Geological Society of America Bulletin*, 117(11–12): 1596–1614. <https://doi.org/10.1130/B25708.1>
- Fildani, A., Cope, T.D., Graham, S.A. & Wooden, J.L. 2003. Initiation of the Magallanes Foreland Basin: Timing of the southernmost Patagonian Andes Orogeny revised by detrital zircon provenance analysis. *Geology*, 31(12): 1081–1084. <https://doi.org/10.1130/G20016.1>
- Folk, R. 1974. *Petrology of sedimentary rocks*. Hemphill Publishing Company, 182 p. Austin, USA.
- García-Ramírez, C.A., Ríos-Reyes, C.A., Castellanos–Alarcón, O.M. & Mantilla–Figueroa, L.C. 2017. Petrology, geochemistry and geochronology of the Arquía Complex’s metabasites at the Pijao–Génova sector, Central Cordillera, Colombian Andes. *Boletín de Geología*, 39(1): 105–126. <http://dx.doi.org/10.18273/revbol.v39n1-2017005>
- Garzanti, E. 2016. From static to dynamic provenance analysis—sedimentary petrology upgraded. *Sedimentary Geology*, 336: 3–13. <https://doi.org/10.1016/j.sedgeo.2015.07.010>
- Gómez-Cruz, A.d.J., Moreno-Sánchez, M. & Pardo-Trujillo, A. 1995. Edad y origen del “Complejo Metasedimentario Aranzazu–Manizales” en los alrededores de Manizales (departamento de Caldas, Colombia). *Geología Colombiana*, 19: 83–93.
- Gómez-Cruz, A.d.J., Moreno-Sánchez, M. & Pardo-Trujillo, A. 2002. Afloramientos fosilíferos del Cretácico Superior en el municipio de Pijao (borde occidental de la cordillera Central, Colombia). *Geo-Eco-Trop*, 26(2): 41–50.
- Gómez, J., Montes, N., Nivia, Á. & Diederix, H., compiladores. 2015. *Geological Map of Colombia 2015*. Scale 1:1 000 000. Servicio Geológico Colombiano, 2 sheets. Bogotá.
- Gómez, P.D. & Lizcano, A. 1990. Estudio tectónico–estratigráfico de la franja sedimentaria cretácea de Berlín, Caldas, cordillera Central. Bachelor thesis, Universidad Industrial de Santander, 120 p. Bucaramanga.
- González, H. 1980. Geología de las planchas 167 Sonsón y 187 Salamina. Scale 1:100 000. Ingeominas, Internal report 1760, 262 p. Medellín.
- González, H. 2001. Memoria explicativa: Mapa geológico del departamento de Antioquia. Scale 1:400 000. Ingeominas, 240 p. Medellín.
- Gradstein, F.M., Ogg, J.G. & Hilgen, F.J. 2012. On the geologic time scale. *Newsletters on Stratigraphy*, 45(2): 171–188. <https://doi.org/10.1127/0078-0421/2012/0020>
- Grosse, E. 1926. Estudio geológico del terciario carbonífero de Antioquia en la parte occidental de la cordillera Central de Colombia, entre el río Arma y Sacaoyal, ejecutado en los años de 1920–1923. Dietrich Reimer, 361 p. Berlin.
- Hall, R.B., Álvarez, J. & Rico, H. 1972. Geología de los departamentos de Antioquia y Caldas (subzona II–A). *Boletín Geológico*, 20(1): 1–85.
- Hincapié–Gómez, S., Cardona, A., Jiménez, G., Monsalve, G., Ramírez–Hoyos, L. & Bayona, G. 2018. Paleomagnetic and gravimetric reconnaissance of Cretaceous volcanic rocks from the western Colombian Andes: Paleogeographic connections with the Caribbean Plate. *Studia Geophysica et Geodaetica*, 62(3): 485–511. <https://doi.org/10.1007/s11200-016-0678-y>
- Horton, B.K. 2018. Tectonic regimes of the central and southern Andes: Responses to variations in plate coupling during subduction. *Tectonics*, 37(2): 402–429. <https://doi.org/10.1002/2017TC004624>
- Horton, B.K., Saylor, J.E., Nie, J., Mora, A., Parra, M., Reyes–Harker, A. & Stockli, D.F. 2010. Linking sedimentation in the northern Andes to basement configuration, Mesozoic extension, and Cenozoic shortening: Evidence from detrital zircon U–Pb ages, Eastern Cordillera, Colombia. *Geological Society of America Bulletin*, 122(9–10): 1423–1442. <https://doi.org/10.1130/B30118.1>
- Ibañez–Mejía, M., Tassinari, C.C.G. & Jaramillo–Mejía, J.M. 2007. U–Pb zircon ages of the “Antioquian Batholith”: Geochronological constraints of late Cretaceous magmatism in the central Andes of Colombia. XI Congreso Colombiano de Geología. Abstracts, 11 p. Bucaramanga.
- Ickert, R.B., Hiess, J., Williams, I.S., Holden, P., Ireland, T.R., Lanc, P., Schram, N., Foster, J.J. & Clement, S.W. 2008. Determining high precision, in situ, oxygen isotope ratios with a SHRIMP II: Analyses of MPI–DING silicate–glass reference materials and zircon from contrasting granites. *Chemical Geology*, 257(1–2): 114–128. <https://doi.org/10.1016/j.chemgeo.2008.08.024>
- Irvine, T.N. & Baragar, W.R.A. 1971. A guide to the chemical classification of the common volcanic rocks. *Canadian Journal of Earth Sciences*, 8(5): 523–548. <https://doi.org/10.1139/e71-055>

- Jaillard, E., Laubacher, G., Bengston, P., Dhondt, A.V. & Bulot, L.G. 1999. Stratigraphy and evolution of the Cretaceous forearc Celica-Lancones Basin of southwestern Ecuador. *Journal of South American Earth Sciences*, 12(1): 51–68. [https://doi.org/10.1016/S0895-9811\(99\)00006-1](https://doi.org/10.1016/S0895-9811(99)00006-1)
- Jaillard, E., Bengston, P., Ordóñez, M., Vaca, W., Dhondt, A., Suárez, J. & Toro, J. 2008. Sedimentary record of terminal Cretaceous accretions in Ecuador: The Yunguilla Group in the Cuenca area. *Journal of South American Earth Sciences*, 25(2): 133–144. <https://doi.org/10.1016/j.jsames.2007.08.002>
- Jaimes, E. & De Freitas, M. 2006. An Albian–Cenomanian unconformity in the northern Andes: Evidence and tectonic significance. *Journal of South American Earth Sciences*, 21(4): 466–492. <https://doi.org/10.1016/j.jsames.2006.07.011>
- Janoušek, V., Farrow, C.M. & Erban, V. 2006. Interpretation of whole-rock geochemical data in igneous geochemistry: Introducing geochemical data toolkit (GCDkit). *Journal of Petrology*, 47(6): 1255–1259. <https://doi.org/10.1093/petrology/egl013>
- Jaramillo, J.S., Cardona, A., León, S., Valencia, V. & Vinasco, C. 2017. Geochemistry and geochronology from Cretaceous magmatic and sedimentary rocks at 6° 35' N, western flank of the Central Cordillera (Colombian Andes): Magmatic record of arc growth and collision. *Journal of South American Earth Sciences*, 76: 460–481. <https://doi.org/10.1016/j.jsames.2017.04.012>
- Kammer, A. & Sánchez, J. 2006. Early Jurassic rift structures associated with the Soapaga and Boyacá faults of the Eastern Cordillera, Colombia: Sedimentological inferences and regional implications. *Journal of South American Earth Sciences*, 21(4): 412–422. <https://doi.org/10.1016/j.jsames.2006.07.006>
- Kerr, A.C., Marriner, G.F., Tarney, J., Nivia, Á., Saunders, A.D., Thirlwall, M.F. & Sinton, C.W. 1997. Cretaceous basaltic terranes in western Colombia: Elemental, chronological and Sr–Nd isotopic constraints on petrogenesis. *Journal of Petrology*, 38(6): 677–702. <https://doi.org/10.1093/petrology/38.6.677>
- Lackey, J.S., Valley, J.W. & Saleeby, J.B. 2005. Supracrustal input to magmas in the deep crust of Sierra Nevada Batholith: Evidence from high- $\delta^{18}\text{O}$ zircon. *Earth and Planetary Science Letters*, 235(1–2): 315–330. <https://doi.org/10.1016/j.epsl.2005.04.003>
- Leal-Mejía, H. 2011. Phanerozoic gold metallogeny in the Colombian Andes: A tectono-magmatic approach. Doctoral thesis, Universitat de Barcelona, 989 p. Barcelona.
- León, S., Cardona, A., Parra, M., Sobel, E.R., Jaramillo, J.S., Glodny, J., Valencia, V., Chew, D., Montes, C., Posada, G., Monsalve, G. & Pardo-Trujillo, A. 2018. Transition from collisional to subduction-related regimes: An example from Neogene Panama–Nazca–South–America interactions. *Tectonics*, 37(1): 119–139. <https://doi.org/10.1002/2017TC004785>
- Litherland, M., Aspden, J.A. & Jemielita, R.A. 1994. The metamorphic belts of Ecuador. Overseas Memoir of the British Geological Survey 11, 147 p. Nottingham, England.
- Lozano, H., Pérez, H. & Mosquera, D. 1975. Prospección geoquímica en los municipios de Salento, Quindío y Cajamarca, Tolima. Ingeominas, Internal report 1692, 103 p. Bogotá.
- Ludwig, K.R. 2003. “User’s Manual for Isoplot/Ex, Version 3.00. A Geochronological Toolkit for Microsoft Excel,” Berkeley Geochronology Center. Special Publication 4(2), 70 p. Berkeley, USA.
- Marsaglia, K.M. 2012. Sedimentation at plate boundaries in transition. In: Busby, C. & Azor, A. (editors), *Tectonics of sedimentary basins: Recent advances*. Blackwell Publishing Ltd, p 291–309. <https://doi.org/10.1002/9781444347166.ch14>
- Martens, U.C., Restrepo, J.J. & Solari, L.A. 2012. Sinifaná metasedimentites and relations with Cajamarca paragneisses of the Central Cordillera of Colombia. *Boletín de Ciencias de la Tierra*, (32): 99–110.
- Martens, U., Restrepo, J.J., Ordóñez-Carmona, O. & Correa-Martínez, A.M. 2014. The Tahamí and Anacona Terranes of the Colombian Andes: Missing links between the South American and Mexican Gondwana margins. *The Journal of Geology*, 122(5): 507–530. <https://doi.org/10.1086/677177>
- Matthews, K.J., Seton, M. & Müller, R.D. 2012. A global-scale plate reorganization event at 105–100 Ma. *Earth and Planetary Science Letters*, 355–356: 283–298. <https://doi.org/10.1016/j.epsl.2012.08.023>
- Maya, M. & González, H. 1995. Unidades litodémicas en la cordillera Central de Colombia. *Boletín Geológico*, 35(2–3): 43–57.
- Mejía-Velásquez, P.J., Dilcher, D.L., Jaramillo, C.A., Fortini, L.B. & Manchester, S.R. 2012. Palynological composition of a Lower Cretaceous South American tropical sequence: Climatic implications and diversity comparisons with other latitudes. *American Journal of Botany*, 99(11): 1819–1827. <https://doi.org/10.3732/ajb.1200135>
- Middlemost, E.A.K. 1994. Naming materials in the magma/igneous rock system. *Earth-Science Reviews*, 37(3–4): 215–224. [https://doi.org/10.1016/0012-8252\(94\)90029-9](https://doi.org/10.1016/0012-8252(94)90029-9)
- Montes, C., Guzmán, G., Bayona, G., Cardona, A., Valencia, V. & Jaramillo, C. 2010. Clockwise rotation of the Santa Marta Massif and simultaneous Paleogene to Neogene deformation of the Plato–San Jorge and Cesar–Ranchería Basins. *Journal of South American Earth Sciences*, 29(4): 832–848. <https://doi.org/10.1016/j.jsames.2009.07.010>
- Moreno, J.M. 1990. Stratigraphy of the Lower Cretaceous Rosablanca and Cumbre Formations, Utica Sandstone and Murca Formation, west flank, Eastern Cordillera, Colombia. *Geología Colombiana*, 17: 65–86.
- Moreno, J.M. 1991. Provenance of the Lower Cretaceous sedimentary sequences, central part, Eastern Cordillera, Colombia. *Revista de la Academia Colombiana de Ciencias Exactas, Físicas y Naturales*, 18(69): 159–173.
- Moreno-Sánchez, M. & Pardo-Trujillo, A. 2003. Stratigraphical and sedimentological constraints on western Colombia: Implications on the evolution of the Caribbean Plate. In: Bartolini,

- C., Buffler, R.T. & Blickwede, J. (editors), The circum-Gulf of Mexico and the Caribbean: Hydrocarbon habitats, basin formation, and plate tectonics. American Association of Petroleum Geologists, Memoir 79, p. 891–924. Tulsa, USA.
- Moreno-Sánchez, M., Gómez-Cruz, A.d.J. & Toro-Toro, L.M. 2008. Proveniencia del material clástico del Complejo Quebradagrande y su relación con los complejos estructurales adyacentes. *Boletín de Ciencias de la Tierra*, (22): 27–38.
- Moulin, M., Aslanian, D. & Unternehr, P. 2010. A new starting point for the south and equatorial Atlantic Ocean. *Earth–Science Reviews*, 98(1–2): 1–37. <https://doi.org/10.1016/j.earsci-rev.2009.08.001>
- Nakamura, N., 1974. Determination of REE, Ba, Fe, Mg, Na, and K in carbonaceous and ordinary chondrites. *Geochimica et Cosmochimica Acta*, 38(5): 757–775. [https://doi.org/10.1016/0016-7037\(74\)90149-5](https://doi.org/10.1016/0016-7037(74)90149-5)
- Naranjo, J.L. 1983. Investigación del potencial uranífero en los shales negros del Sinclinal de Berlín, departamento de Caldas. Bachelor thesis, Universidad Nacional de Colombia, 98 p. Bogotá.
- Nivia, Á., Marriner, G.F., Kerr, A.C. & Tarney, J. 2006. The Quebradagrande Complex: A Lower Cretaceous ensialic marginal basin in the Central Cordillera of the Colombian Andes. *Journal of South American Earth Sciences*, 21(4): 423–436. <https://doi.org/10.1016/j.jsames.2006.07.002>
- Ordóñez-Carmona, O. & Pimentel, M.M. 2001. Consideraciones geocronológicas e isotópicas del Batolito Antioqueño. *Revista de la Academia Colombiana de Ciencias Exactas, Físicas y Naturales*, 25(94): 27–35.
- Ordóñez-Carmona, O., Pimentel, M.M. & Angel-Cárdenas, P. 2001. Consideraciones geocronológicas e isotópicas preliminares del magmatismo cretáceo-paleoceno en el norte de la cordillera Central. VIII Congreso Colombiano de Geología. *Memoirs*, 5 p. Manizales.
- Ordóñez-Carmona, O., Pimentel, M.M., Frantz, J.C. & Chemale, F.F. 2007. Edades U–Pb convencionales de algunas intrusiones colombianas. XI Congreso Colombiano de Geología. Abstracts, p. 45. Bucaramanga.
- Paul, A.N., Spikings, R.A., Ulianov, A. & Ovtcharova, M. 2018. High temperature (>350° C) thermal histories of the long lived (>500 Ma) active margin of Ecuador and Colombia: Apatite, titanite and rutile U–Pb thermochronology. *Geochimica et Cosmochimica Acta*, 228: 275–300. <https://doi.org/10.1016/j.gca.2018.02.033>
- Pearce, J.A. 2008. Geochemical fingerprinting of oceanic basalts with applications to ophiolite classification and the search for Archean oceanic crust. *Lithos*, 100(1–4): 14–48. <https://doi.org/10.1016/j.lithos.2007.06.016>
- Pearce, J.A., Harris, N.B.W. & Tindle, A.G. 1984. Trace element discrimination diagrams for the tectonic interpretation of granitic rocks. *Journal of Petrology*, 25(4): 956–983. <https://doi.org/10.1093/petrology/25.4.956>
- Peccerillo, A. & Taylor, S.R. 1976. Geochemistry of Eocene calc-alkaline volcanic rocks from the Kastamonu area, northern Turkey. *Contributions to Mineralogy and Petrology*, 58(1): 63–81. <https://doi.org/10.1007/BF00384745>
- Pimiento, R. 2011. Mineralogía y petrografía de la mineralización de uranio en fosforitas del Cretácico Inferior, Sinclinal de Berlín, cordillera Central (departamento de Caldas, Colombia). Bachelor thesis, Universidad Industrial de Santander, 156 p. Bucaramanga.
- Pindell, J., Kennan, L., Maresch, W.V., Stanek, K.P., Draper, G. & Higgs, R. 2005. Plate-kinematics and crustal dynamics of circum-Caribbean arc-continent interactions: Tectonic controls on basin development in proto-Caribbean margins. In: Avé-Lallemant, H.G. & Sisson, V.B. (editors), *Caribbean–South American Plate interactions, Venezuela*. Geological Society of America, Special Paper 394, p. 7–52. <https://doi.org/10.1130/0-8137-2394-9.7>
- Pindell, J.L. & Kennan, L. 2009. Tectonic evolution of the Gulf of Mexico, caribbean and northern South America in the mantle reference frame: An update. In: James, K.H., Lorente, M.A. & Pindell, J.L. (editors), *The origin and evolution of the Caribbean Plate*. Geological Society of London, Special Publication 328, p. 1–55. <https://doi.org/10.1144/SP328.1>
- Quiroz, L. 2005. Cartografía y análisis estratigráfico de las formaciones Valle Alto y Abejorral en la región de San Félix, departamento de Caldas, Colombia. Bachelor thesis, Universidad Nacional de Colombia, 53 p. Bogotá.
- Ramos, V.A. 2009. Anatomy and global context of the Andes: Main geologic features and the Andean orogenic cycle. In: Kay, S.M., Ramos, V.A. & Dickinson, W.R. (editors), *Backbone of the Americas: Shallow subduction, plateau uplift, and ridge and terrane collision*. Geological Society of America, *Memoirs* 204, p. 31–65. [https://doi.org/10.1130/2009.1204\(02\)](https://doi.org/10.1130/2009.1204(02))
- Ramos, V.A. 2010. The tectonic regime along the Andes: Present-day and Mesozoic regimes. *Geological Journal*, 45(1): 2–25. <https://doi.org/10.1002/gj.1193>
- Rendón, D.A. 1999. Cartografía y caracterización de las unidades geológicas de la zona urbana de Medellín. Bachelor thesis, Universidad Nacional de Colombia, 113 p. Medellín.
- Restrepo, J.J., Ordóñez-Carmona, O. & Moreno-Sánchez, M. 2009. A comment on “The Quebradagrande Complex: A Lower Cretaceous ensialic marginal basin in the Central Cordillera of the Colombian Andes” by Nivia et al. *Journal of South American Earth Sciences*, 28(2): 204–205. <https://doi.org/10.1016/j.jsames.2009.03.004>
- Restrepo, J.J., Ordóñez-Carmona, O., Armstrong, R. & Pimentel, M.M. 2011. Triassic metamorphism in the northern part of the Tahamí Terrane of the Central Cordillera of Colombia. *Journal of South American Earth Sciences*, 32(4): 497–507. <https://doi.org/10.1016/j.jsames.2011.04.009>
- Restrepo, J.J., Ibañez-Mejía, M. & García-Casco, A. 2012. U–Pb zircon ages of the Medellín Amphibolites (Central Cordillera

- of Colombia) reveal mid-Cretaceous tectonic juxtaposition of Triassic and mid-Cretaceous metamorphic complexes. VIII South American Symposium on Isotope Geology. USB memory device, 33 slides. Medellín.
- Restrepo-Moreno, S.A. 2009. Long-term morphotectonic evolution and denudation chronology of the Antioqueño Plateau, Cordillera Central, Colombia. Doctoral Thesis. University of Florida, 223 p. Gainesville, USA.
- Restrepo-Moreno, S., Foster, D.A. & Kamenov, G. 2007. Formation age and magma sources for the Antioqueño Batholith derived from LA-ICP-MS uranium-lead dating and hafnium-isotope analysis of zircon grains. *GSA Meeting 2007*, 39(6): p. 493. Denver, CO, USA.
- Robertson, A.H.F. 1994. Role of the tectonic facies concept in orogenic analysis and its application to Tethys in the eastern Mediterranean region. *Earth-Science Reviews*, 37(3-4): 139-213. [https://doi.org/10.1016/0012-8252\(94\)90028-0](https://doi.org/10.1016/0012-8252(94)90028-0)
- Rodríguez, C. & Rojas, R. 1985. Estratigrafía y tectónica de la serie infracretácica en los alrededores de San Felix, cordillera Central de Colombia. In: Etayo-Serna, F. & Laverde-Montaño, F. (editors), *Proyecto Cretácico: Contribuciones*. Publicaciones Geológicas Especiales del Ingeominas 16, p. XXIV-1-XXI-21. Bogotá.
- Rodríguez, G. & Celada-Arango, C.M. 2018. Basaltos de San Pablo: un bloque de un arco de islas en el norte de la cordillera Central de Colombia. *Caracterización petrográfica y química*. *Boletín de Geología*, 40(2): 69-85. <https://doi.org/10.18273/revbol.v40n2-2018004>
- Rodríguez, G. & Cetina, L.M. 2016. Caracterización petrográfica y química de rocas de corteza oceánica del Complejo Quebradagrande y comparación con rocas de la unidad Diabasas de San José de Urama. *Boletín de Geología*, 38(3): 15-29. <https://doi.org/10.18273/revbol.v38n3-2016001>
- Rodríguez, G. & Correa-Martínez, A.M. 2015. Edades U-Pb en circón de varias unidades metamórficas al este y noreste de la ciudad de Medellín, cordillera Central de Colombia. XV Congreso Colombiano de Geología. *Memoirs*, p. 287-289. Bucaramanga.
- Rodríguez, G. & Montoya, T. 1993. Evolución magmática del Stock de Altavista. VI Congreso Colombiano de Geología. *Memoirs*, II, p. 497-514. Medellín.
- Rodríguez, G., Arango, M.I., Zapata, G. & Bermúdez, J.G. 2018. Petrotectonic characteristics, geochemistry, and U-Pb geochronology of Jurassic plutons in the Upper Magdalena Valley-Colombia: Implications on the evolution of magmatic arcs in the NW Andes. *Journal of South American Earth Sciences*, 81: 10-30. <https://doi.org/10.1016/j.jsames.2017.10.012>
- Rubatto, D. 2002. Zircon trace element geochemistry: Partitioning with garnet and the link between U-Pb ages and metamorphism. *Chemical Geology*, 184(1-2): 123-138. [https://doi.org/10.1016/S0009-2541\(01\)00355-2](https://doi.org/10.1016/S0009-2541(01)00355-2)
- Ruiz, G.M.H., Seward, D. & Winkler, W. 2007. Evolution of the Amazon Basin in Ecuador with special reference to hinterland tectonics: Data from zircon fission-track and heavy mineral analysis. In: Mange, M.A. & Wright, D.T. (editors), *Heavy Minerals in Use*. *Developments in Sedimentology*, 58: 907-934. [https://doi.org/10.1016/S0070-4571\(07\)58036-2](https://doi.org/10.1016/S0070-4571(07)58036-2)
- Saenz, E.A. 2003. Fission track thermochronology and denudational response to tectonics in the north of the Colombian Central Cordillera. Master Thesis, Shimane University, 138 p. Shimane, Japan.
- Sarmiento-Rojas, L.F., van Wess, J.D. & Cloetingh, S. 2006. Mesozoic transtensional basin history of the Eastern Cordillera, Colombian Andes: Inferences from tectonic models. *Journal of South American Earth Sciences*, 21(4): 383-411. <https://doi.org/10.1016/j.jsames.2006.07.003>
- Schmitt, A.K., Konrad, K., Andrews, G.D.M., Horie, K., Brow, S.R., Koppers, A.A.P., Pecha, M., Busby, C.J. & Tamura, Y. 2017. $^{40}\text{Ar}/^{39}\text{Ar}$ ages and zircon petrochronology for the rear arc of the Izu-Bonin-Marianas intra-oceanic subduction zone. *International Geology Review*, 60(8): 956-976. <https://doi.org/10.1080/00206814.2017.1363675>
- Sdrolias, M. & Müller, R.D. 2006. Controls on back-arc basin formation. *Geochemistry, Geophysics, Geosystems*, 7(4): 1-40. <https://doi.org/10.1029/2005GC001090>
- Seton, M., Müller, R.D., Zahirovic, S., Gaina, C., Torsvik, T.H., Shephard, G., Talsma, A., Gurnis, M., Turner, M., Maus, S. & Chandler, M. 2012. Global continental and ocean basin reconstructions since 200 Ma. *Earth-Science Reviews*, 113(3-4): 212-270. <https://doi.org/10.1016/j.earscirev.2012.03.002>
- Seton, M., Mortimer, N., Williams, S., Quilty, P., Gans, P., Meffre, S., Micklethwaite, S., Zahirovic, S., Moore, J. & Matthews, K.J. 2016. Melanesian back-arc basin and arc development: Constraints from the eastern Coral Sea. *Gondwana Research*, 39: 77-95. <https://doi.org/10.1016/j.gr.2016.06.011>
- Sláma, J., Kosler, J., Condon, D.J., Crowley, J.L., Gerdes, A., Hanchar, J.M., Horstwood, M.S.A., Morris, G.A., Nasdala, L., Norberg, N., Schaltegger, U., Schoene, B., Tubrett, M.N. & Whitehouse, M.J. 2008. Plešovice zircon-A new natural reference material for U-Pb and Hf isotopic microanalysis. *Chemical Geology*, 249(1-2): 1-35. <https://doi.org/10.1016/j.chemgeo.2007.11.005>
- Smyth, H.R., Hall, R. & Nichols, G.J. 2008. Significant volcanic contribution to some quartz-rich sandstones, east Java, Indonesia. *Journal of Sedimentary Research*, 78(5): 335-356. <https://doi.org/10.2110/jsr.2008.039>
- Spadea, P. & Espinosa, A. 1996. Petrology and chemistry of late Cretaceous volcanic rocks from the southernmost segment of the Western Cordillera of Colombia (South America). *Journal of South American Earth Sciences*, 9(1-2): 79-90. [https://doi.org/10.1016/0895-9811\(96\)00029-6](https://doi.org/10.1016/0895-9811(96)00029-6)
- Spikings, R., Cochrane, R., Villagómez, D., van der Lelij, R., Vallejo, C., Winkler, W. & Beate, B. 2015. The geological history of northwestern South America: From Pangaea to the early collision of the Caribbean Large Igneous Province (290-75 Ma).

- Gondwana Research, 27(1): 95–139. <https://doi.org/10.1016/j.gr.2014.06.004>
- Stern, R.J. 2012. Subduction zones. *Reviews of Geophysics*, 40(4): 3–38. <https://doi.org/10.1029/2001RG000108>
- Suárez, M.B., González, L.A. & Ludvigson, G.A. 2010. Estimating the oxygen isotopic composition of equatorial precipitation during the mid–Cretaceous. *Journal of Sedimentary Research*, 80(5): 480–491. <https://doi.org/10.2110/jsr.2010.048>
- Sun, S.S. & McDonough, W.F. 1989. Chemical and isotopic systematics of oceanic basalts: Implications for mantle composition and processes. In: Saunders, A.D. & Norry, M.J. (editors), *Magma-tism in the ocean basins*. Geological Society of London, Special Publication 42, p. 313–345. <https://doi.org/10.1144/GSL.SP.1989.042.01.19>
- Tamayo, J. & Correa, V. 2010. Petrografía y datación de circones detríticos en las facies cuarzosas del complejo Quebradagrande (Cretácico Inferior) de la cordillera Central. Bachelor thesis, Universidad de Caldas, 76 p. Manizales.
- Torsvik, T.H., Rouse, S., Labails, C. & Smethurst, M.A. 2009. A new scheme for the opening of the South Atlantic Ocean and the dissection of an Aptian salt basin. *Geophysical Journal International*, 177(3): 1315–1333. <https://doi.org/10.1111/j.1365-246X.2009.04137.x>
- Toussaint, J.F. 1996. Evolución geológica de Colombia: 3 Cretácico. Universidad Nacional de Colombia, 277 p. Medellín.
- Trail, D., Mojzsis, S.J., Harrison, T.M., Schmitt, A.K., Watson, E.B. & Young, E.D. 2007. Constraints on Hadean zircon protoliths from oxygen isotopes, Ti–thermometry, and rare earth elements. *Geochemistry, Geophysics, Geosystems*, 8(6): 1–22. <https://doi.org/10.1029/2006GC001449>
- Tunik, M., Folguera, A., Naipauer, M., Pimentel, M. & Ramos, V.A. 2010. Early uplift and orogenic deformation in the Neuquén Basin: Constraints on the Andean uplift from U–Pb and Hf isotopic data of detrital zircons. *Tectonophysics*, 489(1–4): 258–273. <https://doi.org/10.1016/j.tecto.2010.04.017>
- Uyeda, S. & Kanamori, H. 1979. Back–arc opening and the mode of subduction. *Journal of Geophysical Research: Solid Earth*, 84(B3): 1049–1061. <https://doi.org/10.1029/JB084iB03p01049>
- van der Lelij, R., Spikings, R. & Mora, A. 2016. Thermochronology and tectonics of the Mérida Andes and the Santander Massif, NW South America. *Lithos*, 248–251: 220–239. <https://doi.org/10.1016/j.lithos.2016.01.006>
- Vásquez, M., Altenberger, U., Romer, R.L., Sudo, M. & Moreno–Murrillo, J.M. 2010. Magmatic evolution of the Andean Eastern Cordillera of Colombia during the Cretaceous: Influence of previous tectonic processes. *Journal of South American Earth Sciences*, 29(2): 171–186. <https://doi.org/10.1016/j.jsames.2009.02.003>
- Vavra, G., Schmid, R. & Gebauer, D. 1999. Internal morphology, habit and U–Th–Pb microanalysis of amphibolite–to–granulite facies zircons: Geochronology of the Ivrea zone (southern Alps). *Contribution to Mineralogy and Petrology*, 134(4): 380–404. <https://doi.org/10.1007/s004100050492>
- Vervoort, J.D. & Blichert–Toft, J. 1999. Evolution of the depleted mantle: Hf isotope evidence from juvenile rocks through time. *Geochimica et Cosmochimica Acta*, 63(3–4): 533–556. [https://doi.org/10.1016/S0016-7037\(98\)00274-9](https://doi.org/10.1016/S0016-7037(98)00274-9)
- Vervoort, J.D. & Patchett, P.J. 1996. Behavior of hafnium and neodymium isotopes in the crust: Constraints from Precambrian crustally derived granites. *Geochimica et Cosmochimica Acta*, 60(19): 3717–3733. [https://doi.org/10.1016/S0016-7037\(98\)00274-9](https://doi.org/10.1016/S0016-7037(98)00274-9)
- Vervoort, J.D., Patchett, P.J., Söderlund, U. & Baker, M. 2004. Isotopic composition of Yb and the determination of Lu concentrations and Lu/Hf ratios by isotope dilution using MC–ICPMS. *Geochemistry, Geophysics, Geosystems*, 5(11): 1–15. <https://doi.org/10.1029/2004GC000721>
- Villagómez, D. & Spikings, R. 2013. Thermochronology and tectonics of the Central and Western Cordilleras of Colombia: Early Cretaceous–Tertiary evolution of the northern Andes. *Lithos*, 160–161: 228–249. <https://doi.org/10.1016/j.lithos.2012.12.008>
- Villagómez, D., Spikings, R., Magna, T., Kammer, A., Winkler, W. & Beltrán, A. 2011. Geochronology, geochemistry and tectonic evolution of the Western and Central Cordilleras of Colombia. *Lithos*, 125(3–4): 875–896. <https://doi.org/10.1016/j.lithos.2011.05.003>
- Villamil, T. 1999. Campanian–Miocene tectonostratigraphy, depocenter evolution and basin development of Colombia and western Venezuela. *Palaeogeography, Palaeoclimatology, Palaeoecology*, 153(1–4): 239–275. [https://doi.org/10.1016/S0031-0182\(99\)00075-9](https://doi.org/10.1016/S0031-0182(99)00075-9)
- Villamil, T. & Arango, C. 1998. Integrated stratigraphy of latest Cenomanian and Early Turonian facies of Colombia. In: Pindell, J.L. & Drake, C.L. (editors), *Paleogeographic evolution and non–glacial eustacy, northern South America*. Society for Sedimentary Geology, Special Publication 58, p. 129–159. <https://doi.org/10.2110/pec.98.58.0129>
- Vinasco, C.J., Cordani, U.G., González, H., Weber, M. & Peláez, C. 2006. Geochronological, isotopic, and geochemical data from Permo–Triassic granitic gneisses and granitoids of the Colombian central Andes. *Journal of South American Earth Sciences*, 21(4): 355–371. <https://doi.org/10.1016/j.jsames.2006.07.007>
- Weber, M., Gómez–Tapias, J., Cardona, A., Duarte, E., Pardo–Trujillo, A. & Valencia, V. 2015. Geochemistry of the Santa Fé Batholith and Buriticá Tonalite in NW Colombia—Evidence of subduction initiation beneath the Colombian Caribbean Plateau. *Journal of South American Earth Sciences*, 62: 257–274. <https://doi.org/10.1016/j.jsames.2015.04.002>
- Whattam, S.A. & Stern, R.J. 2015. Late Cretaceous plume–induced subduction initiation along the southern margin of the Caribbean and NW South America: The first documented example with implications for the onset of plate tectonics.

- Gondwana Research, 27(1): 38–63. <https://doi.org/10.1016/j.gr.2014.07.011>
- Wiedenbeck, M., Hanchar, J.M., Peck, W.H., Sylvester, P., Valley, J., Whitehouse, M., Kronz, A., Morishita, Y., Nasdala, L., Fiebig, J., Franchi, I., Girard, J.P., Greenwood, R.C., Hinton, R., Kita, N., Mason, P.R.D., Norman, M., Ogasawara, M., Piccoli, P.M., Rhede, D., Satoh, H., Schulz–Dobrick, B., Skår, O., Spicuzza, M.J., Terada, K., Tindle, A., Togashi, S., Vennemann, T., Xie, Q. & Zheng, Y.F. 2004. Further characterisation of the 91 500 zircon crystal. *Geostandards and Geoanalytical Research*, 28(1): 9–39. <https://doi.org/10.1111/j.1751-908X.2004.tb01041.x>
- Williams, I.S. 1998. U–Th–Pb geochronology by ion microprobe. In: Mckibben, M.A., Shanks III, W.C. & Ridley, W.I. (editors.), *Applications of microanalytical techniques to understanding mineralizing processes*. *Reviews in Economic Geology* 7, p. 1–35. Littleton, USA.
- Zapata, J.P., Restrepo, J.J., Cardona, A. & Martens, U. 2017. Geoquímica y geocronología de las rocas volcánicas básicas y el Gabro de Altamira, cordillera Occidental (Colombia): Registro de ambientes de plateau y arco oceánico superpuestos durante el Cretácico. *Boletín de Geología*, 39(2): 13–30. <https://doi.org/10.18273/revbol.v39n2-2017001>
- Zapata, S., Cardona, A., Jaramillo, J. S., Patiño, A., Valencia, V., Leon, S., Mejía, D., Pardo–Trujillo, A. & Castañeda, J. P. 2018. Cretaceous extensional and compressional tectonics in the Northwestern Andes, prior to the collision with the Caribbean oceanic plateau. *Gondwana Research*, 66: 207–226. <https://doi.org/10.1016/j.gr.2018.10.008>

Explanation of Acronyms, Abbreviations, and Symbols:

CLIP	Caribbean Large Igneous Province	LA–ICP–MS	Laser ablation inductively coupled plasma mass spectrometry
E–MORB	Enriched mid–ocean ridge basalt	LILE	Large–ion lithophile element
FC	Faraday cup	LREE	Light rare earth element
DM	Depleted mantle	MORB	Mid–ocean ridge basalt
HFSE	High field strength element	MREE	Middle rare earth element
HREE	Heavy rare earth element	TDM	Depleted mantle model ages
ICP–AES	Inductively coupled plasma atomic emission spectroscopy	TIMS	Thermal ionization mass spectrometry
ICP–MS	Inductively coupled plasma mass spectrometry	VSMOW	Vienna standard mean ocean water

Authors' Biographical Notes



Agustín CARDONA is graduated with a degree in geology from Universidad EAFIT in 1999. He obtained MS and PhD degrees in geochemistry and geotectonics, respectively, from the Universidade de São Paulo, Brasil. Subsequently, he was a postdoctoral fellow at the Smithsonian Tropical Research Institute (2006–2011), working in several paleogeographic-oriented projects in

northern Colombia and Panamá. Since 2012, he has served as full-time professor at the Universidad Nacional de Colombia in Medellín. His main interest is related to regional tectonics of convergent margins, especially the Andean and Caribbean Orogens.



Santiago LEÓN is graduated with a degree in geological engineering from the Universidad Nacional de Colombia in 2015 and obtained a MS degree in geochemistry and geotectonics from the Universidade de São Paulo, Brasil in 2017. He is currently enrolled as a PhD student at the Universidad Nacional de Colombia and as a predoctoral fellow at the Smithsonian Tropical Research Institute in Panamá.

Santiago uses zircon U–Pb geochronology, petrography, geochemistry, and low-temperature thermochronology to reconstruct the Neogene tectono-stratigraphic and magmatic record of northwesternmost Colombia as the product of changing collisional and subduction-related tectonics.



Juan S. JARAMILLO is graduated as a geological engineer from the Universidad Nacional de Colombia in 2016 and master of mineral resources in 2018 from the same university. He is interested in the tectono–magmatic evolution of the northern Andes and the integration of geological mapping, geochemistry, and the geochronological and the stratigraphic evolution of magmatic arcs. He

has examined the reconstruction of the Cretaceous, Paleocene, and Miocene volcanic arcs of the northern Andes. Currently, Juan is studying the tectono–magmatic processes of the Miocene compositional arc variation of the Colombian Andes.



Victor A. VALENCIA is currently a research scientist at the School of the Environment, Washington State University, he received his BEng in geosciences from CESUES, México, MS in geology from the Universidad de Sonora, and PhD from the Department of Geosciences, University of Arizona. His research interests include U–Pb geochronology, economic geology, and the magmatic

evolution of convergent margins. He has been involved in various regional projects examining the Mesozoic – Cenozoic tectonomagmatic and metallogenetic evolution of the Andes and México.



Sebastian ZAPATA is a geologist, who received his PhD from the University of Potsdam (Germany). He performed his undergraduate and master's studies at the Universidad Nacional de Colombia Sede Medellín. He is interested in examining the structural, sedimentological, and thermochronological characteristics of exposed orogenic systems in rock sequences that are generated at shallow–

to–intermediate depths of the Earth. His research approach involves the application of multitechnique methodologies that are oriented towards a better understanding and the reconstruction of paleogeographic and tectonic conditions during the evolution of convergent margins. In particular, he aims to understand the processes responsible for mountain building, topographic evolution, and relief development in combination with climate–driven impacts on surface processes and structural patterns in orogeny development. The research of Sebastian ZAPATA has been focused on “source–to–sink” topics along the Andean flanks in the northern and central Andes but also includes the Caribbean Plateau, using low–temperature thermochronology, U/Pb geochronology, tectonostratigraphy, structural geology, and sediment provenance analysis.



Andrés PARDO–TRUJILLO is a geologist in the Departamento de Ciencias Geológicas at the Universidad de Caldas (Manizales, 1998). Andres obtained his MS in vegetal micropaleontology in 1997 and his PhD in Science from Liège University (Belgium, 2004). He has worked since 1989 as a professor in the Departamento de Ciencias Geológicas at Universidad de Caldas, Colombia, in

sedimentology, regional geology, palynology, and field geology. From 2006–2009, he worked as an advisor at the Agencia Nacional de Hidrocarburos (ANH), where he participated in the geological study of several Colombian sedimentary basins. Andres is currently the director of the Instituto de Investigaciones en Estratigrafía (IIES) and of the Grupo de Investigación en Estratigrafía y Vulcanología (GIEV) at the Universidad de Caldas. His main interest is the study of the geological and biological evolution of the NW corner of South America during the Cretaceous – Cenozoic.



Axel K. SCHMITT is currently a professor at the Institute of Earth Sciences at Ruprecht–Karls–Universität Heidelberg, Germany and is part of the petrology and isotope geology research group. He was formerly a professor and researcher at the University of California, Los Angeles, USA. Some major lines of research include, among others, the analysis of the time scales of magmatic processes;

the origin, growth, and recycling of the continental crust; continental rifting and magmatism, magma–driven geothermal systems and their thermal history; and geoarchaeology.



Dany MEJÍA as an MS student of mineral resources at the Facultad de Minas at the Universidad Nacional de Colombia Sede Medellín, he is studying Jurassic metamorphism at the Central Cordillera of Colombia, using structural geology, mineral chemistry, whole–rock geochemistry, and isotope geology to understand Andean continental arc growth and responses to changes in the

subduction angle and convergence obliquity. Dany obtained his degree as an engineer geologist from the same university in 2015 and has experience in structural geology, geological mapping, petrology, heavy mineral analysis, geochronology, geochemistry, and low–to–medium–grade thermobarometry.



Juan Camilo ARENAS has worked as a geologist engineer since 2018. He obtained his degree from the Universidad Nacional de Colombia, where he developed his work in geochemistry and geochronology from north zone of Central Cordillera to understand the Cretaceous tectonic evolution in this region. He is currently engaged in hydrogeological modulation as an employee of a private company dedicated to the development of environmental impact studies.

